

REPORT DOCUMENTATION PAGE

AFRL-SR-AR-TR-04-

0555

The public reporting burden for this collection of information is estimated to average 1 hour per response, including the time for gathering and maintaining the data needed, and completing and reviewing the collection of information. Send comments regarding this burden estimate or any other aspect of this collection of information, including suggestions for reducing the burden, to the Department of Defense, Executive Service and Communications, Washington, DC 20301-4070. That notwithstanding any other provision of law, no person shall be subject to any penalty for failing to comply with a collection of information if it does not display this control number.

PLEASE DO NOT RETURN YOUR FORM TO THE ABOVE ORGANIZATION.

1. REPORT DATE (DD-MM-YYYY) 11-10-2004		2. REPORT TYPE Final		3. DATES COVERED (From - To) Oct 2001 - Sept 2004	
4. TITLE AND SUBTITLE Organic glasses and crystals for miniature electro-optic devices: synthesis, characterization, and applications				5a. CONTRACT NUMBER	
				5b. GRANT NUMBER F49620-01-1-0561	
				5c. PROGRAM ELEMENT NUMBER	
				5d. PROJECT NUMBER	
6. AUTHOR(S) Fernandez, Felix, E. Timofeeva, Tanja Sarkisov, Sergey, S.				5e. TASK NUMBER	
				5f. WORK UNIT NUMBER	
7. PERFORMING ORGANIZATION NAME(S) AND ADDRESS(ES) University of Puerto Rico Highway #2, Post Street, Bldg. 2A Mayaguez, PR 00931				8. PERFORMING ORGANIZATION REPORT NUMBER	
9. SPONSORING/MONITORING AGENCY NAME(S) AND ADDRESS(ES) Air Force Office of Research 801 N Randolph Street Arlington, VA 22203				10. SPONSOR/MONITOR'S ACRONYM(S) AFOSR	
				11. SPONSOR/MONITOR'S REPORT NUMBER(S)	
12. DISTRIBUTION/AVAILABILITY STATEMENT Approved for public release. Distribution unlimited.					
13. SUPPLEMENTARY NOTES <div style="text-align: center; font-size: 2em; font-weight: bold;">20041109 017</div>					
14. ABSTRACT A high-level computational analysis of two-photon absorbing derivatives of piperidone and cyclohexanone was carried out. Obtained data were compared with the experimental results. The molecular cross-section of the two-photon absorption of these compounds, as high as $3000 \times 10^{-50} \text{ cm}^4 \text{ s/photon}$ at nanosecond pumping, makes then promising nonlinear materials for optical limiting in near-infrared region. They also exhibit an intense two-photon exciting fluorescence, of the same order as that of Rhodamine B. In addition, these compounds have previously demonstrated strong anticancer effect. Both features combined in a single compound also open the way for more efficient treatment of cancer. Characterization of the infrared absorption spectrum of the solutions of fullerene C_{60} with 2-cyclooctylamino-5-nitropyridine additive known as COANP has been performed with the focus on possible bonding with the amino-group of the additive. No occurrence of such bonding was found at normal conditions. Also no change of optical absorption in visible region and optical limiting of fullerene due to chemical bonding with the additive was detected even for a molar proportion of the additive to fullerene approaching 200:1. A miniature electro-optic (E-O) modulator that comprises a Fabry-Perot (F-P) etalon integrated with an optical fiber was theoretically analyzed. The estimations indicated that the finesse of the F-P cavity is a highly critical factor in achieving low driving voltage of the modulator. Thin films of E-O polymers LD-3 and polyimide were prepared using spin casting technique followed by corona poling. The electro-optic coefficient r_{33} was measured and found to be between 3 and 5 pm/V.					
15. SUBJECT TERMS two-photon absorption, two-photon excited fluorescence, piperidone, cyclohexanone, optical limiting, fullerene, COANP, FTIR					
16. SECURITY CLASSIFICATION OF:			17. LIMITATION OF ABSTRACT UU	18. NUMBER OF PAGES 102	19a. NAME OF RESPONSIBLE PERSON Félix E. Fernández
a. REPORT U	b. ABSTRACT U	c. THIS PAGE U			19b. TELEPHONE NUMBER (Include area code) 787-265-3844

Standard Form 298 (Rev. 8/98)
Prescribed by ANSI Std. Z39.18

BEST AVAILABLE COPY

AFOSR Grant F49620-01-1-0561

**ORGANIC GLASSES AND CRYSTALS FOR MINIATURE ELECTRO-OPTIC
DEVICES: SYNTHESIS, CHARACTERIZATION, AND APPLICATIONS**

Felix E. Fernandez (University of Puerto Rico at Mayaguez))
Tatiana Timofeeva (New Mexico Highlands University)
Sergey Sarkisov (Alabama Agricultural and Mechanical University)

University of Puerto Rico at Mayaguez
Department of Physics
Mayaguez, Puerto Rico 00681-9016

October 2004

Final Report

October 1, 2001 – September 30, 2004

Preface

This is the final report of research conducted for the Air Force Office of Research. The research was conducted under Grant F49620-01-1-0561 from 1 October 2001 through 30 September 2004 and was coordinated with Dr. Charles Lee, Scientific Program Officer.

The research was conducted by the University of Puerto Rico at Mayaguez (leading institution), the New Mexico Highlands University, and the Alabama Agricultural and Mechanical University, which are the members of the Alliance for Nonlinear Optics sponsored in the past by NASA.

This report elaborates on aspects of the work described in Annual Reports submitted in August 2002, 2003.

The objectives of the research were the following:

1. Computational evaluation of molecular structure and optical properties of materials before synthesis.
2. Synthesis of the compounds of interest, including synthesis of precursors.
3. Single-crystal X-ray analysis of monomers to prove their structure and to get information about structural features responsible for optical properties.
4. Preparation of thin films of polymer materials by conventional methods for preliminary evaluation properties.
5. Structural/chemical modification of the compounds to improve and/or optimize their NLO/EO and OL characteristics.
6. Characterization of organic-inorganic materials and devices.
7. Investigation of materials for optical limiting. Exploring of two-photon absorption mechanism.
8. To explore a modulator comprised of thin film and a prism coupler.

9. To study the feasibility of the proposed design of a miniature electro-optic modulator based on Fabry-Perot cavity integrated with an optical fiber.
10. To characterize the performance of new organic electro-optic glasses, polymers, and single-crystal films using the modulator.
11. To characterize the performance of new synthesized photorefractive, optical limiting and two-photon absorbing materials using the basic design of the modulator as a research platform.

It has been shown before that compounds, such as piperidone and cyclohexanone, that belong to a class of conjugated ketone derivatives are prospective two-photon absorbing (TPA) materials. TPA involves electronic excitation of a molecule induced by a pair of photons of the same or different energy. Unlike single-photon absorption (OPA), TPA is quadratically proportional to the intensity of the incident light, and hence, by focusing the beam, one can precisely localize TPA in a small volume up to one wavelength in size deep inside the bulk of the material, that directs practical applications of TPA to 3D microfabrication, TPA photodynamic therapy, and molecular biosensing.

This report presents a high-level computational analysis of TPA activity of these compounds. Computational analysis of the compounds was carried out in collaboration with Theoretical Division at Los Alamos National Laboratory (Dr. Tretiak). Obtained data have been compared with the experimental results obtained by Dr. Sarkisov's group at the Department of Physics, AAMU.

Characterization of the infrared absorption spectrum of the solutions of fullerene C₆₀ with 2-cyclooctylamino-5-nitropyridine additive has been performed with the focus on possible bonding with the amino-group of the additive. No occurrence of such bonding was found at normal conditions. Also no change of optical absorption in visible region and optical limiting of fullerene due to chemical bonding with the additive was detected. The resulting optical properties of the mixture were simply a sum of the properties of the components for a molar proportion of the additive to fullerene approaching 200:1.

The two-photon absorption and two-photon excited fluorescence of a selected group of new derivatives of cyclohexanone and piperidone was studied in relation to

their molecular structure. The molecular cross-section of the two-photon absorption of these compounds, as high as $3000 \times 10^{-50} \text{ cm}^4 \text{ s/photon}$ at nanosecond pumping, makes them promising nonlinear materials for optical limiting in near-infrared region. They also exhibit an intense two-photon exciting fluorescence. Similar compounds have previously demonstrated strong anticancer effect. Both features combined in a single compound thus open the way for more efficient treatment of cancer, when bio-chemical destruction of malignant cells is accompanied by their two-photon fluorescent imaging.

A miniature electro-optic (E-O) modulator that comprises a Fabry-Perot (F-P) etalon integrated with an optical fiber was theoretically analyzed. The theoretical evaluation of the performance of the modulator was conducted for a single crystal film of organic compound *N*-4-Nitrophenyl-*N*-(*L*)-prolinol known as NPP, which have been recently grown and used in a longitudinal E-O modulator known as a conventional Pockels cell. The estimations indicated that the finesse of the F-P cavity is a highly critical factor in achieving low driving voltage of the modulator. An E-O modulator based on a planar thin film waveguide was also considered as another approach to a miniature E-O device. Thin films of E-O polymers were prepared using spin casting technique. An experimental setup for characterization of electro-optic properties of poled polymer films was built. The electro-optic coefficients of poled polymer films were measured. Coefficient r_{33} was found to be between 3 and 5 pm/V.

Acknowledgments

The authors wish to express their thanks to Dr. Paul Fleitz, Air Force Research Lab, for conducting characterization of two-photon compounds and providing very helpful comments.

The authors also appreciate the help of Aracelis Cardona and Sindia Ramos, instrumentation specialists at the Department of Chemistry, UPR, in performing some of the FTIR measurements.

Our good friend and colleague Alex Leyderman passed away prior to publication of this paper. His co-authors dedicate this work to him.

Table of contents

List of figures.....	3
List of tables.....	7

Part 1

Evaluation, synthesis, and preparation of materials

1. Computational evaluation of two-photon absorption cross-section for potential optical limiting materials (piperidone (I) and cyclohexanone (II) derivatives).....	8
2. Synthesis of piperidone and cyclohexanone derivatives with high two-photon activity and high solubility.....	19
3. Synthesis of surfactants for coating of nano-particles.....	21
4. Synthesis of 3,5-bis(Benzylidene)-4-piperidone hydrochloride.....	22
5. Synthesis of 3,5-bis(Benzylidene)-4-piperidone.....	23
6. Synthesis of 11- <i>N</i> -[3,5-bis(Benzylidene)-4-piperidone]undecan-1-ol.....	24
7. Synthesis of 3,5-bis(4-Dimethylaminobenzylidene)-4-piperidone hydrochloride.....	25
8. Synthesis of 3,5-bis(4-Dimethylaminobenzylidene)-4-piperidone.....	26
9. Conclusions and recommendations.....	26
References for Part 1.....	26

Part 2

Studies of Photosensitivity, Optical Limiting, Device Fabrication, and Characterization

1. Introduction.....	27
2. Optical limiting in mixtures of fullerene C ₆₀ with COANP.....	29
2.1. FTIR spectroscopy.....	29
2.2. Optical spectroscopy in visible region.....	31
2.3. Optical limiting.....	32
3. Optical limiting and two-photon excited fluorescence in derivatives of cyclohexanone and piperidone.....	34
3.1. Materials.....	34
3.2. Experiment.....	35

3.3. Experimental results and discussion.....	39
3.3.1. Two-photon absorption.....	39
3.3.2. Single-photon and two-photon fluorescence.....	41
4. Conclusions and recommendations.....	45
References for Part 2.....	46

Part 3

Miniature Device Fabrication

1. Design.....	73
2. Evaluation of the figures-of-merit.....	73
3. Alternative designs.....	77
4. Suggested fabrication procedure.....	82
5. Experimental results: conductive coating of optical fibers.....	84
6. Electro-optic modulator based on a planar waveguide.....	87
7. Conclusions and recommendations.....	92
References for Part 3.....	92

Appendix

A1. Participants.....	A1
A2. Presentations.....	A2
A3. Papers published.....	A3
A4. Papers submitted.....	A4
A5. Students graduated.....	A5

List of figures

Part 1

Fig. 1. HOMO and LUMO orbitals in molecules 3c and 2a.

Fig. 2. Structure of molecule **c1** in crystal.

Fig. 3. Structure of molecule **c3** in crystal.

Part 2

Fig. 1. Chemical structure of (a) the molecules of fullerene C_{60} and 2-cyclooctylamino-5-nitropyridine (COANP) and (b) their hypothetical covalent bonding through the amino-group.

Fig. 2. FTIR transmission spectra of (a) solvent carbon disulfide (dotted curve 1) and COANP solution (60 mg/ml) in carbon disulfide (solid curve 2); (b) solvent carbon tetrachloride (dotted curve 1) and COANP solution (60 mg/ml) in carbon tetrachloride (solid curve 2).

Fig. 3. FTIR transmission spectra of COANP solution in (a) carbon tetrachloride at a concentration of 4mg/ml (dotted curve 1); carbon tetrachloride at a concentration of 60 mg/ml (curve 2); carbon disulfide at a concentration of 20 mg/ml (dotted curve 3); carbon disulfide at a concentration of 60 mg/ml (curve 4); carbon disulfide after casting on an IR-card and evaporation of the solvent (curve 5); (b) carbon disulfide after casting on an IR-card and evaporation of the solvent for 1 hour (curve 1) and for 2 days (curve 2).

Fig. 4. FTIR transmission spectrum of (1) solvent (carbon disulfide); (2) fullerene C_{60} solution (7 mg/ml) in carbon disulfide.

Fig. 5. FTIR transmission spectra (a) in spectral region 550 to 1425 cm^{-1} of solvent carbon disulfide (curve 1); fullerene C_{60} solution (7mg/ml) in carbon disulfide (curve 2); COANP solution (20 mg/ml) in carbon disulfide (curve 3); fullerene C_{60} (7 mg/ml) and COANP (20 mg/ml) solution in carbon disulfide (curve 4); (b) in spectral region 1600 to 3700 cm^{-1} of solvent carbon disulfide (curve 1); fullerene C_{60} solution (7mg/ml) in carbon disulfide (curve 2); COANP solution (20 mg/ml) in carbon disulfide

(curve 3); fullerene C_{60} (7 mg/ml) and COANP (20 mg/ml) solution in carbon disulfide (curve 4); (c) of the films deposited from solution in CS_2 on AgCl plate of COANP (dotted curve 1) and COANP plus fullerene C_{60} (curve 2).

Fig. 6. Optical absorption spectra of the solutions in CS_2 of (1) pure C_{60} ; (2) C_{60} and COANP at molar proportion 1:0.5; (3) C_{60} and COANP at molar proportion 1:1; (4) C_{60} and COANP at molar proportion 1:2; (5) C_{60} and COANP at molar proportion 1:5; (6) C_{60} and COANP at molar proportion 1:10; (7) C_{60} and COANP at molar proportion 1:20; (8) C_{60} and COANP at molar proportion 1:50; (9) C_{60} and COANP at molar proportion 1:100; (10) C_{60} and COANP at molar proportion 1:200. Dotted line shows marks the position of the absorption peak of C_{60} near 600 nm. Fullerene C_{60} was initially dissolved at a maximum concentration of 7.9 mg/ml (6.6×10^{-4} molar fraction)³⁰ before COANP was added and then the solution was filtered through a 0.2- μ m-pore-size filter.

Fig. 7. Spectrum of optical absorption of (1) pure CS_2 ; (2) COANP in CS_2 at the same concentration as in the mixture of C_{60} and COANP in molar proportion 1:5; (3) C_{60} in CS_2 ; (4) mixture of C_{60} and COANP in CS_2 in molar proportion 1:5. Fullerene C_{60} was initially dissolved at a maximum concentration of 7.9 mg/ml (6.6×10^{-4} molar fraction)³⁰ before COANP was added.

Fig. 8. Optical density of the solutions of C_{60} and COANP in CS_2 versus molar proportion of COANP (number of moles per one mole of C_{60}) at (1) 434-nm wavelength; (2) 452-nm wavelength; (3) 597-nm wavelength.

Fig. 9. Schematic of the experimental setup for the characterization of optical limiting properties of fullerene/COANP solutions.

Fig. 10. Normalized transmittance of the solution of C_{60} and COANP in CS_2 versus the fluence of laser light at 532-nm wavelength. Molar proportion of C_{60} to COANP was: (1) 1:0 (pure C_{60}); (2) 1:0.5; (3) 1:1; (4) 1:5; (5) 1:10; (6) 1:50. Dataset (7) corresponds to pure COANP at a concentration that would make molar proportion 1:100 if C_{60} were added. Dataset (8) corresponds to pure solvent CS_2 . The concentration of C_{60} was always kept at maximum. The measurements were taken with frequency double Nd:YAG laser, 180-ns pulse duration, 5-Hz pulse repetition rate.

Fig. 11. Generalized chemical structure of the derivatives of cyclohexanone/piperidone (1 through 8) studied in this work: (a) molecular layout and (b)

distribution of electro-positive and negative fragments. Molecular structure with $X=CH$ and $R_2=Ph$ (phenyl) corresponds to a derivative of cyclohexanone, and the one with $X=N$ and $R_2=CH_3$ corresponds to a derivative of piperidone. Compound 9 is a piperidone derivative that has R_1 and benzene ring on both ends replaced by ferrocene Fc.

Fig. 12. Setup for measurements of TPA, SPEF and TPEF with pulsed laser sources. In case of measurements of SPEF under continuous pumping with UV lamp, the light was modulated by a mechanical chopper and the boxcar averager was replaced by a lock-in amplifier synchronized by the chopper.

Fig. 13. Typical plot of the inversed transmissivity of a TPA compound (compound 2 in this case) versus input intensity of IR radiation.

Fig. 14. Power of the two-photon excited fluorescence versus the power of pumping IR radiation plotted in: (a) linear scale and (b) log-log scale. The experimental data correspond to compound 4.

Fig. 15. Spectra of TPA cross-section of compounds (1) 7, (2) 8, (3) 1, (4) 2, (5) 3, (6) 5, (7) 6, and (8) 4.

Fig. 16. Single-photon absorption, single-photon excited (SPEF) and two-photon excited fluorescence (TPEF) of compound 1 dissolved in chloroform. The arrows mark the positions of the spectrum lines for: 1) 876 nm tunable IR pulsed dye laser; 2) pulsed frequency double Nd:YAG laser (532 nm); 3) double energy of photon of the IR dye laser; 4) Nitrogen pulsed UV laser (337 nm). The slant lines indicate the range of the emission spectrum of the UV lamp (302 nm to 580 nm). Single-photon absorption was taken at a concentration of 0.675 mM/L, SPEF was taken at concentration of 100, 5, and 5 mM/L, and TPEF was taken at a concentration of 100 mM/L.

Fig. 17. Single-photon absorption, SPEF and TPEF of compounds 2 and 3 (dotted lines) both dissolved in chloroform. Notations and the conditions at which the spectra were taken are the same as for Fig. 16.

Fig. 18. Single-photon absorption, SPEF and TPEF of compound 4 dissolved in chloroform. Notations and the conditions at which the spectra were taken are the same as for Fig. 16.

Fig. 19. Single-photon absorption, SPEF and TPEF of compounds 5 and 6 (dotted lines) both dissolved in chloroform. Notations and the conditions at which the spectra were taken are the same as for Fig. 16.

Fig. 20. Single-photon absorption and SPEF of compounds 7 and 8 (dotted lines) both dissolved in chloroform. Notations and the conditions at which the spectra were taken are the same as for Fig. 16.

Part 3

Fig. 1. Schematic of a miniature E-O modulator based on a Fabry-Perot (F-P) etalon integrated with an optical fiber.

Fig. 2. Transmittance of a F-P modulator (solid curves) as compared to a Pockels cell (dashed curve 1). Curve 2 corresponds to the finesse of the F-P cavity 10, curve 3 – to 100.

Fig. 3. A schematic of a F-P E-O modulator made of fiber Bragg reflectors.

Fig. 4. Schematic of a transversal E-O modulator using optical fibers to inject light in and collect light out from a single crystal film of an organic crystal grown by the plate guiding method.

Fig. 5. Schematic of a longitudinal E-O modulator using optical fibers to inject light in and collect light out from a single crystal film of an organic crystal grown by the plate guiding method.

Fig. 6. The schematic of the suggested experimental cell for growing a single-crystal film of an organic E-O material as a part of a F-P E-O modulator.

Fig. 7. The schematic of the experimental set-up used to deposit ITO conductive coating on the end of an optical fiber using the RF magnetron sputtering technique.

Fig. 8. The schematic of the experimental set-up used to test the electric contact between the sidewalls of the ITO coated fiber and its end face.

Fig. 9. The oscillogram of the signal proportional to the varying intensity of light reflected from the film of poled polyimide from GSU (top) and the alternating voltage applied to it (bottom).

Fig. 10. Amplitude of the modulation signal from the E-O polyimide film versus amplitude of the alternating voltage in (a) linear and (b) log-log scale.

List of tables

Part I

Table 1. Piperidone derivatives (series I)

Table 2. Cyclohexanone derivatives (series II)

Table 3. Positions of absorption and emission peaks for studied compounds

Table 4. Crystal data on compounds **c1** and **c3**

Part 2

Table 1. Energy position of vibrational spectra bands in COANP in solution and in solid phase.

Table 2. Cross-section of TPA of cyclohexanone/piperidone derivatives and reference materials.

Table 3. Intensity of SPEF and TPEF of cyclohexanone/piperidone derivatives relative to reference dyes Rhodamine 6G and Rhodamine B respectively.

Part 3

Table 1: Driving voltage V_{10dB} (V) of the F-P modulator for various values of finesse as compared to a Pockels cell. The material is a single crystal film of organic compound NPP

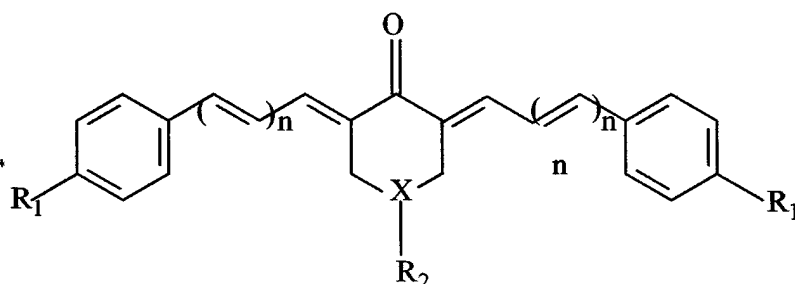
Table 2. Resistance of the ITO coating between the sidewall and the end face of optical fibers

Part 1

Evaluation, synthesis, and preparation of materials

1. Computational evaluation of two-photon absorption cross-section for potential optical limiting materials (piperidone (I) and cyclohexanone (II) derivatives)

It was shown before that compounds with general formula presented below



I: X=N, R₁=Donor, R₂=H, Alk

II: X=CH, R₁=Donor, R₂=Ph

that belongs to a class of conjugated keton derivatives are prospective two-photon absorbing (TPA) materials in case when R₁ are strong donor substituents. General scheme of synthesis of such compounds was presented in our 2001-02 report. Preliminary computational analysis of TPA characteristics of these compounds was presented at the same report. TPA involves electronic excitation of a molecule induced by a pair of photons of the same or different energy. Unlike one-photon absorption (OPA), TPA is quadratically proportional to the intensity of the incident light, and hence, by focusing the beam, one can precisely localize TPA in a small volume up to one wavelength in size deep inside the bulk of the material, that directs practical applications of TPA such as 3D microfabrication, TPA photodynamic therapy, and biosensing on molecular level.

In the final report we are presenting a high-level computational analysis of TPA activity of these compounds. Computational analysis of series of compounds I and II have been carried out in collaboration with Theoretical Division at Los Alamos National Laboratory (Dr. Tretiak). Obtained data have been compared with the experimental results obtained by Dr. Sarkisov's group at Physics Department AA&MU.

Time-dependent density-functional theory (TDDFT) described in Ref.1 was applied to calculate one- and two-photon absorption spectra (related to linear and third-order optical responses, respectively) in a series of molecules **II** and **I**.

Experimental results on molecular structure of series **I** and **II** in crystal have shown that molecules adopt two conformations according to substituent position at X atom – axial or equatorial. Our experimental data and computations show that equatorial conformation is the most common for these compounds. So for several molecules we evaluated energy difference between two conformations and also presented TPA and other molecular electronic characteristics for two conformations.

In Tables 1 and 2 calculational and experimental results on piperidone derivatives (series **I**) and cyclohexanone derivatives (series **II**) with different length of π -conjugated chain (one and two C=C bonds) are presented. It is obvious that experimental and computational results have the same qualitative trend, but does not correspond exactly numerically and should be scaled for quantitative agreement. It should be mentioned that the same problem occurs for other NLO properties such as second and third harmonic generation. Partial improvement of the results might be achieved by account of the solvent, and for several compounds we introduced consideration of solvent in our calculations. These results are presented in parenthesis.

Another important characteristic of TPA compounds is HOMO – LUMO gap. When gap is low, potential to manifest TPA for particular compound is high. The orbitals special distribution is also an important characteristic of TPA activity. Figure 1 shows HOMO and LUMO orbitals of two molecules under consideration in ground and excited states. Computational evaluation of TPA activity is still in progress and we plan to submit publication describing our results by the end of 2004.

Table 1. Piperidone derivatives (series I)

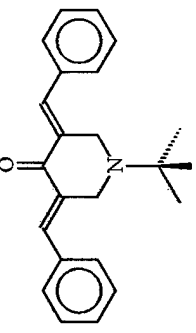
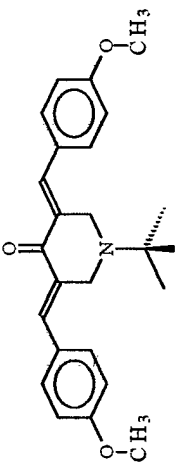
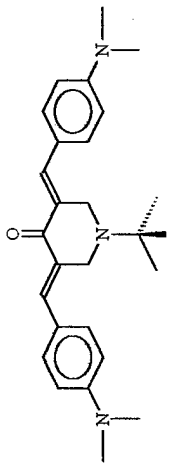
Number	Structure	μ , D (HF)	ΔE , kJ/ mol	Linear transm it- tance (1 cm cell)	Molecular cross-section of TPA $\sigma_2 \times$ 10^{-50} [cm ⁴ s photon ⁻¹ molecule ⁻¹]	Calculated TPA cross section σ_2 $\times 10^{-50}$ [cm ⁴ s photon ⁻¹ molecule ⁻¹]
3q		ax				
		eq				53 (2.06)(88) 62 (2.64)(102)
3k		ax 4.42	2.75			76 (1,92)
		eq 5.90	0			
3c				0.88	600±150 162±73	181 (1.69) (298) 135 (2.4) (223)
		eq 3.66				

Table 1 continued. Piperidone derivatives (series I)

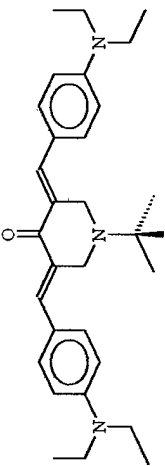
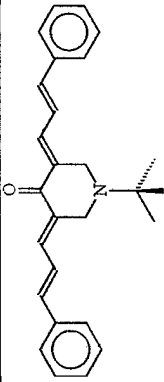
Number	Structure	μ , D (HF)	E_h kJ/ mol	Linear transmittance (1 cm cell)	Molecular cross- section of TPA $\sigma'_2 \times 10^{-50}$ [cm ⁴ s photon ⁻¹ molecule ⁻¹]	Calculated TPA cross section $\sigma_2 \times 10^{-50}$ [cm ⁴ s photon ⁻¹ molecule ⁻¹]
3a		ax		~1.00	1950±110 504±140	177 (1.68) (291) 148 (2.38) (244)
		eq				
3r		ax				188(309) (1.74eV) 108(2.2) 405 (668) (2.37)
		eq				

Table 1 continued. Piperidone derivatives (series I)

Number	Structure	μ , D (HF)	E_h kJ/ mol	Linear transmittance (1 cm cell)	Molecular cross- section of TPA $\sigma'_2 \times 10^{-50}$ [cm ⁴ s photon ⁻¹ molecule ⁻¹]	Calculated TPA cross section $\sigma_2 \times 10^{-50}$ [cm ⁴ s photon ⁻¹ molecule ⁻¹]
3e		ax 4.49	2.80	0.84	460±80	220 (1.65) (363)
		eq 5.73	0		130±40	232 (2.18) (382) 341 (1.66) (562) 322 (2.2) (531)
3g		ax 2.36	2.69	0.88	2650±100	623 (1.5) (1028)
		eq 4.06	0		683±178	346 (2.07) 377 (1.51) (623) 250 (2.09)

Table 1 continued. Piperidone derivatives (series I)

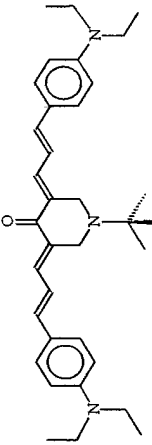
Number	Structure	μ , D (HF)	E_h kJ/ mol	Linear transmittance (1 cm cell)	Molecular cross- section of TPA $\sigma'_2 \times 10^{-50}$ [cm ⁴ s photon ⁻¹ molecule ⁻¹]	Calculated TPA cross section $\sigma_2 \times 10^{-50}$ [cm ⁴ s photon ⁻¹ molecule ⁻¹]
3i				0.91	3230±70	
		eq			829±200	672 (1.5)
		5.73 eq	0			341 (1.66) (562) 322 (2.2) (531)

Table 2. Cyclohexanone derivatives (series II)

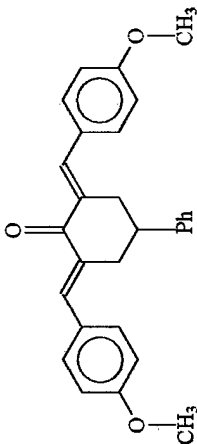
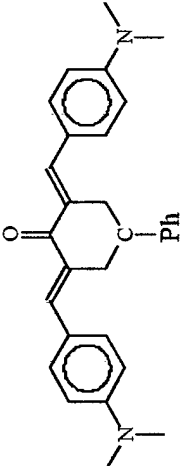
Number	Structure	μ , D (HF)	E_h kJ/ mol	Linear transmit- tance (1 cm cell)	Molecular cross- section of TPA $\sigma_2 \times$ 10^{-50} [cm ⁴ s photon ⁻¹ molecule ⁻¹]	Calculated TPA cross section $\sigma_2 \times$ 10^{-50} [cm ⁴ s photon ⁻¹ molecule ⁻¹]
31		eq 5.17				114(188) (1.87eV) 87 (143) (2.47eV)
3b		eq 3.51				179 (295) (1.69) 38 (62) (2.33)

Table 2 continued. Cyclohexanone derivatives (series II)

Number	Structure	μ , D (HF)	E_h kJ/ mol	Linear transmit- tance (1 cm cell)	Molecular cross- section of TPA $\sigma'_2 \times$ 10^{-50} [cm ⁴ s photon ⁻¹ molecule ⁻¹]	Calculated TPA cross section $\sigma_2 \times$ 10^{-50} [cm ⁴ s photon ⁻¹ molecule ⁻¹]
3d		eq 3.82				289 (477) (1.65) 189 (311) (2.33)

Table 2 continued. Cyclohexanone derivatives (series II)

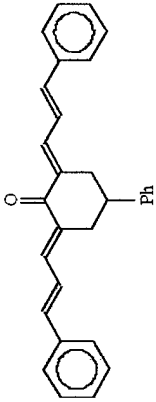
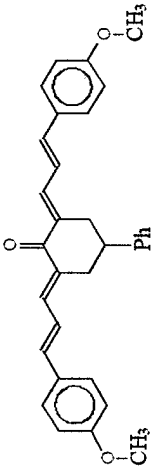
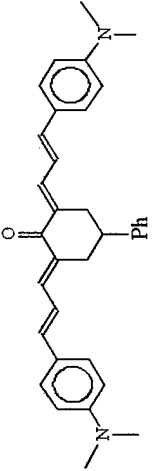
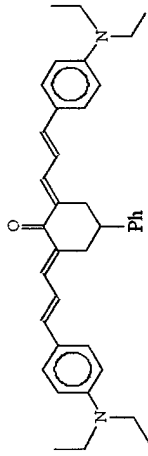
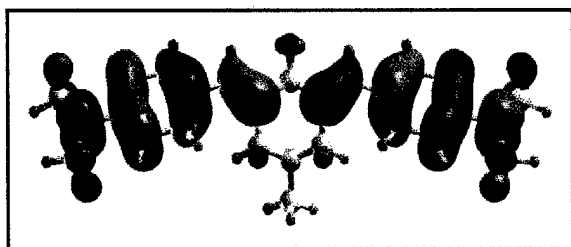
Number	Structure	μ , D (HF)	E_h kJ/ mol	Linear transmit- tance (1 cm cell)	Molecular cross- section of TPA $\sigma'_2 \times$ 10^{-50} [cm ⁴ s photon ⁻¹ molecule ⁻¹]	Calculated TPA cross section $\sigma_2 \times$ 10^{-50} [cm ⁴ s photon ⁻¹ molecule ⁻¹]
						
3M				0.92	520±10 135±30	208(343)(1.63) 239 (394)(2.17)
3N				0.90	2470±70 635±160	595 (981)(1.48) 358 (590)(2.04)

Table 2 continued. Cyclohexanone derivatives (series II)

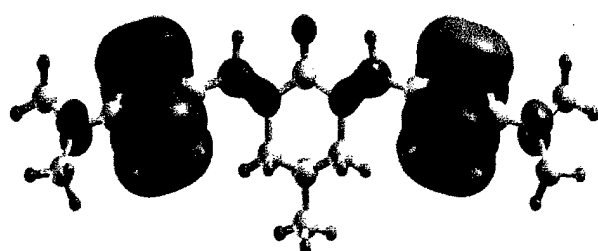
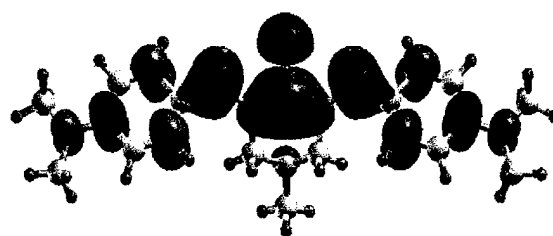
Number	Structure	μ , D (HF)	E_h kJ/ mol	Linear transmit- tance (1 cm cell)	Molecular cross- section of TPA $\sigma'_2 \times$ 10^{-50} [cm ⁴ s photon ⁻¹ molecule ⁻¹]	Calculated TPA cross section $\sigma_2 \times$ 10^{-50} [cm ⁴ s photon ⁻¹ molecule ⁻¹]
3P				0.87	2600±200 675±200	660 (1089)(1.47) 385 (635)(2.03)

HOMO

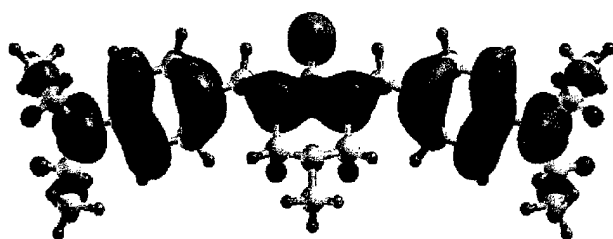
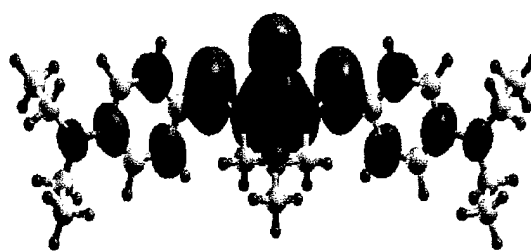
LUMO



Compound 3c, ground state



Compound 3c, 4-th excited state



Compound 3a, ground state

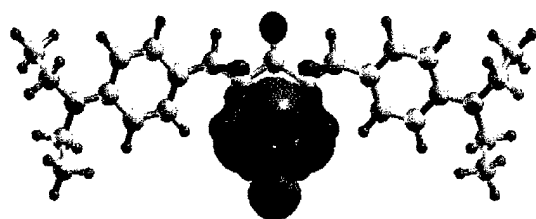
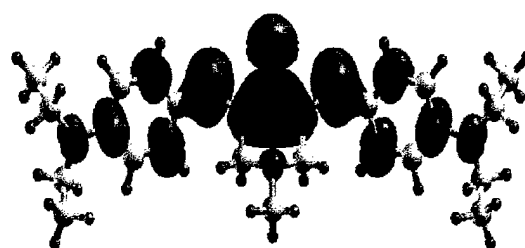
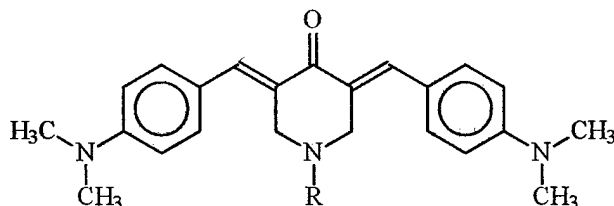
Compound 3a, 10th excited state

Fig. 1. HOMO and LUMO orbitals in molecules 3c and 2a.

2. Synthesis of piperidone and cyclohexanone derivatives with high two-photon activity and high solubility

In many cases application of TPA materials depends on material concentration in particular media (solvent or polymer matrix). Most of materials described above (series I and II) have pretty low solubility. To increase solubility of this series of materials we started synthesis of compounds with different substituents (see scheme below)

n



	R	MM, g·mol ⁻¹
c1	$\text{CH}_3\text{CH}_2\text{O}-\overset{\textstyle }{\text{C}}=\text{O}$	433.54
c2	$\text{H}_3\text{C}-\overset{\textstyle }{\text{C}}=\text{O}$	403
c3	$\text{CF}_3\text{CH}_2\text{O}-\overset{\textstyle }{\text{P}}=\text{O}$ $\text{CF}_3\text{CH}_2\text{O}$	605.51
c4	$\text{PhO}-\overset{\textstyle }{\text{P}}=\text{O}$ OPh	593

For compounds with P-organic substituents at N atom (**c3** and **c4**) solubility grow significantly that make them prospective for potentials applications including optical limiting and bio-sensing.

We measured one-photon absorption and fluorescence characteristics of compounds **c1-c4**, which is presented in Table 3.

Table 3. Positions of absorption and emission picks for studied compounds

Compound	λ_{ex} , nm	λ_{em} , nm
c1	287.0	398.0/533.0
	449.0	533.0
c2	284.0	355.0/537.0
	452.0	537.0
c3	281.0	400.0/536.0
	458.0	536.0
c4	277.0	400.0/523.0
	454.0	529.0

For compounds **c1** and **c3** structure was supported by single crystal X-ray analysis. The X-ray diffraction experiments were carried out using SMART 1000 CCD diffractometer at 293K [$\lambda(\text{MoK}\alpha) = 0.71073 \text{ \AA}$, ω scans with 0.3° step and 20 s per frame exposure]. The parameters of data collection and crystal refinement for structures **c1** and **c3** are given in Table 4.

Table 4. Crystal data on compounds **c1** and **c3**

	c1	c3
Formula	C ₂₆ H ₃₁ N ₃ O ₃	C ₂₇ H ₃₀ F ₆ N ₃ O ₄ P
M _r	433.54	605.51
Crystal system	Triclinic	Triclinic
Space group	P-1	P-1
a(Å)	9.295(3)	9.4914(19)
b(Å)	11.174(3)	9.6298(19)
c(Å)	11.531(3)	17.836(4)
$\alpha(^{\circ})$	97.162(6)	92.135(4)
$\beta(^{\circ})$	105.505(5)	98.602(4)
$\gamma(^{\circ})$	98.308(6)	119.344(4)
V (Å ³)	1125.2(5)	1393.4(5)
Z	2	2
D _c (g cm ⁻³)	1.280	1.443
μ (mm ⁻¹)	0.084	0.178
F(000)	464	628
T (K)	293(2)	293(2)
R1 [F > 4 σ (F)]	0.0646	0.0747

In both compounds studied (Figures 2 and 3) substituents at nitrogen atom are in axial position.

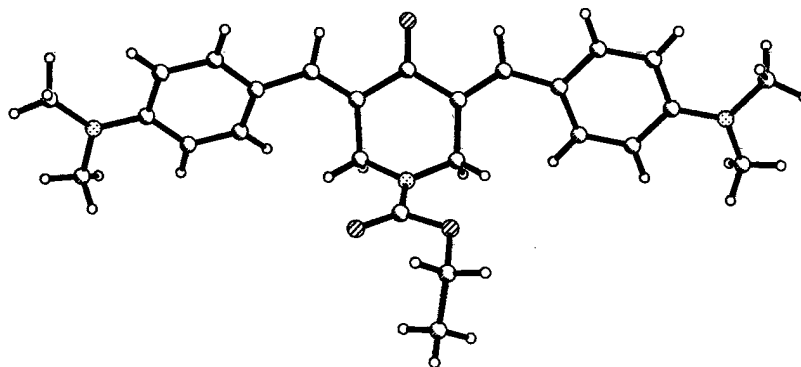


Fig. 2. Structure of molecule **c1** in crystal.

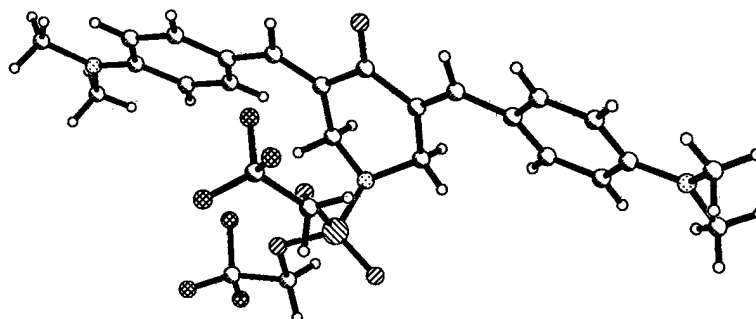
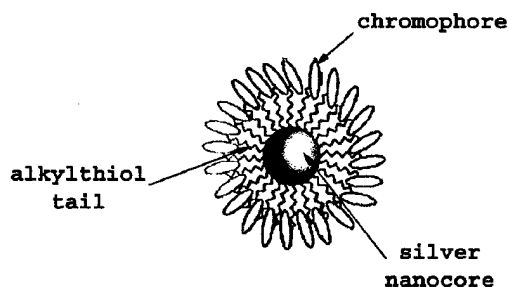


Fig. 3. Structure of molecule **c3** in crystal.

Incorporation of substituent at N atom was also useful for development of synthetic route for creation of chromophore-bearing surfactants (see Section 3).

3. Synthesis of surfactants for coating of nano-particles

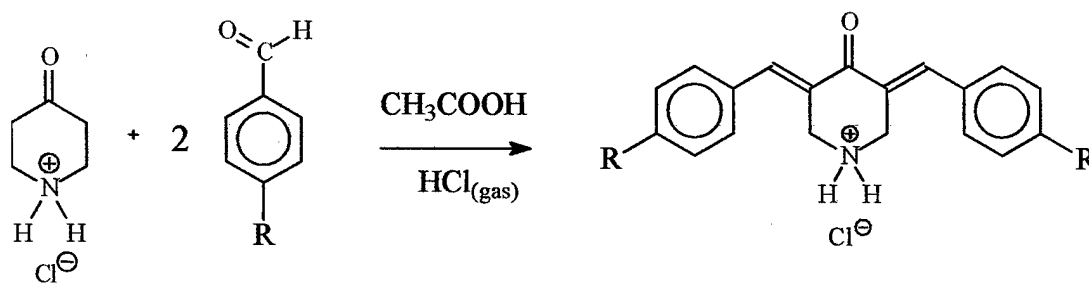
At present we are working on synthesis of metal coated nanoparticles with chromophores that may effect in significant enhancement of two-photon absorption cross-section.



Synthetic procedure to obtain long-tail chromophores that might be used in coating of metal nanoparticles is presented below.

4. Synthesis of 3,5-bis(Benzylidene)-4-piperidone hydrochloride

The general reaction for synthesis of 3,5-(Benzylidene)-4-piperidone hydrochloride para-derivatives is the next:



Where $R = -H, -N(CH_3)_2, -N(CH_2H_3)_2, -OCH_3$

The procedure was common for all synthesis. The first step was mixing 0.01 mol of 4-piperidone hydrochloride with 30 mL of glacial acetic acid. Then 0.206 mols of appropriate benzaldehyde was added to the suspension (benzaldehyde was taken in a slight excess toward 4-piperidone). After that the mixture was treated with dry hydrogen chloride gas for 30 minutes (~2-3 bubbles per second), at this step mixture became clear (4-piperidone and benzaldehyde dissolved in acetic acid) and then lived for 24 hours at room temperature to complete reaction under stirring. After reaction was completed the product was filtered and washed with ethanol. Then product was dried under open air.

Reaction load: mass of 4-piperidone hydrochloride (M.M. = 153.61 g/mol) was 1.56 grams, volume of benzaldehyde (M.M. = 106 g/mol, $d = 1.044 \text{ g/cm}^3$) was 2.9 mL. Compounds were purchased from Aldrich and used without any purification.

Precipitate formation took about 4 hours. After product was filtrated, washed with ethanol and dried a yellow powder was obtained (mass = 1.511 grams). Then pH of the filtrate was made ~ 6 (NaHCO_3 and potassium hydroxide were used), precipitated substance was filtrated and washed. Dry powder had pale yellow color (mass = 0.476 grams). Thus, total reaction yield is equal to 63%.

Measured melting points were 241°C for the first fraction, 240°C for recrystallized from 95% ethanol first fraction. Compound melted with decomposition. Second fraction didn't melt up to 300°C .

As NMR solvent a mixture of unisol and tiny amount of DMSO-d_6 (to increase solubility) was used for both fractions.

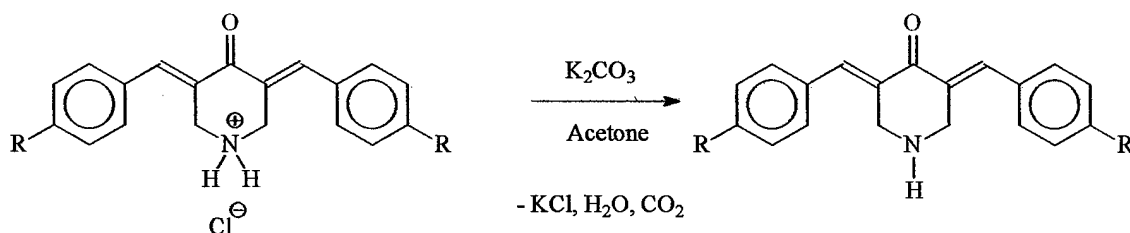
First fraction: $^1\text{H-NMR}$: δ (ppm) 9.76 (s, 2H), 7.94 (s, 2H), 7.5 (t, 10H), 4.52 (s, 8H). $^{13}\text{C-NMR}$: δ (ppm) 181.87, 139.38, 133.40, 130.07, 129.71, 128.59, 127.26, 43.89.

Second fraction: $^1\text{H-NMR}$: δ (ppm) 10.11 (s, 1H), 7.90 (s, 2H), 7.5 (t, 10H), 4.51 (s, 2H). $^{13}\text{C-NMR}$: δ (ppm) 181.70, 139.83, 133.17, 129.88, 129.69, 128.51, 126.73, 43.88.

5. Synthesis of 3,5-bis(Benzylidene)-4-piperidone

General procedure for free base preparation was as follows. To the boiling solution of the salt in acetone (about 30 mL) saturated aqueous potassium carbonate solution was added (about 30 mL). The mixture was stirred at reflux for 2-3 hours. On cooling distilled water was added which made the free base to precipitate. Then it was collected by filtration, washed by DI water and dried on open air. Free bases were purified by recrystallization from the appropriate solvents.

The general reaction for synthesis of 3,5-(Benzylidene)-4-piperidone para-derivatives is the next:



Where R = $-\text{H}$, $-\text{N}(\text{CH}_3)_2$, $-\text{N}(\text{CH}_2\text{H}_3)_2$, $-\text{OCH}_3$

Reaction load: mass of 3,5-bis(Benzylidene)-4-piperidone hydrochloride was about 1.2 g, volumes of acetone and saturated potassium carbonate solutions were 30 mL of each.

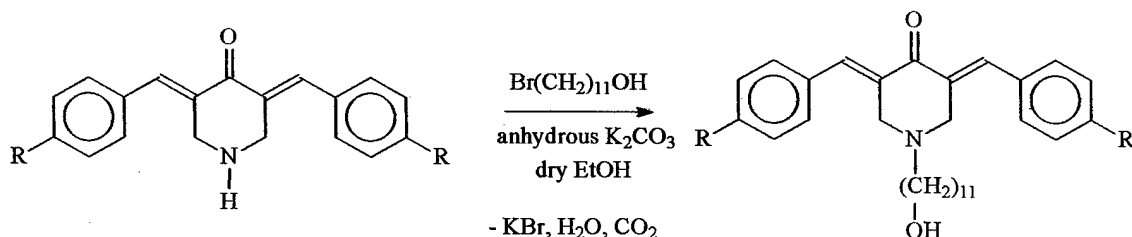
After reaction took place the reaction mixture was cooled down and distilled water was added. The precipitate was collected, washed with DI water and dried. The free base was purified by recrystallization from ethanol. As a result a yellow glitter crystals were obtained with the mass of 0.90 g (yield 85%). Crystals melted at 178 – 179 °C without decomposition. As NMR solvent DMSO- d_6 was used.

^1H -NMR: δ (ppm) 7.59 (s, 2H), 7.47 (m, 10H), 3.99 (s, 4H). ^{13}C -NMR: δ (ppm) 187.69, 136.03, 134.90, 133.72, 130.42, 129.02, 128.65, 47.57.

If to compare ^1H -NMR spectrum of the salt and of free base one can see that there is no peak from amino proton on the second spectrum, also in case of free base peak from methylene protons shifted by 0.5 ppm to lower values.

6. Synthesis of 11-*N*-[3,5-bis(Benzylidene)-4-piperidone]undecan-1-ol

The procedure of *N*-alkylation reaction was general for all synthesis for the case of 11-bromoundecanol.



Where R = -H, -N(CH₃)₂, -N(CH₂H₃)₂, -OCH₃

The appropriate free base (0.002 mol) was dissolved in ethyl alcohol (15 mL), which was dried over molecular sieves prior to the reaction. To that mixture 0.003 mol of 11-bromoundecanol, 0.0025 mol of K₂CO₃ and extra 15 mL of dry ethanol were added. The reaction mixture was brought to boiling and left under reflux for 1.5 weeks. The reaction was monitored by TLC.

After solvent was evaporated (rotevap) the reaction mixture was dissolved in methylene chloride, than water was added and organic layer was separated. The water layer was washed 2-3 times with CH₂Cl₂. The combined organic layers were dried over anhydrous MgSO₄. After removing the volatiles the product was purified by column chromatography on silica 60 in appropriate solvent.

7. Synthesis of 3,5-bis(4-Dimethylaminobenzylidene)-4-piperidone hydrochloride

Reaction load: mass of 4-piperidone hydrochloride (M.M. = 153.61 g/mol) was 1.56 grams, mass of p-dimethylaminobenzaldehyde (M.M. = 149 g/mol) was 3.545 grams. Compounds were purchased from Aldrich and used without further purification.

After the mixture was treated with dry HCl gas for 0.5 hours it became clear (piperidone and benz aldehyde dissolved in acetic acid). As 24 hours passed by the yellow suspension was obtained which was then filtered, washed with ethanol and dried. When ethyl alcohol got in touch with the product its color immediately changed from yellow to deep red. The product was recrystallized from hot methyl alcohol (small snowflake like crystals were obtained). After drying under open air mass of the compound was 2.744 grams (yield 69%). The product didn't melt up to 300 °C.

NMR solvent DMSO-d₆ (poorly soluble). ¹H-NMR: δ (ppm) 7.73 (s, 2H), 7.37 (d, 4H), 6.81 (d, 4H), 4.42 (s, 4H), 3.02 (s, 12H). Due to low solubility of the product in available NMR solvents it was impossible to get ¹³C spectrum.

8. Synthesis of 3,5-bis(4-Dimethylaminobenzylidene)-4-piperidone

The same procedure was used as for synthesis of 3,5-bis(Benzylidene)-4-piperidone. Reaction load: mass of 3,5-bis(4-Dimethylaminobenzylidene)-4-piperidone hydrochloride was about 1.2 g, volume of acetone and saturated potassium carbonate solution was 30 mL of each. After reaction completed and DI water was added orange precipitate was formed, which was collected by gravity filtration. After recrystallization from *N,N*-dimethylformamide 1.58 g of the product were collected. While measuring melting point crystals changed color to dark red at 190 °C, as temperature increased further the compound started to decompose and at 210 °C all crystals were black. Up to 250 °C no changes observed.

¹H-NMR (CDCl₃): δ (ppm) 7.76 (s, 2H), 7.35 (d, 4H), 6.71 (d, 4H), 4.17 (s, 4H), 3.03 (s, 12H). ¹³C-NMR (CDCl₃): δ (ppm) 187.60, 150.61, 136.11, 132.62, 131.19, 123.39, 111.68, 48.36, 40.10.

9. Conclusions and recommendations

Computational results on TPA active molecules are at present on stage of analysis of results and writing of corresponding publication.

The same situation is with synthesized derivatives with elevated solubility. At present we are discussing obtained results and preparing corresponding publication.

Chromophore-bearing surfactants for coating of silver nanoparticles with elevated TPA activity have been synthesized. Now we plan to use them for synthesis of nanoparticles with enchanted TPA activity. This part of the project is still in progress.

References for Part 1

1. A. Masunov, S. Tretiak. *J. Phys. Chem.*, 2004, *B*, **108** (3), 899 –907.

Part 2

Studies of Photosensitivity, Optical Limiting, Device Fabrication, and Characterization

1. Introduction

It is well known that fullerene C_{60} in various liquid solutions and solid matrices exhibits remarkable nonlinear optical properties such as optical limiting at relatively low threshold energy levels of incoming laser radiation.¹⁻³ It is also well known that adding some compounds to fullerene, such as those with amino-groups, can bring up additional desirable features including enhanced electro-conductivity, solubility in some solvents, formation of thin films, etc.⁴⁻⁵ Organic substance 2-cyclooctylamino-5-nitropyridine (COANP) is a typical representative of such amino-compounds.⁶⁻⁹ It is also a prominent electro-optic organic material¹⁰⁻¹² with noncentrosymmetric molecules¹³ (Fig.1a) that have a large dipole moment due to transfer of electron cloud from donor NH group to acceptor NO_2 group.¹⁴ Molecules of COANP can readily pack into noncentrosymmetric crystalline structure.¹⁵ It is also possible to bring COANP to a glass-like amorphous phase in a form of thin film with sufficiently good optical quality.^{16, 17} The films of such sort could work as solid matrices for fullerene thus making up solid-state optical limiters.

However, there is always a risk of getting the properties of fullerene significantly changed in unpredictable direction or even corrupted due to chemical interaction with an additive.¹⁸ One of the possibilities here is the formation of covalent bonding between fullerene and the amino-group of COANP similar to that shown in Fig. 1b. There have been a number of studies where this bonding was identified as being responsible for attaching organic molecules to fullerenes.^{4,5,19} There is also a possibility that fullerene, being a good electron pair acceptors (Lewis acid), can form charge-transfer complexes with COANP as an electron donating amine (Ref. 19, p. 62). In this paper we analyze the occurrence of such covalent bonding or complex formation using the dynamics of vibrational spectra of the solutions of fullerene with COANP in the IR region. Additionally, we used optical spectroscopy in visible region and the analysis of optical

limiting to look for a change of optical properties of fullerene due to the presence of COANP. In Section 2 we explain the experimental approach and the results of the FTIR spectroscopy. Section 3 describes the results of optical spectroscopy in visible region. Section 4 focuses on the optical limiting experiments and is followed up by the conclusions.

Organic materials with two-photon absorption and two-photon excited fluorescence can be also used for optical limiting. An ideal optical limiter should fulfill the following conditions: (1) complete transmission at low incident intensity, (2) wide spectral coverage, (3) fast operation (response time of the order of 10^{-9} s or less), and (4) high pulsed energy suppression.²⁰ The combinations of these requirements place severe restrictions on materials, which must respond quickly, and provide protection from a variety of laser sources. There are many ways of achieving optical limiting effects including the use of nonlinear optical absorbers,^{21,22} thermal defocusing,²³ frustrated total internal reflection,^{5 24} etc. The advantage of an optical limiter based on two-photon absorbing material is that its response (10^{-12} s or less)^{21,22} is fast enough to block short pulse laser radiation. Additionally, there is a need for multi-photon fluorescent markers in bio-medical applications. The newly synthesized derivatives of cyclohexanone/piperidone demonstrate both, strong two-photon absorption (TPA) and two-photon excited fluorescence (TPEF) and thus can be potentially useful for optical limiting and fluorescent labeling. By coincidence, similar derivatives of piperidone have been recently reported by Dimmock et al. as strong anticancer agents.²⁵ If fluorescent labeling and anticancer action can be combined in a single compound, it opens new avenues for more efficient medical diagnostics and treatment of cancer. This is an additional important reason for detailed study of the two-photon processes in derivatives of cyclohexanone and piperidone. The main focus is on how the two-photon absorption and fluorescence relate to the molecular structure of the compounds. This could point to the direction of synthesis of the most efficient two-photon absorbers and fluorophores among these materials.

2. Optical limiting in mixtures of fullerene C₆₀ with COANP

2.1. FTIR spectroscopy

A powder of fullerene C₆₀ of 99.5% purity was obtained from Alfa Aesar. COANP was synthesized and purified at the New Mexico Highlands University.

Tetrachlormethane (CCl₄) and carbon disulfide (CS₂) were chosen as solvents for fullerene with the COANP additive. These solvents have relatively low number of intense vibrational absorption bands in the region, where the absorption peaks of fullerene/COANP could be expected. Measurements were performed with FTIR spectrophotometers 2000 GS-IR from Perkin-Elmer and Tensor 27 from Bruker in the 10- μ m thick cuvette with KBr and NaCl windows. In order to avoid possible errors due to interference effects we recorded the transmission spectra of solutions with various concentrations of COANP (4, 7, 20 and 60 mg/ml) and related to the vibrational spectrum of COANP only those bands, which have the intensity growing with the concentration.

Fig. 2 shows the transmission spectra of the solution of COANP in CS₂ in region 500 through 1400 cm⁻¹ and in CCl₄ in region 1400 through 3700 cm⁻¹. These spectral regions match the windows of transparency of solvents CS₂ and CCl₄, respectively. The observed absorption bands are summarized in Table 1.

Previously the vibrational spectrum of COANP has been studied in Ref. 26 with the use of crystalline plates and powders. The minimum thickness of the plates used for transmission measurements was limited by the mechanical strength of the crystals and could not be less than 50 microns. At such thickness, the plates were practically opaque in a substantial part of the spectrum. Because of that the authors also used tablets of KBr powder mixed with the powder of COANP. Their data on the vibrational spectrum are presented in Table 1 for comparison. The energies of the spectrum are referred to certain types of molecular vibrations.

We also measured the transmission spectra of COANP in solid phase: a thin layer obtained by deposition from a solution poured on a substrate made of polyethylene (IR-card) and on AgCl window and subsequently dried. The data is also presented in Table 1. As can be seen from Table 1, the energies of the absorption bands of COANP in solid phase obtained in our experiments are in good agreement with those of Ref. 26. This

served as an additional indication that we chose correct experimental arrangements and approaches.

With the experimental data obtained, we could trace the effect of transition of COANP from solution to solid phase on its absorption. This can be most explicitly observed in the region between 3330 and 3430 cm^{-1} (Fig. 3a). A detailed structure of the absorption bands in this region is shown for two concentrations of COANP in CCl_4 (curves 1 and 2) and CS_2 (curves 3 and 4) and also for a thin layer of COANP deposited from solution on a polyethylene (PE) IR card (curve 5). In solutions COANP has two well defined absorption peaks. The peak at higher energy (to very right in curves 1 through 4 in Fig. 3a) can be attributed to the N-H stretching vibration.^{27, 28} The second peak 30 cm^{-1} below is due to intra-molecular hydrogen bonding that occurs in some secondary amines in non-polar solvents and gets stronger at higher concentrations.²⁹ When COANP undergoes crystallization, instead of two above-mentioned peaks we start getting the peak at 3341 cm^{-1} (curve 5 in Fig. 3a). The origin of this peak was discussed in Ref. 26. The authors believe that the peak is due to N-H...O stretch vibration resulting from hydrogen bonding between the amino-group and the oxygen of the nitro-group of adjacent molecules in the crystal. The likelihood of such bonding is supported by the data of the X-ray diffraction analysis of COANP crystals.¹⁵ It is worthwhile to mention that, when we let the solvent to evaporate at slow rate (for one/two days), we could observe a wide absorption band in the intermediate position between N-H bands and the H-O band as shown in Fig.3b. This is probably due to rather gradual increase of the strength hydrogen bonding between the molecules of COANP held up at relatively large distances from each other by the residual solvent. There is also some relatively weak peak both in solutions and in solid phase near 3383 cm^{-1} that we could not interpret.

COANP dissolves very well in many polar and non-polar solvents while the solubility of fullerene in the most of solvents is relatively poor. The concentration of C_{60} in CS_2 , solvent suitable for FTIR spectroscopy, at room temperature approaches 7.9 mg/ml (6.6×10^{-4} molar fraction).³⁰ Fig. 4 shows the absorption spectrum of C_{60} in carbon disulfide together with the spectrum of the solvent only. One can see clearly defined narrow lines at 527, 576, and 1182 cm^{-1} that are due to F_{1u} active vibrations.³¹ We also measured the absorption spectra of C_{60} and COANP at a maximum concentration of C_{60}

in the solution and two concentrations of COANP: 7 and 20 mg/ml (which corresponds to molar proportion of fullerene to COANP 1:2.6 and 1:7.3 respectively) as is shown in Fig. 5. Here, for comparison, we also present the spectra of pure solvent CS_2 and separate solutions of pure C_{60} and pure COANP in CS_2 . In order to investigate the changes in the absorption spectrum that is blocked by the absorption band of carbon disulfide (1400 through 1600 cm^{-1}) we prepared thin layers of COANP and C_{60} +COANP by means of casting solutions in toluene onto AgCl substrates and subsequent evaporation of the solvent. The corresponding absorption spectra are shown in Fig. 5c. It can be clearly seen in Fig. 5 that the absorption spectrum of C_{60} with COANP additive is a simple sum of the unchanged absorption bands of the individual components. FTIR spectrum thus shows no sign of formation of either covalent bonding or molecular complexes between COANP and fullerene C_{60} at the conditions described above.

2.2. Optical spectroscopy in visible region

We also performed optical spectroscopy of the solutions of fullerene C_{60} with COANP in visible region. We dissolved C_{60} in CS_2 at maximum concentration and then added COANP. In the obtained solutions the molar proportion of C_{60} to COANP varied from 1:0.5 to 1:200 respectively. The solutions were filtered with a 0.2-pore-size filter and poured into a 1-mm spectroscopic cell. The absorption spectra (Fig. 6) were taken with a Cary 3E UV-VIS spectrophotometer from Varian. It can be clearly seen that there was no noticeable change in the positions of the spectral peaks of the mixtures with respect to those of pure C_{60} (line 1) despite a substantial increase of the concentration of COANP (400 times). However the magnitude of absorption in mixtures is not exactly the sum of the magnitudes of absorption of the components. In Fig. 7 the absorption spectrum of the mixture of C_{60} and COANP at a proportion of 1:5 is shown compared against the spectra of pure CS_2 (line 2), COANP in CS_2 (line 2) at the same concentration as in the mixture, and C_{60} in CS_2 (at maximum concentration). In region 450 to 700 nm COANP does not have any significant optical absorption. However, the optical density of the mixture stands higher than that of pure fullerene by approximately 0.5 (in terms of optical density). This uniform increase of the optical density is probably due to additional

reflection and extinction of light in the sample. The latter one could be due to some scattering of light on newly formed aggregates of the molecules of the additive. The absorption of COANP falls into a short-wavelength region starting from 425 nm and below. Fig. 8 shows that the growth of optical density near the peak at 600 nm (typical for C_{60}) becomes saturated when the molar proportion of COANP reaches 20 and higher while the growth of optical density at 434 and 452 nm, where the major contribution comes from COANP, keeps growing exponent-like. This is again more likely due to light scattering on COANP aggregates. Mixing COANP with fullerene solution at high molar proportions (1:20 and above) leads to high concentrations of the additive: from approximately one molecule of COANP per 80 molecules of solvent at a proportion of 1:20 to one molecule per 8 molecules of solvent at a proportion 1:200. Despite very good solubility of COANP, the probability of aggregation of its molecules could become significant. The fact that the optical density of the mixture is not a simple sum of the optical densities of the components thus can serve as an indication of aggregation of the molecules of the components at high concentrations. No change in the absorption band structure, which might be associated with chemical interaction C_{60} – COANP, was detected.

2.3. Optical limiting

Fullerene C_{60} in various solutions is known as a good optical limiting substance that reduces its transmittance in response to the high power laser radiation. The mechanism of optical limiting in fullerenes is mostly due to opening an additional channel of absorption through a transition from the first to the second triplet state.³² We studied optical limiting in solutions of fullerene/COANP in search for some additional signs of interaction between fullerene and the additive that can possibly go unchecked by optical spectroscopy. The experimental setup similar to that described in Ref. 33 is presented in Fig. 9. A frequency-doubled Nd:YAG laser (Antares 76s from Coherent in Q-switched operational mode) generates 180-ns pulses of green light (532 nm) with 5-Hz repetition rate. The laser beam passes through a variable attenuator made of two Glan-Thompson polarizers (one is fixed, another is mounted on a dial). After passing the

attenuator, the beam is focused by a lens in a 1-mm-thick cuvette with the sample solution. The cuvette is mounted on a translational stage in order to adjust its position precisely in the focus of the lens. The criterion for choosing the focal distance of the lens is based on the condition that the so-called Rayleigh range z_R , the distance at which a focused Gaussian beam propagates without significant divergence,³⁴ must be greater than the thickness of the cuvette d :

$$z_R = \pi w_0^2 / \lambda > d, \quad (1)$$

where λ is the wavelength of the laser radiation; w_0 is the beam waist in the focal point determined as

$$w_0 = (2\lambda/\pi)(F/D), \quad (2)$$

where F is the focal distance of the lens, D is the diameter of the beam before passing through the lens. For $\lambda \approx 532$ nm and $d = 1$ mm Eqs. (1) and (2) give us

$$F/D > 122 \quad (3)$$

Under this condition the diameter of the incident beam can be considered constant along its path in the cuvette. In our case diameter of the beam $D \approx 1.2$ mm. So the focal distance of the lens had to be $F > 146$ mm. We chose the lens with focal distance 150 mm.

The beam after the cuvette is collected by a focusing lens in the face of a liquid light guide that transmits light to a photo-multiplying tube (PMT). On its way from the output face of the light guide to PMT the light beam is focused and reduced in intensity by a neutral density filter with an optical density (OD) of 5.0. This is done for the purpose of keeping the intensity of incoming light within the linear operational range of PMT or, in other words, to exclude the effect of the nonlinearity of PMT on the experimental data describing nonlinear transmittance of the sample solutions. PMT is powered by a high-voltage power supply. The signal from PMT proportional to the intensity of the incoming light is sent to a digital oscilloscope.

The setup was used to measure the transmittance of the sample solutions in the following way. Initially, the cuvette with a solution was removed and the amplitude of the incoming laser pulses $I_{in}^{(k)}$ was measured with the oscilloscope with regard to certain fixed angular positions $\theta^{(k)}$ of the dial of the attenuator. Then the cuvette was replaced and the amplitude of the laser pulses passing through the cuvette $I_{out}^{(k)}$ was measured

exactly at the same angular positions of the dial $\theta^{(k)}$ as in the case without the cuvette. The values of the transmittance $T^{(k)}$ were calculated as $T^{(k)} = I_{out}^{(k)} / I_{in}^{(k)}$ and plotted versus $I_{in}^{(k)}$.

Fig. 10 shows the normalized transmittance versus fluence for the solutions of fullerene C_{60} and COANP in CS_2 at various molar proportions of C_{60} to COANP together with transmittance of pure COANP dissolved in CS_2 and pure solvent. The concentration of fullerene was kept at its maximum level. The concentration of the solution of pure COANP in CS_2 was such that, if C_{60} would be added at maximum concentration, the molar proportion of C_{60} to COANP would be 1:100. One can see that for all the solutions containing fullerene optical limiting starts at the same threshold level (marked up by a vertical line) and after that the transmittance drops down at the same rate (within the limits given by the experimental error). The concentration of COANP, which varies from zero to 50 molecules of COANP per one molecule of C_{60} , turns out to be insignificant as far as optical limiting is concerned. Optical limiting of pure COANP is much weaker than that of the fullerene solutions (dataset 7 in Fig.10). The optical limiting in pure solvent is negligible.

3. Optical limiting and two-photon excited fluorescence in derivatives of cyclohexanone and piperidone

3.1. Materials

Two-photon absorbers studied in this work belong to the group of cyclohexanone/piperidone derivatives. They were synthesized and analyzed at the New Mexico Highlands University. The generalized molecular structure of the compounds is presented in Fig. 11. All the compounds have symmetric molecules of the general structure $D-\pi-A-\pi-D$, where D stands for the electron donor (electro-positive fragment), π - stands for a bond by means of conjugated π -electrons ($-C=$ or $-C=C-C=$ bridge), and A stands for electron acceptor (electro-negative fragment). In case of cyclohexanone derivative, the central core is electro-negative cyclohexanone, where oxygen is attached to carbon on one end and phenyl group (the monovalent group $-C_6H_5$, derived from benzene) is attached to carbon on another end of the ring. In case of piperidone

derivative, the central core of the molecule is electro-negative piperidone, a six-member ring with oxygen attached to carbon on one end and nitrogen atom on another end with methyl group ($-\text{CH}_3$) attached. All the compounds, except one, have benzene rings attached on two sides of the core through a bridge $-\text{C}=$ or $-\text{C}=\text{C}-\text{C}=$ with conjugated π -electrons. A distinct feature of each molecule is pendant electro-positive groups attached to benzene rings on both sides of the molecule. There are four types of pendant groups: (a) $-\text{N}(\text{CH}_3)_2$, (b) $-\text{N}(\text{C}_2\text{H}_5)_2$, (c) $-\text{OCH}_3$, and (d) ferrocene. The last group is the weakest donor of electrons (slightly electro-positive). The correspondence between the chemical structure and the designation numbers given to the compounds at the New Mexico Highlands University is presented in Table 2.

All the compounds are well soluble in most conventional organic solvents, including methyl alcohol and chloroform. There is a shift of the peak in optical single photon absorption spectra of the solutions in the visible region due to solvent. The compounds were dissolved in chloroform at concentrations of 0.675 mM/L (for single-photon optical absorption spectroscopy), 5 mM/L (for single-photon fluorescence spectroscopy with pumping provided by a mercury arc UV lamp and pulsed lasers in visible and UV region), and 100 mM/L for TPA measurements and TPEF spectroscopy with an infrared pulsed dye laser. As will be shown below, all the compounds have strong single photon absorption in the region between 2.25 and 3.5 eV. Each compound has exhibited shelf life of more than six months in solution being stored in a dark bottle at room temperature.

3.2. Experiment

The experimental setup for characterization of two-photon compounds is shown in Fig. 12. Measurements of TPA were done with a tunable IR dye laser PDL-2 from Quanta Ray pumped by a frequency doubled Q-switched Nd:YAG laser DCR-2A from Quanta Ray (9-ns pulse duration, 10-Hz pulse repetition rate). Laser dye LDS-867 from Exciton was used. TPA was measured at a wavelength of 876 nm where the power of the laser reached maximum. Radiation from the laser was reflected by a mirror and passed through a variable attenuator (a set of fixed and rotating Glen-Thompson polarizers). Then IR radiation was reflected by another mirror through a focusing lens onto a 10-mm

thick cuvette with sample solution of a two-photon compound. On its path through the solution, the IR radiation is absorbed in the solution. A power meter is used to measure the total power of the IR radiation transmitted through the sample.

Measurements of TPA could be significantly simplified if the size of the IR beam does not change substantially along its path through the cuvette. This puts a limitation on the focal distance of the focusing lens. The criteria for choosing the focal distance is based on the condition that the Rayleigh range z_R , the distance at which the focused Gaussian beam travels without significant divergence³⁵, must be greater than the thickness of the cuvette d :

$$z_R = \pi w_0^2 / \lambda > d, \quad (4)$$

where λ is the wavelength of the IR radiation; w_0 is the radius of the beam waist in the focal point determined by

$$w_0 = (2\lambda/\pi)(f/D), \quad (5)$$

where f is the focal distance of the lens; and D is the diameter of the beam before entering the lens. For $\lambda \approx 0.9 \mu\text{m}$ and $d = 1 \text{ cm}$ Equations (4) and (5) give

$$f/D > 95. \quad (6)$$

The diameter of the IR beam D was approximately 10 mm. According to condition in Eq. (6) the focal distance of the lens must be $f > 950 \text{ mm}$. However, the beam coming out of the laser was diverging. So, to account for such divergence, which is not included in Eqs. (4) through (6), a lens with a focal distance of $f = 150 \text{ mm}$ was chosen. This made the equivalent focal distance f_{eq} of the system laser – lens close to the criterion $f_{eq} \sim 950 \text{ mm}$. However, the condition in Eq. (6) is fully applicable to a Gaussian beam only. In our case, the laser produced a non-Gaussian beam with a complicated intensity profile and wavefront. Because of that, we could not fully maintain constant the size of the beam and, correspondingly, its intensity along the path through the cuvette.

We extracted the cross section of the TPA of the compounds from the transmission measurements in the following manner. Taking into account complicated actual intensity profile of the beam and its variation along the path through the cuvette, the approach suffers the lack of accuracy. However, it gives an estimate of the order of magnitude of TPA of the compounds and makes possible to compare them against each other and against the known materials that were characterized in the same experimental

arrangement. The intensity I of the beam passing through the solution of a two-photon absorbing compound is assumed constant across the beam. As a function of travel distance z , it is given by²¹

$$dI/dz + \alpha I + \beta I^2 = 0, \quad (7)$$

where α is the coefficient of linear (single-photon) absorption, β is the coefficient of TPA. If $\alpha z < 1$, the intensity at a certain distance z within the absorbing medium can be derived from Eq. (7) as

$$I(z) \approx I(0)\exp(-\alpha z)/[1 + \beta z I(0)], \quad (8)$$

where $I(0)$ is the intensity of the beam at the entry to the medium ($z = 0$). The transmittance T of the layer of the medium of thickness d can be found from Eq. (8) as

$$T[I(0)] = I(d)/I(0) = T_1/[1 + \beta d I(0)], \quad (9)$$

where $T_1 = \exp(-\alpha d)$ is the linear (single-photon) component of the transmittance. Eq. (9) can be rewritten as

$$I/T[I(0)] = (1/T_1)[\beta d I(0) + 1]. \quad (10)$$

Equation (7) explains the experimental procedure. Using the setup in Figure 2 with the sample removed, the input intensity $I(0)$ was measured with the power meter. Each experimental value of input intensity $I(0)_k$ corresponded to a certain angle of rotation of the dial of the variable laser attenuator θ_k . Next, the sample was replaced into the setup and the output intensity $I(d)$ was again measured with the power meter. Experimental values $I(d)_k$ corresponded to the same angles of rotation of the attenuator θ_k that were previously used to measure $I(0)_k$. Therefore, there was a direct correspondence between $I(d)_k$ and $I(0)_k$. Then, the values of the inverse transmissivity $(1/T)_k = I(0)_k/I(d)_k$ were calculated and plotted versus $I(0)_k$. A linear least mean square fit of the experimental plot, in accordance with Eq. (10), was performed. The two parameters of fitting were $1/T_1$ and βd . For the thickness of the cuvette $d = 10$ mm, the coefficient of TPA β was extracted from the second fitting parameter. The molecular cross-section of TPA (in terms of absorbed power) σ_2 was extracted from β using equation

$$\sigma_2 = \beta N_A C_M, \quad (11)$$

where N_A is the Avogadro number and C_M is the molar concentration of a two-photon compound in the solution. The molecular cross-section of TPA (in terms of the number of absorbed photons) σ_2' was calculated as

$$\sigma_2' = h\nu\sigma_2, \quad (12)$$

where $h\nu$ is the energy of the incident photons.

As was mentioned above, Eqs. (7) through (12) can be used only for estimate of the true cross-section of TPA. More precise evaluation would require usage of a rather complicated model, which accounts for the beam shape. A laser source with more predictable beam shape, such as Gaussian, would be preferable for this purpose. Additionally, it might be necessary to include in the model the temporal profile of the laser pulse if nonlinear absorption processes have characteristic times comparable or longer than the laser pulse duration. The response time of the true TPA process (usually, of the order of 10^{-12} s) was assumingly much shorter than the laser pulse duration (~ 9 ns). In fact, many authors emphasize that the cross-section of intrinsic TPA can only be measured with ultra-short (picosecond or femtosecond) laser pulses that exclude contribution to absorption of long-lived excited states.²⁰ In case of compound 4 the laser flash photolysis experiment with a nanosecond UV (355 nm) laser was conducted in order to check if there was any significant absorption through long-lived excited state (usually the triplet). The results of the experiment indicated that such absorption was very weak. The strong fluorescence was another indicator that the majority of molecules were relaxing before they get to the triplet state. This means that the approximation of the CW pumping (very long laser pulse) implicitly assumed in the model holds on at least for some of the compounds.

The setup shown in Fig. 12 was also used for measurements of the single-photon excited fluorescence (SPEF) and TPEF with pulsed laser sources. For SPEF two lasers were used: frequency doubled Q-switched Nd:YAG laser (DCR-11 from Quanta Ray, 532-nm wavelength, 9-ns pulse duration, 10-Hz pulse repetition rate), and pulsed UV nitrogen laser (Model VSL-337ND-S from ThermoOriel, 337-nm wavelength, ~ 4 -ns pulse duration, 10-Hz pulse repetition rate). Spectroscopy of TPEF was done with the same tunable IR dye laser that was used for TPA measurements. All the TPEF spectra were taken at 876 nm, the wavelength of maximum laser emission. The fluorescence

radiation from the sample was collected by a multi-mode optic fiber placed near the path of the exciting beam. The fiber was mounted on a platform with five degrees of freedom (three translational and two rotational). The position of the cleaved flat tip of the fiber was maneuvered with respect to the fluorescent region in order to collect most of the fluorescent light and the least exciting radiation. The light was then transmitted by the fiber to the entrance slit of a scanning monochromator MS257 from Oriel. A photomultiplier tube (PMT) was attached to the output slit of the monochromator. The output of the PMT was connected to a gated boxcar averager SR250 from SRS triggered by the laser. The signal from the averager, which was proportional to the intensity of fluorescent radiation, was routed to a computer running LabVIEW where the data was recorded and plotted. We also measured SPEF excited by continuous UV lamp (500-W mercury arc lamp Model 6285 from Oriel). In this case the light from the UV lamp was chopped with a mechanical chopper. The gated boxcar averager was replaced with a lock-in amplifier synchronized by the chopper.

3.3. Experimental results and discussion

3.3.1. Two-photon absorption

A typical experimental plot of the inverse transmissivity I/T versus intensity of IR radiation is presented in Fig. 13. Linear least mean square fitting of the experimental points produced the following parameters: linear transmittance, coefficient of nonlinear absorption, and the errors of fitting (taken as experimental errors). Their values are presented in Table 2 for all the compounds along with the molecular cross-section of TPA. The energy of IR photons was 1.43 eV (876-nm wavelength). As will be shown below, the double energy of the IR photon falls well in the single-photon absorption band of all the studied materials. For comparison, Table 2 presents the values for the TPA cross-section of some highly efficient two-photon absorbers known from the literature. It also contains the TPA cross-section of Rhodamine B (100 mM solution in chloroform) measured in experimental setup in Fig. 12 at the same conditions as that of materials 1 through 9. Some compounds, such as 2, 3, 4, and 5, have the TPA cross-section approximately three times greater than that of Rhodamine B, a well-known TPA material. A very efficient material BDBAS³⁶ has a TPA cross-section just 6 times greater than

compound 4. This is a clear indication, that the derivatives of cyclohexanone/piperidone have the potential of being used as efficient two-photon absorbers and optical limiters.

Experimental data in Table 2 can be used for finding relation between the chemical structure of the compounds and their cross-section of TPA. Compounds are grouped according to their pending donor fragments. First group is made of three compounds 1, 2, and 3 with pending group $R_1 = N(CH_3)_2$. It can be clearly seen that the central acceptor core, either cyclohexanone or piperidone, does not play a significant role in achieving high TPA. The length of the bridge made of conjugated π -electrons is the factor that contributes mostly to the TPA. Compounds 2 (derivative of piperidone) and 3 (derivative of cyclohexanone) with long conjugated π -electron C–C bridge have similar cross-section of TPA, which is more than four times greater than that of compound 1 (derivative of piperidone) with short conjugated π -electron bridge.

Similar trend can be observed for the group of compounds 4, 5, and 6 with pending donor group $R_1 = N(C_2H_5)_2$. Here compounds 5 (derivative of piperidone) and 6 (derivative of cyclohexanone) with long conjugated π -electron C–C bridge, have larger cross-section of TPA than compound 4 with short bridge. In fact, material 5 has the largest cross-section of TPA among all the studied compounds. The next group is made of compound 7 (derivative of cyclohexanone) and 8 (derivative of piperidone) with the same pending methoxy group $R_1 = OCH_3$. Despite the presence of long C–C bridge in both compounds, they have weak TPA, even comparing to short-bridge compounds 1 and 4 from previous groups. We believe that this is due to the fact that the methoxy group is a relatively weak donor of electrons comparing to previously discussed pendants $N(CH_3)_2$ and $N(C_2H_5)_2$. The results obtained for compound 9 support our hypothesis. It is a derivative of piperidone with short C–C bridge and ferrocene complex, very weak donor, as a pendant. Despite its very strong single-photon absorption (linear transmittance is almost twice as low as for the other compounds), compound 9 exhibits weak TPA. According to our findings, a hypothetical compound with large cross-section of TPA should have a long bridge made of conjugated π -electrons between the central acceptor core and the donor pending groups on both sides. The pending groups should be chosen from strong donors. The central core would be preferably cyclohexanone, since piperidone derivatives showed some tendency to light-induced transformation after being

exposed to intense UV radiation. It is worthwhile to mention that these results are in good agreement with early findings of Perry, Marder, and co-workers (see review in Ref. 20) who also considered molecular structure $D-\pi-A-\pi-D$ as having potentially high cross-section of TPA and application in optical limiters.

An additional test was conducted to verify whether the nonlinear optical absorption of the compounds is a true TPA process. The intensity of TPEF was measured and plotted as a function of the input intensity. A typical example of the experimental plot in log-log scale gives linear dependence as is shown in Fig. 14. The slope of the linear graph is approximately 1.5. This means that the power of TPEF (P_{TPEF}) depends on the power of IR radiation P_{IR} as

$$P_{TPEF} \sim P_{IR}^{3/2} \quad (13)$$

It has been shown in the literature³⁸ that this is exactly the dependence, which should be expected for a true TPA in a material illuminated by a focused IR beam that causes an onset of saturation of multi-photon absorption in its waist. Since the size of the laser beam varied along its path and the distribution of the intensity across the beam was complex with some sharp maxima in various locations where the saturation of TPA could occur, we believe the relation described by Eq. (13) can be applied to our case. The obtained result can thus be reasonably used as another evidence of the true, intrinsic, TPA in the investigated compounds.

Spectroscopy of TPA was performed for the compounds in the tuning range of the dye laser from 851 nm (1.46-eV photon energy) to 901 nm (1.38-eV photon energy). The experimental spectra are presented in Fig. 15. The spectra look relatively flat without any narrow and steep peaks. Those peaks usually appear when there are some intermediate states in the energy gap between states S_0 and S_1 that dramatically increase the efficiency of TPA comparing to less probable TPA through the virtual state. The absence of such peaks is a clear indication that the main mechanism of two-photon excitation of the cyclohexanone/piperidone derivatives is the one through a virtual state.

3.3.2. Single-photon and two-photon fluorescence

The spectroscopy of single-photon absorption of the compounds was performed using a UV-VIS spectrophotometer Cary 3E from Varian. Each solution had a

concentration of 0.675 mM/L and was placed in a 1-mm-thick spectroscopic quartz cell. Below the spectra of single-photon absorption are discussed together with the spectra of SPEF and TPEF.

The spectra of single photon absorption, SPEF and TPEF of the compounds are presented in Figs. 16 through 20. The relative intensity of SPEF and TPEF of the compounds is presented in Table 3. The discussion of the spectra will be given with regard to the chemical structure of the compounds. Three compounds with pending group $-N(CH_3)_2$ on both ends (1, and especially 2, and 3) have strikingly similar spectra of single-photon absorption and fluorescence. The band of single-photon absorption is located between 2.4 and 3.0 eV (the energy of 532-nm photon and the double energy of 876-nm photon are on the left and right edges of the band respectively). The absorption peak of the compounds is near 2.6 eV. The fluorescence spectra of all the compounds have two peaks and do not follow the conventional pattern of "mirror" image of the absorption spectrum. The positions of the peaks are almost the same for CW and pulsed single-photon pumping and TPEF. Some shift of the right (in energy scale) peaks is more likely due to re-absorption. As one can see, the right tail of the fluorescence spectrum slightly overlaps with the absorption band. So, re-absorption was quite possible, especially if the optic fiber used to collect fluorescent emission was at some small but poorly controlled distance from the region where the fluorescence was excited by the beam passing through solution. In case of compound 1 the left, less energetic peak, is relatively stronger for CW wide band pumping with the UV lamp. This left, less energetic peak is more likely due to the transition from triplet state T_1 to the ground state S_0 . Continuous pumping could provide sufficient time for the triplet state to be occupied through the intersystem crossing mechanism. This emission is relatively slow phosphorescence that is very weak for the pulsed SPEF and TPEF. In case of compounds 2 and 3 the left peak came up strong for the pulsed fluorescence. For compound 2 the right peak virtually diminishes at continuous pumping with the UV lamp while the material undergoes irreversible photochemical reaction, possibly polymerization. In terms of intensity of the SPEF and TPEF, compounds 2 and 3 stand close to each other, as can be seen from Table 3. The peak intensity of SPEF generated by the UV lamp is 4% and 1% for compound 2 and 3 respectively, as compared against that of Rhodamine 6G in

chloroform. For the pulsed pumping either with 532-nm visible or 337-nm UV laser the intensities of SPEF are greater and closer to each other: around 10%. This clearly indicates that at CW pumping with UV lamp radiationless transitions are significant and empty excited state S_1 before a strong fluorescence can occur. The TPEF of both compounds is relatively strong (with respect to Rhodamine B used as a reference) and close to 35%. In terms of SPEF and TPEF compound 1 is less efficient (1000 times weaker fluorescence for the UV lamp pumping). The conclusion can be derived here that the chemical structure of the core of the molecule does not matter too much in determining the fluorescence spectrum and its intensity, particularly for TPEF. What really matters is the pending group on both sides of the molecule, $-N(CH_3)_2$, and the length of the carbon bridge with conjugated π -electrons between the core and the ends.

Similar trend, though not so prominent, could be observed for compounds 4, 5, and 6. They have the same pending donor group $-N(C_2H_5)_2$ on both ends of their molecules. Compound 4 has piperidone core and short carbon bridges between donor and acceptor parts on each side. The absorption spectrum (Fig. 18) for compound 4 is shifted towards higher energies: the line of the UV laser is near the peak, and the band of the UV lamp completely covers the absorption spectrum. Fluorescent spectra always have right higher energy peak dominant. As was mentioned above, the laser flash photolysis showed no significant role of the long-lived triplet state in absorption. The absence of an intense low energy, left peak of fluorescence (phosphorescence) due to downward transition from the triplet state, especially at pulsed pumping, is in good agreement with this finding. The intensity of SPEF is not that strong: 0.14% of that of Rhodamine 6G for UV lamp, 0.8% for 532-nm, and 0.34% for 337-nm pumping. However, this material takes the lead in TPEF. In relative rating, its intensity of TPEF is 43.5% of that for Rhodamine B (see Table 3). Compounds 5 and 6 have different cores: piperidone and cyclohexanone respectively. There is a long carbon bridge between donor and acceptor parts on each side in both compounds. Compounds 5 and 6 differ more significantly from short-bridge compound 4 in terms of their spectra than materials 2, and 3 from 1. Their single-photon absorption spectra both have substantial UV tails (Fig. 19). The peak of absorption of compound 5 is shifted more towards lower energy than that of 6. Apparently, 532-nm and 337-nm photons are now falling well within the absorption band (for compound 5,

532-nm photon is close to the absorption peak). Both long-bridge compounds demonstrate two-peak fluorescent spectra, especially in case of SPEF. The band of fluorescence for the SPEF, and the TPEF, is located between 1.6 and 2.0 eV. The intensity of SPEF is higher for compound 6 (in case of UV pumping – 10 times higher, probably due to stronger absorption of UV photons). However, the intensity of TPEF is approximately 90% of that for material 4 for both compounds. Again, comparison of compounds 4, 5, and 6 reveals that the attachments and the length of the carbon bridge determines the spectrum features of the compounds rather than the structure of the core: piperidone or cyclohexanone.

Compounds 7 and 8 make up yet another group with different cores (cyclohexanone and piperidone for 7 and 8 respectively), but with the same attachment (methoxy group $-\text{OCH}_3$ in this case) and the same length of carbon bridge (long). Both compounds have linear absorption spectrum shifted towards the UV region with the 532-nm photon falling completely out of the absorption band (Fig. 20). However, their SPEF is relatively weak even for UV pumping, both CW and pulsed, and they demonstrate no significant TPEF. This result correlates with the fact that the methoxy attachments on both sides of the molecules of the compounds 7 and 8 are much weaker donors of electrons (electro-positive) than those in the previously discussed substances.

The last material studied was compound 9. It is a piperidone derivative with ferrocene attachments. Ferrocene is a weak donor. Compound 9 has its peak of absorption far in UV region (337-nm laser line is located near the peak). Despite its rather strong single-photon absorption, it did not demonstrate any significant fluorescence at all. This is one more confirmation of important role of the attachments and the length of the carbon bridge in the spectral features of the compounds.

There was one occasion when the structure of the molecular core played an important role in spectroscopy experiments. When the compounds 2 and 5 were pumped with the UV lamp for several seconds, this caused the solutions to change color from dark red to purple. That was accompanied by the drop of the left fluorescent peak in the SPEF spectrum as can be seen in Figs. 17 and 19. A remarkable feature of this process was that the change in color continued even after the UV radiation was turned off until all the solutions had turned purple. This clearly indicated that a photo-initiated chain reaction,

possibly polymerization, took place in the solutions. Both compounds have different attachments but the same piperidone core, which was probably the molecular fragment participating in photo-polymerization. The same piperidone core was also responsible for cytotoxicity of similar anticancer compounds.²⁵

Spectroscopy in relation with molecular structure clearly indicated that the best hypothetical derivative of cyclohexanone/piperidone in terms of the efficiency of TPEF would be the one that has attachments pending on both sides with strong donor (electro-positive) properties and long carbon bridge $-C=C-C=$, possibly even longer.

4. Conclusions and recommendations

Analysis of the dynamics of the IR spectra of the solutions of fullerene C_{60} with the COANP additive led us to the conclusion that the interactions between the molecules of the fullerene and the additive associated with covalent or hydrogen-like bonding practically do not occur at normal conditions. Additional experimental techniques, such as optical spectroscopy in visible region and optical limiting, also do not indicate any noticeable effect of COANP on the optical properties of fullerene, both linear and nonlinear. The practical significance of these findings is that COANP and possibly other similar compounds with amino-groups can be mixed at large concentrations with solutions of fullerene C_{60} without risk of corrupting its useful optical property of optical limiting. The resulting optical properties of the mixture, including that in the form of solid glass matrix made of COANP or similar compound, are simply summarized. This opens new way to a greater control of functional properties of fullerene preserving its remarkable feature of optical limiting.

Derivatives of cyclohexanone/piperidone have demonstrated a TPA cross-section of the order of $3000 \times 10^{-50} \text{ cm}^4/\text{s/photon}$ for pulsed nanosecond IR laser radiation. They compare well against materials known from the literature. Stronger TPA should be expected for more stable derivatives of cyclohexanone with long bridges made of conjugated π -electrons and strong donor pending groups. This makes them promising nonlinear optical absorbers and optical limiters. The important feature is that the energy is absorbed in the IR region, where the protection is needed for remote IR sensors and

night-vision systems. It is also important that substantial portion of the energy of the dissipated IR radiation is converted into fluorescence instead of heat that can damage the optical limiter. The two-photon excited fluorescence occurs in the visible spectral region. The most efficient TPEF material studied was compound 4 (piperidone derivative with $N(C_2H_5)_2$ pending group). Comparative study of the TPEF with regard to the chemical structure of the compounds suggested that the most efficient two-photon fluorophores would be those with structure $D-\pi-A-\pi-D$, where the pendant groups D have to be strong electron donors. The efficiency of TPEF is almost the same for both electron acceptor cores: cyclohexanone or piperidone.

Compounds with a piperidone core have a tendency to undergo a chain chemical reaction initiated by UV radiation. They are more reactive and thus more likely can create chemical bonding with bio-agents that must be necessary for using them as fluorescent markers in bio-imaging and medical diagnostics.

References for Part 2

1. Lee W. Tutt, Alan Kost, *Nature* **335**, (1992).
2. S. Couris, E.Koudoumas, A. A. Ruth, S. Leach, *J.Phys.* **B28**, 4537 (1995).
3. N.V. Kamanina, L.N. Kaporskii, B.V. Kotov, *Optics Communications* **152**, 280 (1998).
4. L. Dai, *J.M.S.-Rev. Macromol. Chem. Phys.* **39**, 273 (1999).
5. Yu. Chen, Zu-En Huang, Rui-Fang Cai and Bo-Cheng Yu, *Eur. Polym. J.* **34**, 137 (1998).
6. J. Hulliger, B. Brezina, M. Ehrensperger, *Journal of Crystal Growth*, **106**, 605 (1990).
7. K. Sutter, J. Huliger, P. Gunter, *Solid State Commun.* **74**, 867 (1990).
8. Hulliger, K. Sutter, Y. Schumacher, B. Brezina, V.A. Ivanshin, *Journal of Crystal Growth* **128**, 886 (1993).
9. Ch. Bosshard, K. Sutter, R. Schlessler, P.Gunter, *J. Opt. Soc. Am.* **10**, 867 (1993).
10. Ch. Bosshard, K. Sutter, P.Gunter, G. Chapuis, *J. Opt. Soc. Am.* **B6**, 721, 1989.
11. M. Eich, H. Looser, Do Y. Yoon, R. Twieg, G. Bjorklund, J. C Baumert, *J. Opt. Soc Am.* **B6**, 1590 (1989).

12. Leyderman, Y. Gui, *Optics. Lett.* **23**, 909 (1998).
13. P. Gunter, Ch. Bosshard, K. Sutter, H. Arend, G. Chapuis, R. J. Twieg, D. Dobrovolski, *Appl. Phys. Lett.* **50**, 486, 1986.
14. J. F. Nicoud, R. J. Twieg, in "*Nonlinear Optical Properties of Organic Molecules and Crystals*", eds. D. S. Chemla, J. Zyss (Academic Press, Inc., Orlando, 1987), p. 229.
15. M. Yu. Antipin, T. V. Timofeeva, R. O. Clark, V. N. Nesterov, F. M. Dolgushin, J. Wu, A. Leyderman, *J. Mater. Chem.* **11**, 351 (2001).
16. Shi-Xian Qu, Hairong Zheng, A. Barrientos, A. Leyderman, *Phys. Lett.* **A268**, 360 (2000).
17. A. Leyderman, Shi-Xian Qu, *Phys. Rev.* **E62**, 3293 (2000).
18. Yu. E. Biryulin, V. S. Vichnin, V. N. Zgonik, *Physica Tverdogo Tela* **42**, 188 (2000).
19. F. Wudl, A. Hirsh, K. S. Khemani, T. Suzuki, P.-M. Allemand, A. Koch, H. Eskert, G. Sradnov, H. M. Webb in *Fullerenes, - synthesis, properties and chemistry of large carbon clusters*, eds. G. S. Hammond, V. J. Kuck (American Chemical Society, Washington, 1992), p. 161.
20. C. W. Spangler, *Journal Mater. Chem.* **9**, 2013 (1999).
21. R. L. Sutherland, *Handbook of Nonlinear Optics* (Marcel Dekker, Inc., New York, 1996) p. 541.
22. E. W. Van Stryland, D. J. Hagan, T. Xia, and A. A. Said, *Application of nonlinear optics to passive optical limiting, in Nonlinear Optics of Organic Molecules and Polymers*, H. S. Nalwa and S. Miyata, eds. (CRC Press, Boca Raton, 1996) pp. 841-860.
23. B. L. Justus, Z. H. Kafafi, and A. L. Huston, *Opt. Lett.* **19**, 1603 (1993).
24. E. J. Sharp, G. L. Wood, R. R. Shurtz II, and J. L. W. Pohlmann, *Frustrated total internal reflection optical power limiter*, US Pat. 5561541 (1996).
25. J. R. Dimmock, M. P. Padmanilayam, R. N. Puthucode, A. J. Nazarali, N. L. Motaganahalli, G. A. Zello, J. W. Quail, E. O. Oloo, H. B. Kraatz, J. S. Prisciak, T. M. Allen, C. L. Santos, J. Balzarini, E. D. Clercq, and E. K. Manavathu, *J. Med. Chem.* **44**, 586 (2001).
26. J. Petzelt, J. Hrabovska, S. Kamba, I. Gregora, V. Vorlicek, K. Kokesova, Brezina, J. Hulliger, *Nonlinear optics* **7**, 7 (1994).

27. B. Smith, *Infrared spectral interpretation, A systematic approach*. (CRC Press, Boca Raton, 1999), p. 135.
28. M. Avram, Gh. Mateescu, *Infrared Spectroscopy. Application in Organic Chemistry*, (Wiley-Interscience, New York, 1972), p.317.
29. C.N.R. Rao, *Chemical Applications of Infrared Spectroscopy*, (Academic Press, New York, 1963), p. 248.
30. *Fullerenes (Chemistry, Physics and Technology)* eds. K. M. Kadish, R. S. Ruoff (A. John Wiley and Sons Inc. Publication, 2002). p. 53.
31. P. S. Eklund, P. Zhou, K.-A. Wang, G. Dresselhaus, M. S. Dresselhaus, *J. Phys. Chem. Solids* **53**, 1391 (1992).
32. J. W. Arbogast, A. P. Darmanyan, C.S. Foote, Y. Rubin, F.N. Diederich, M. M. Alvarez, S. J. Anz and R. L. Whetten, *J. Phys. Chem.* **95**, 11 (1991)
33. R.L. Sutherland, *Handbook of nonlinear optics* (Marcel Dekker, New York, 1996) p. 558
34. A. Yariv, *Quantum Electronics*, (John Wiley & sons, New York, 1989) p. 119.
35. A.E. Siegman, *Lasers* (University Science Books, Sausalito, California, 1986) p.669.
36. J.E. Ehrlich, X. L. Wu, I. Y. S. Lee, Z. Y. Hu, H. Rockel, S. R. Marder, and J. W. Perry, *Opt. Lett.* **24**, 1843 (1997).
37. G. S. He, G.C. Xu, P.N. Prasad, B.A. Reinhardt, J.C. Bhatt, and A.G. Dillard, *Opt. Lett.* **20**, 435 (1995).
38. S.H. Lin, Y. Fujimura, H. J. Neusser, and E. W. Schlag, *Multiphoton Spectroscopy of Molecule* (Academic Press, Inc., Orlando, Florida, 1984) pp. 90-97.

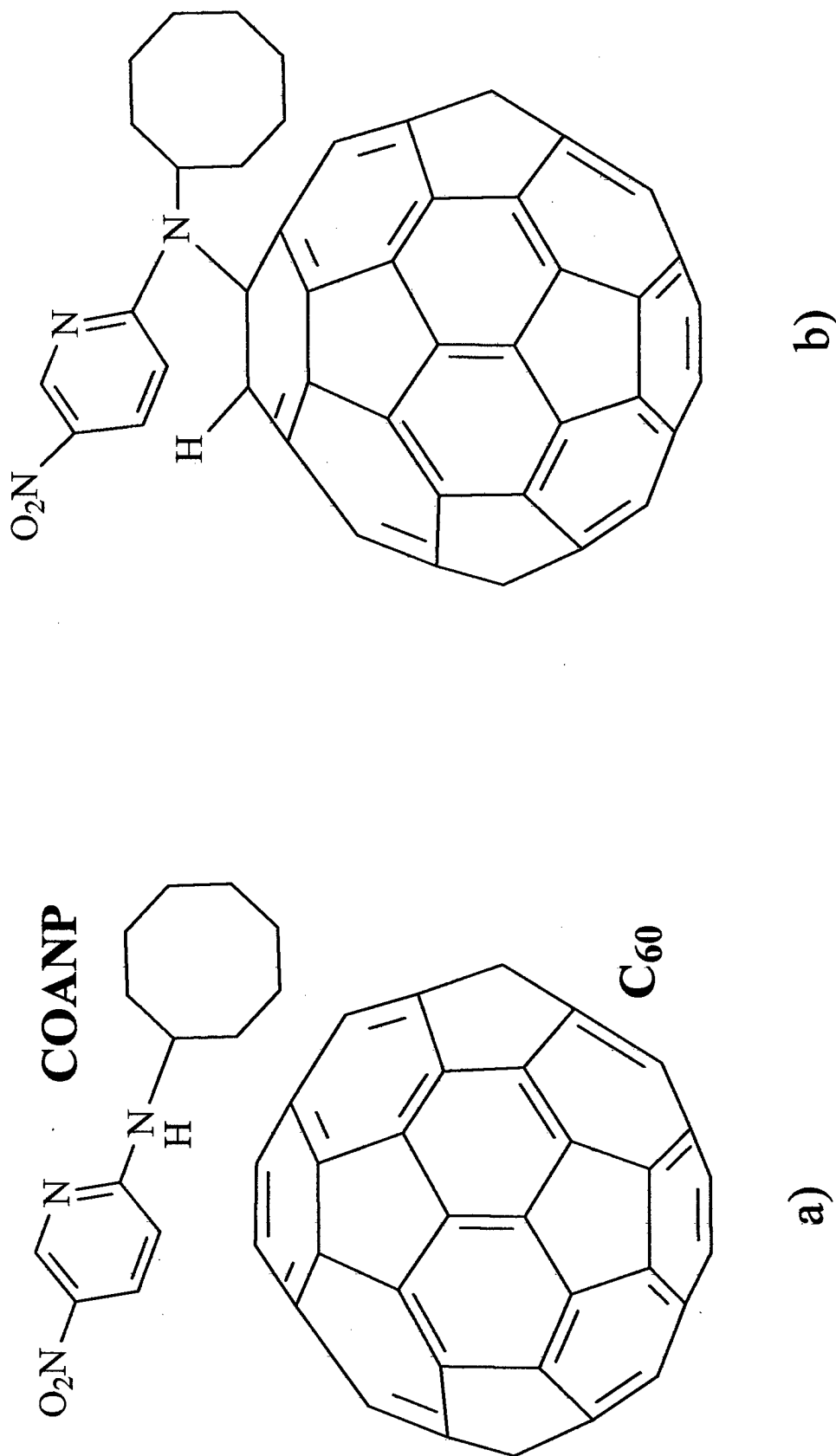


Fig. 1. Chemical structure of (a) the molecules of fullerene C₆₀ and 2-cyclooctylamino-5-nitropyridine (COANP) and (b) their hypothetical covalent bonding through the amino-group.

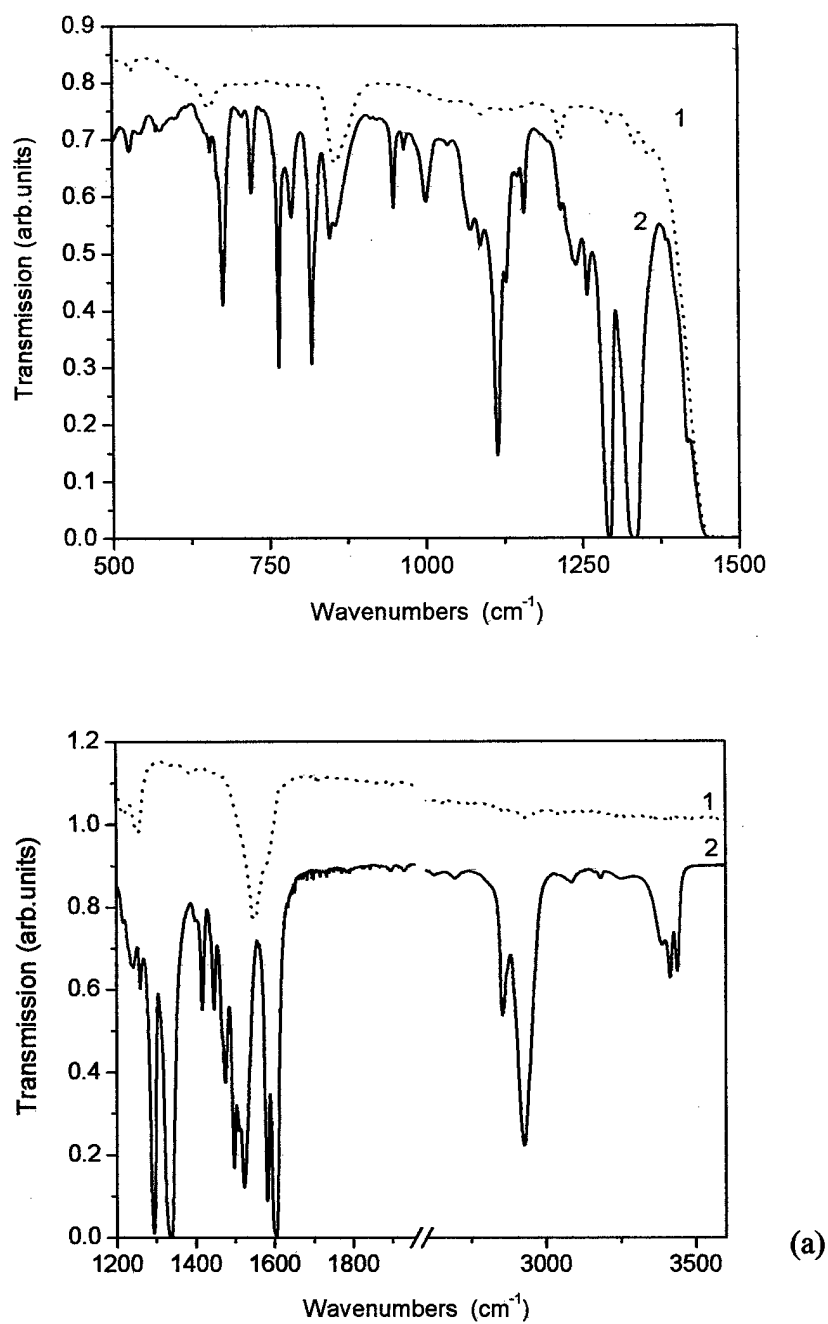


Fig. 2. FTIR transmission spectra of (a) solvent carbon disulfide (dotted curve 1) and COANP solution (60 mg/ml) in carbon disulfide (solid curve 2); (b) solvent carbon tetrachloride (dotted curve 1) and COANP solution (60 mg/ml) in carbon tetrachloride (solid curve 2).

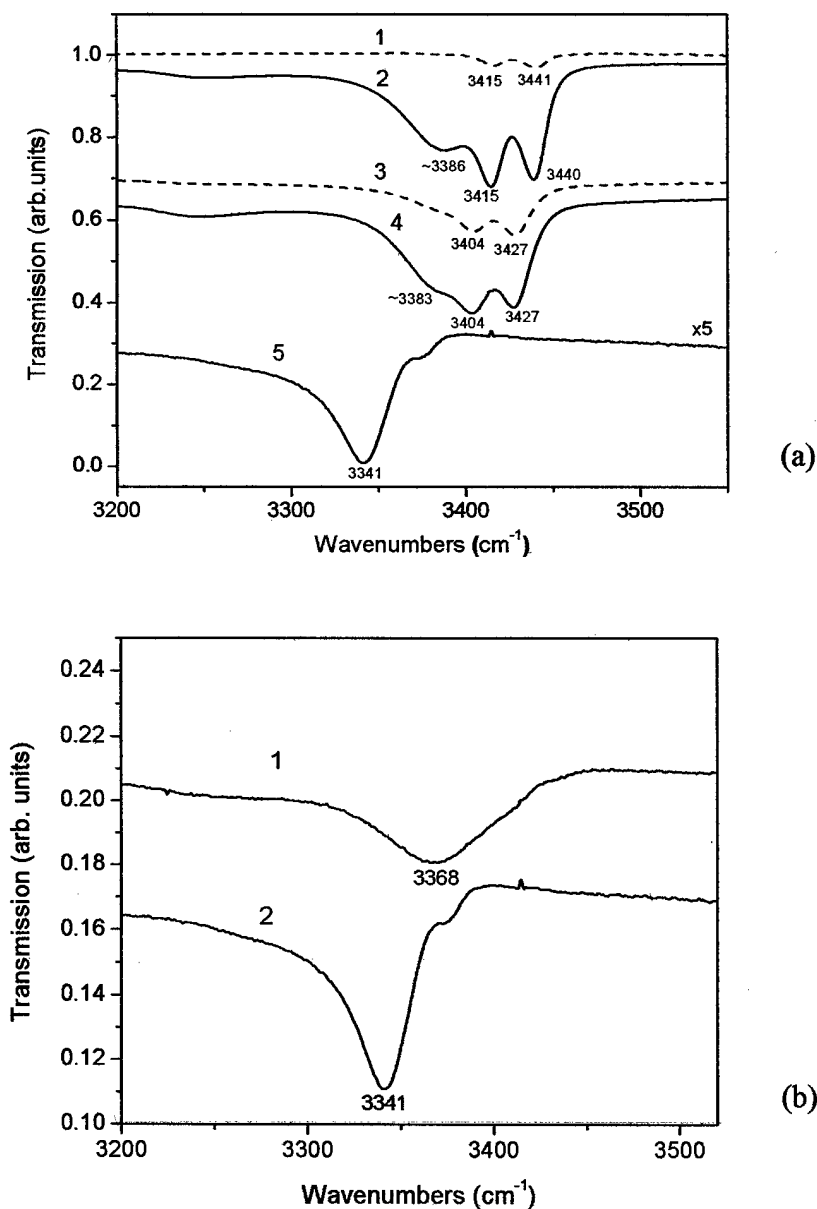


Fig. 3. FTIR transmission spectra of COANP solution in (a) carbon tetrachloride at a concentration of 4mg/ml (dotted curve 1); carbon tetrachloride at a concentration of 60 mg/ml (curve 2); carbon disulfide at a concentration of 20 mg/ml (dotted curve 3); carbon disulfide at a concentration of 60 mg/ml (curve 4); carbon disulfide after casting on an IR-card and evaporation of the solvent (curve 5); (b) carbon disulfide after casting on an IR-card and evaporation of the solvent for 1 hour (curve 1) and for 2 days (curve 2).

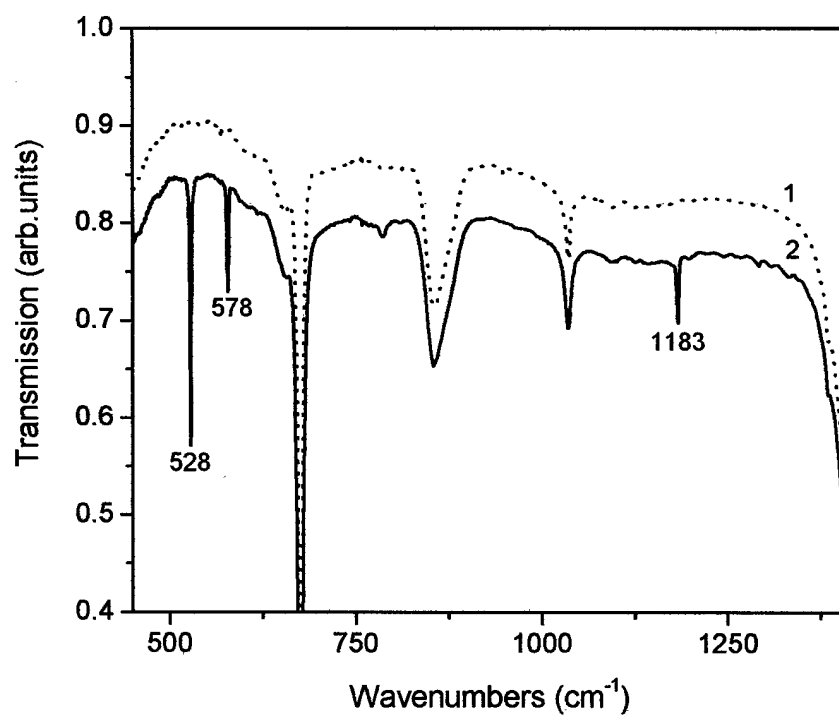


Fig. 4. FTIR transmission spectrum of (1) solvent (carbon disulfide); (2) fullerene C₆₀ solution (7 mg/ml) in carbon disulfide.

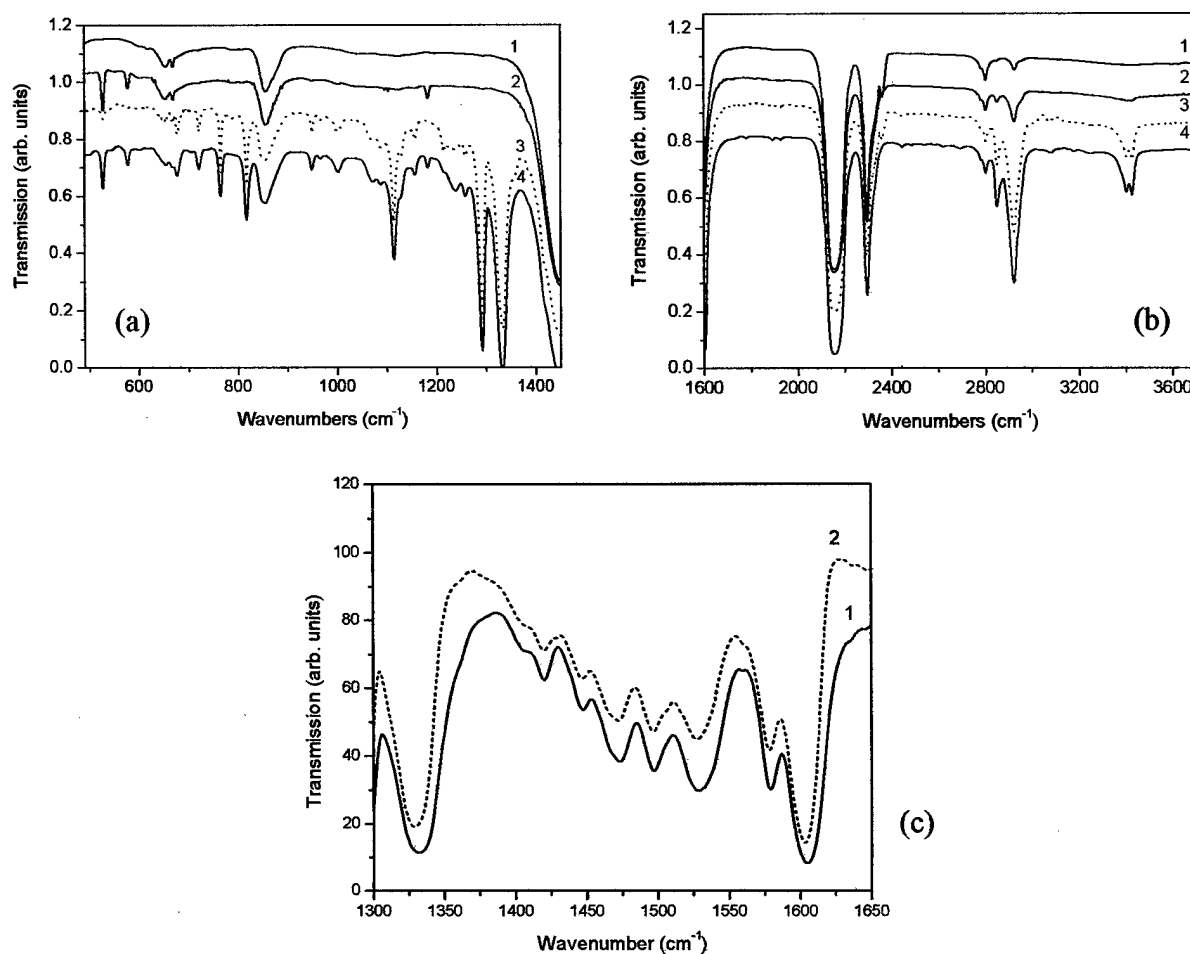


Fig. 5. FTIR transmission spectra (a) in spectral region 550 to 1425 cm^{-1} of solvent carbon disulfide (curve 1); fullerene C_{60} solution (7mg/ml) in carbon disulfide (curve 2); COANP solution (20 mg/ml) in carbon disulfide (curve 3); fullerene C_{60} (7 mg/ml) and COANP (20 mg/ml) solution in carbon disulfide (curve 4); (b) in spectral region 1600 to 3700 cm^{-1} of solvent carbon disulfide (curve 1); fullerene C_{60} solution (7mg/ml) in carbon disulfide (curve 2); COANP solution (20 mg/ml) in carbon disulfide (curve 3); fullerene C_{60} (7 mg/ml) and COANP (20 mg/ml) solution in carbon disulfide (curve 4); (c) of the films deposited from solution in CS_2 on AgCl plate of COANP (dotted curve 1) and COANP plus fullerene C_{60} (curve 2).

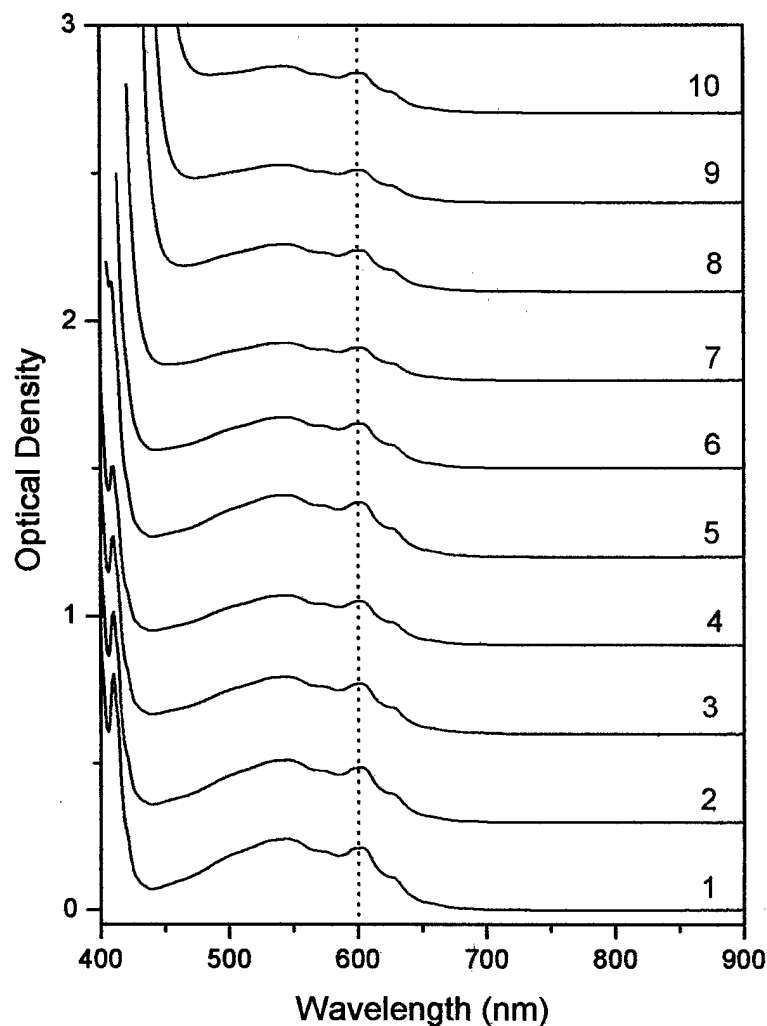


Fig. 6. Optical absorption spectra of the solutions in CS_2 of (1) pure C_{60} ; (2) C_{60} and COANP at molar proportion 1:0.5; (3) C_{60} and COANP at molar proportion 1:1; (4) C_{60} and COANP at molar proportion 1:2; (5) C_{60} and COANP at molar proportion 1:5; (6) C_{60} and COANP at molar proportion 1:10; (7) C_{60} and COANP at molar proportion 1:20; (8) C_{60} and COANP at molar proportion 1:50; (9) C_{60} and COANP at molar proportion 1:100; (10) C_{60} and COANP at molar proportion 1:200. Dotted line shows marks the position of the absorption peak of C_{60} near 600 nm. Fullerene C_{60} was initially dissolved at a maximum concentration of 7.9 mg/ml (6.6×10^{-4} molar fraction)³⁰ before COANP was added and then the solution was filtered through a 0.2- μm -pore-size filter.

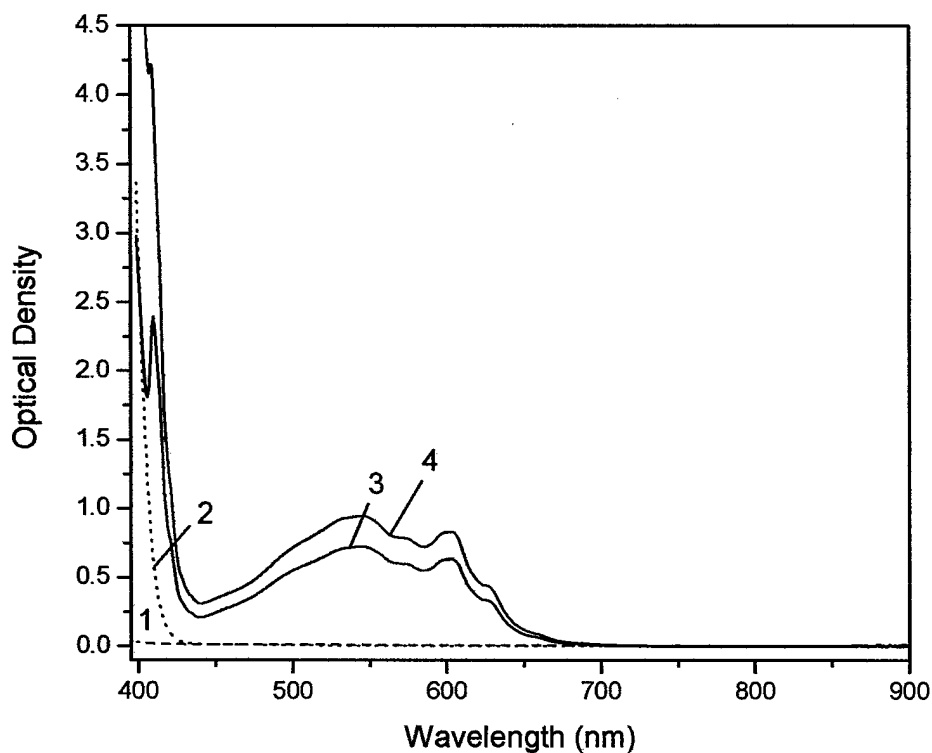


Fig. 7. Spectrum of optical absorption of (1) pure CS₂; (2) COANP in CS₂ at the same concentration as in the mixture of C₆₀ and COANP in molar proportion 1:5; (3) C₆₀ in CS₂; (4) mixture of C₆₀ and COANP in CS₂ in molar proportion 1:5. Fullerene C₆₀ was initially dissolved at a maximum concentration of 7.9 mg/ml (6.6×10^{-4} molar fraction)³⁰ before COANP was added.

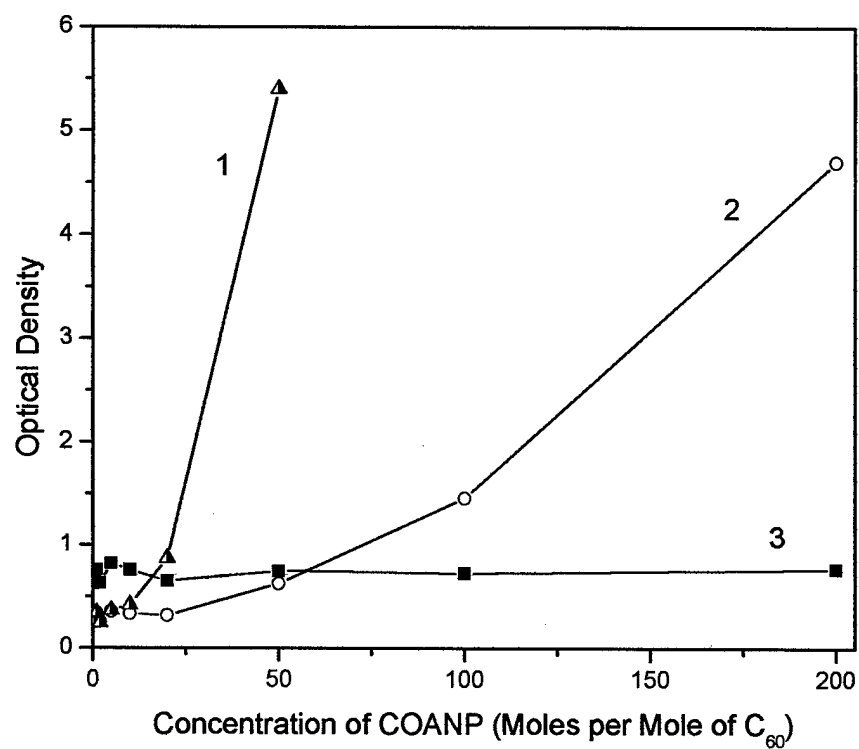


Fig. 8. Optical density of the solutions of C_{60} and COANP in CS_2 versus molar proportion of COANP (number of moles per one mole of C_{60}) at (1) 434-nm wavelength; (2) 452-nm wavelength; (3) 597-nm wavelength.

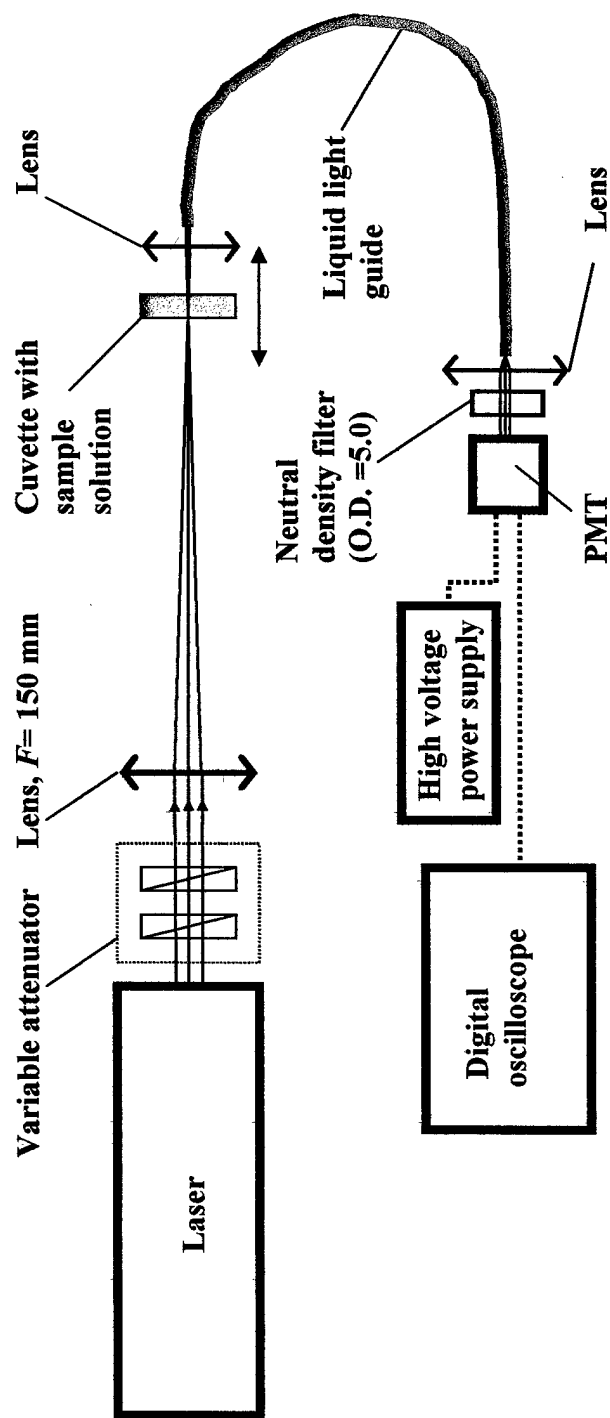


Fig. 9. Schematic of the experimental setup for the characterization of optical limiting properties of fullerene/COANP solutions.

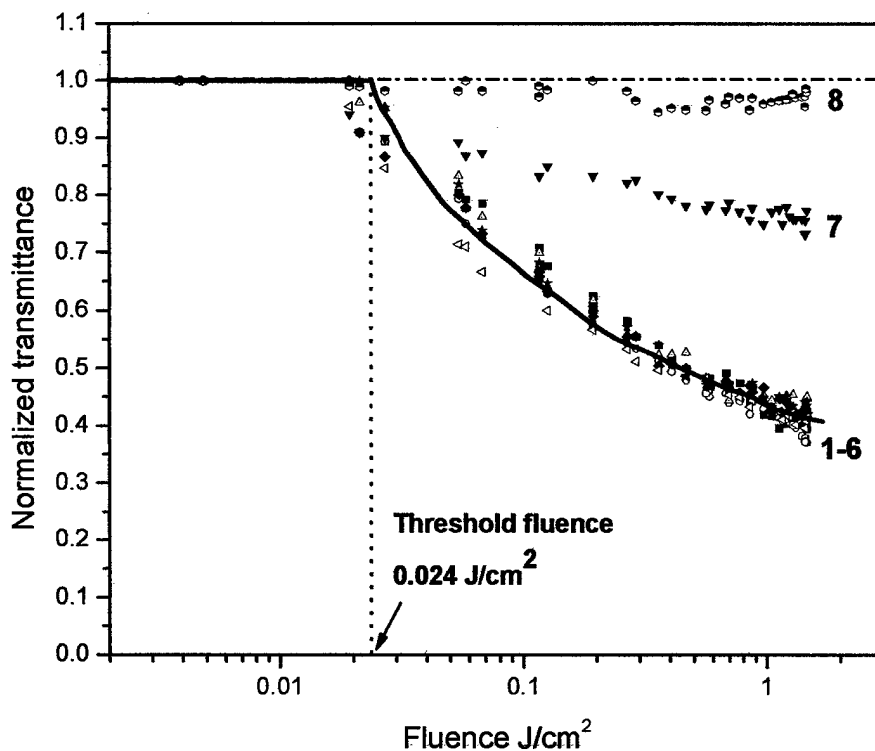
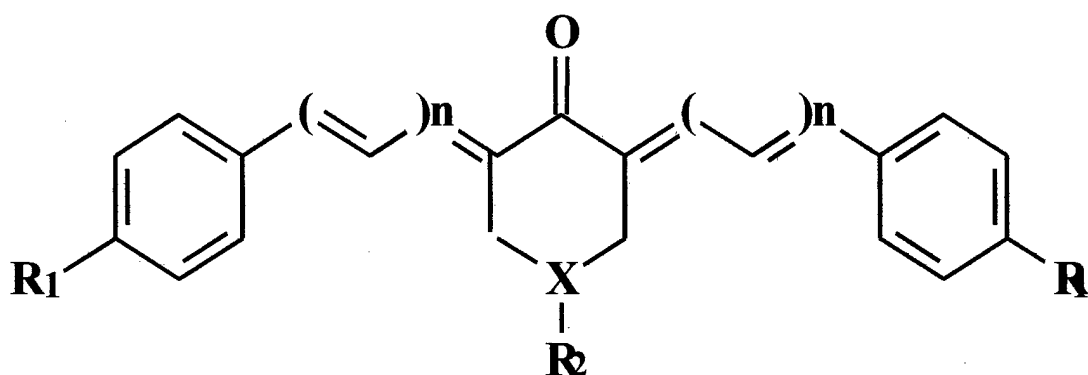
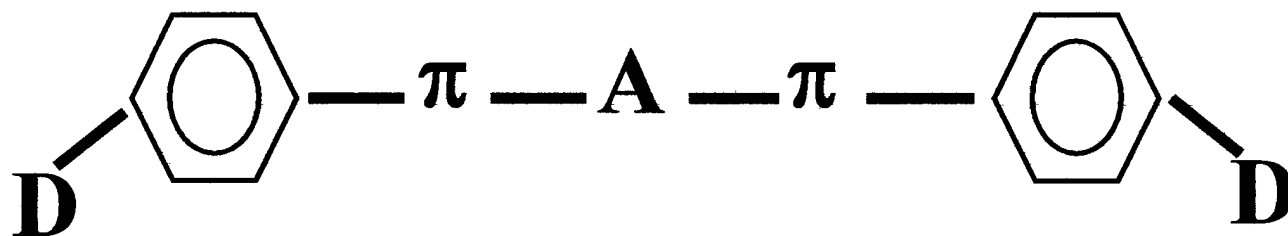


Fig. 10. Normalized transmittance of the solution of C_{60} and COANP in CS_2 versus the fluence of laser light at 532-nm wavelength. Molar proportion of C_{60} to COANP was: (1) 1:0 (pure C_{60}); (2) 1:0.5; (3) 1:1; (4) 1:5; (5) 1:10; (6) 1:50. Dataset (7) corresponds to pure COANP at a concentration that would make molar proportion 1:100 if C_{60} were added. Dataset (8) corresponds to pure solvent CS_2 . The concentration of C_{60} was always kept at maximum. The measurements were taken with frequency double Nd:YAG laser, 180-ns pulse duration, 5-Hz pulse repetition rate.



(a)



(b)

Fig. 11. Generalized chemical structure of the derivatives of cyclohexanone/piperidone (1 through 8) studied in this work: (a) molecular layout and (b) distribution of electro-positive and negative fragments. Molecular structure with $X=CH$ and $R_2=Ph$ (phenyl) corresponds to a derivative of cyclohexanone, and the one with $X=N$ and $R_2=CH_3$ corresponds to a derivative of piperidone. Compound 9 is a piperidone derivative that has R_1 and benzene ring on both ends replaced by ferrocene Fc.

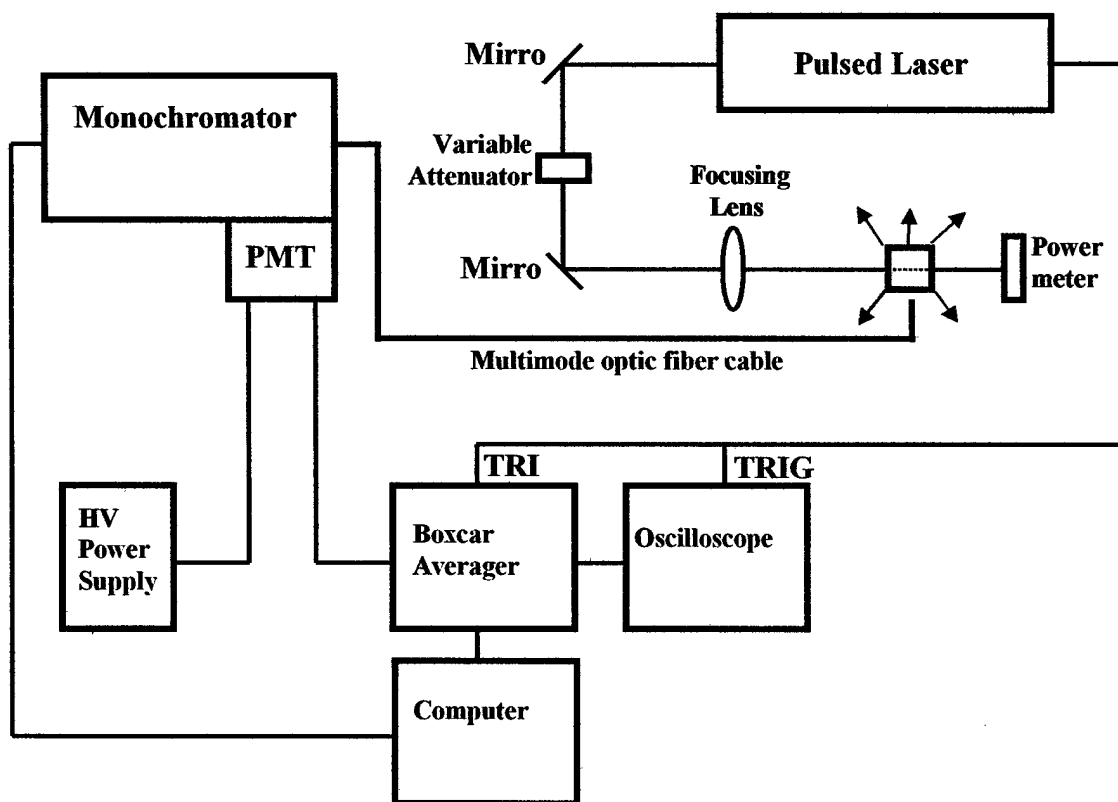


Fig. 12. Setup for measurements of TPA, SPEF and TPEF with pulsed laser sources. In case of measurements of SPEF under continuous pumping with UV lamp, the light was modulated by a mechanical chopper and the boxcar averager was replaced by a lock-in amplifier synchronized by the chopper.

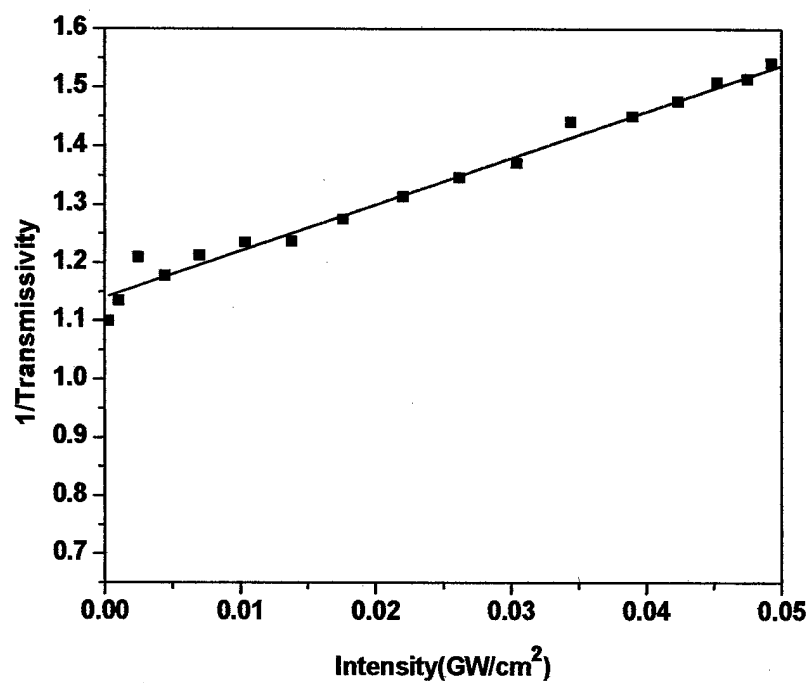


Fig. 13. Typical plot of the inversed transmissivity of a TPA compound (compound 2 in this case) versus input intensity of IR radiation.

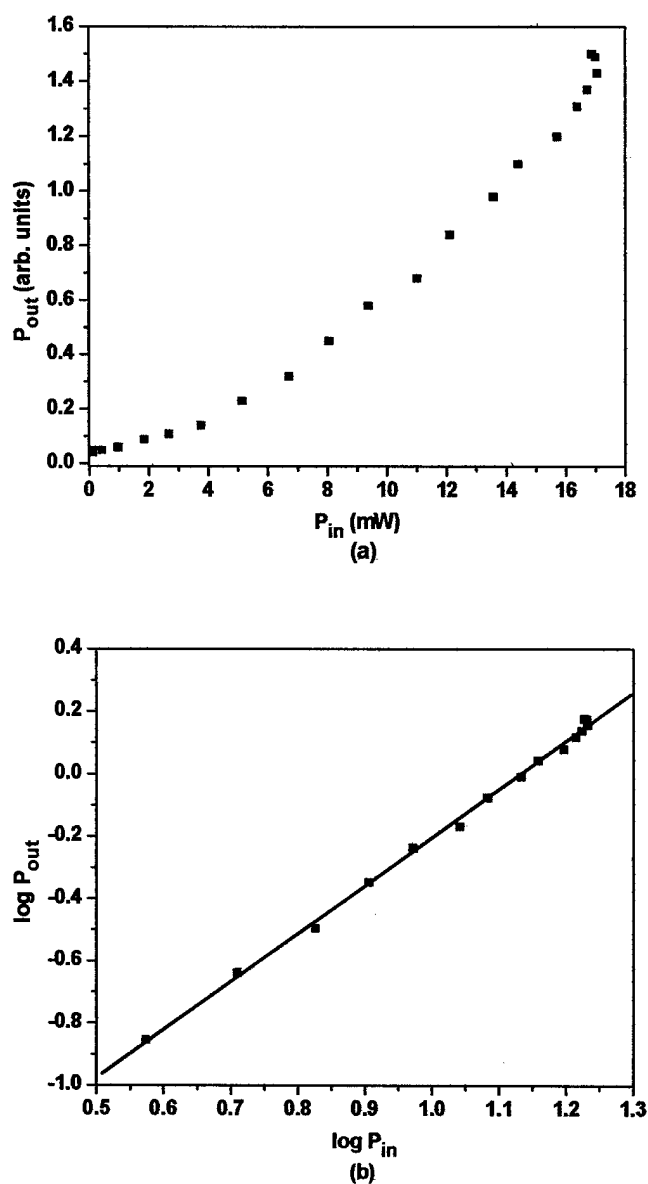


Fig. 14. Power of the two-photon excited fluorescence versus the power of pumping IR radiation plotted in: (a) linear scale and (b) log-log scale. The experimental data correspond to compound 4.

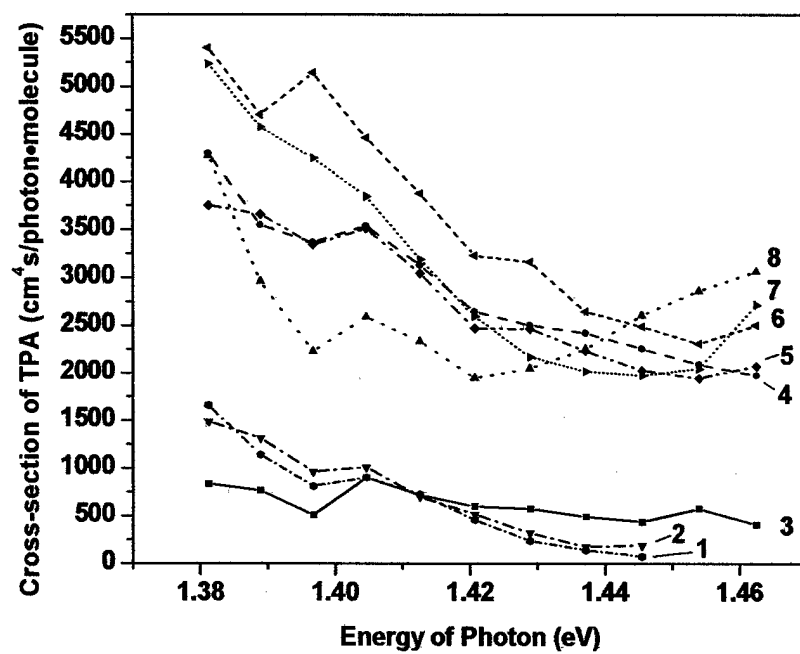


Fig. 15. Spectra of TPA cross-section of compounds (1) 7, (2) 8, (3) 1, (4) 2, (5) 3, (6) 5, (7) 6, and (8) 4.

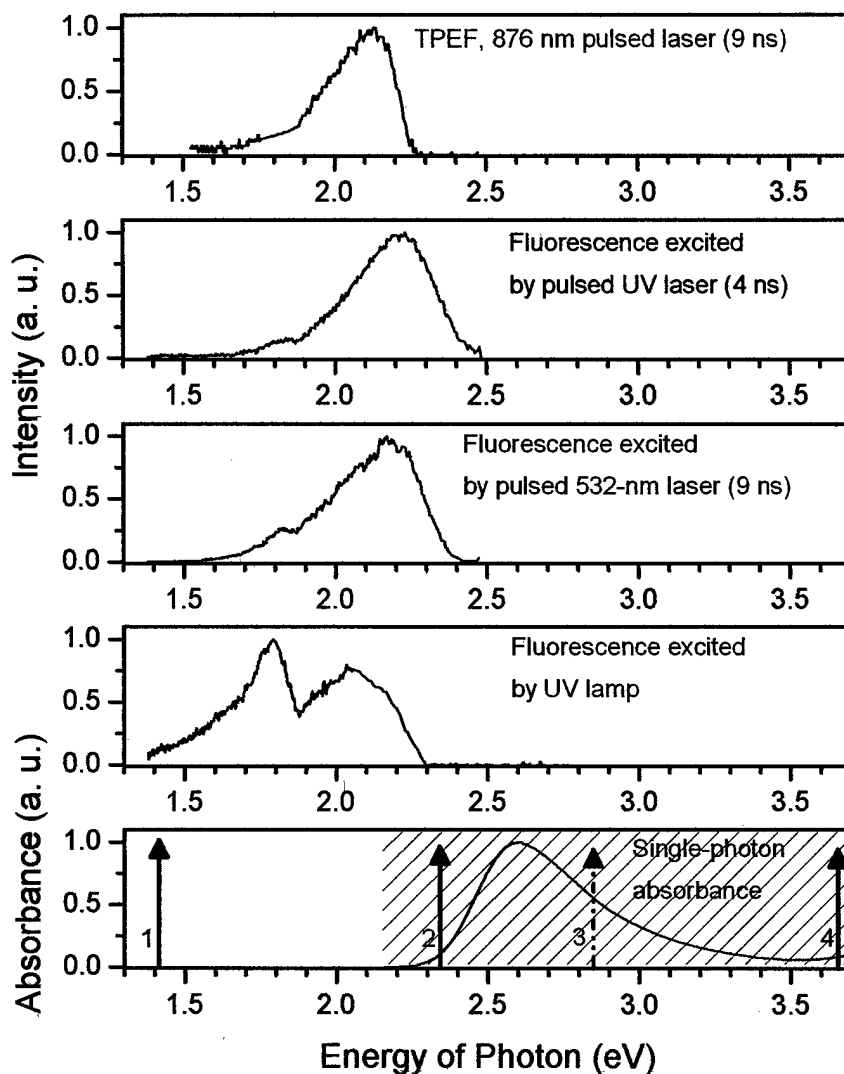


Fig. 16. Single-photon absorption, single-photon excited (SPEF) and two-photon excited fluorescence (TPEF) of compound 1 dissolved in chloroform. The arrows mark the positions of the spectrum lines for: 1) 876 nm tunable IR pulsed dye laser; 2) pulsed frequency double Nd:YAG laser (532 nm); 3) double energy of photon of the IR dye laser; 4) Nitrogen pulsed UV laser (337 nm). The slant lines indicate the range of the emission spectrum of the UV lamp (302 nm to 580 nm). Single-photon absorption was taken at a concentration of 0.675 mM/L, SPEF was taken at concentration of 100, 5, and 5 mM/L, and TPEF was taken at a concentration of 100 mM/L.

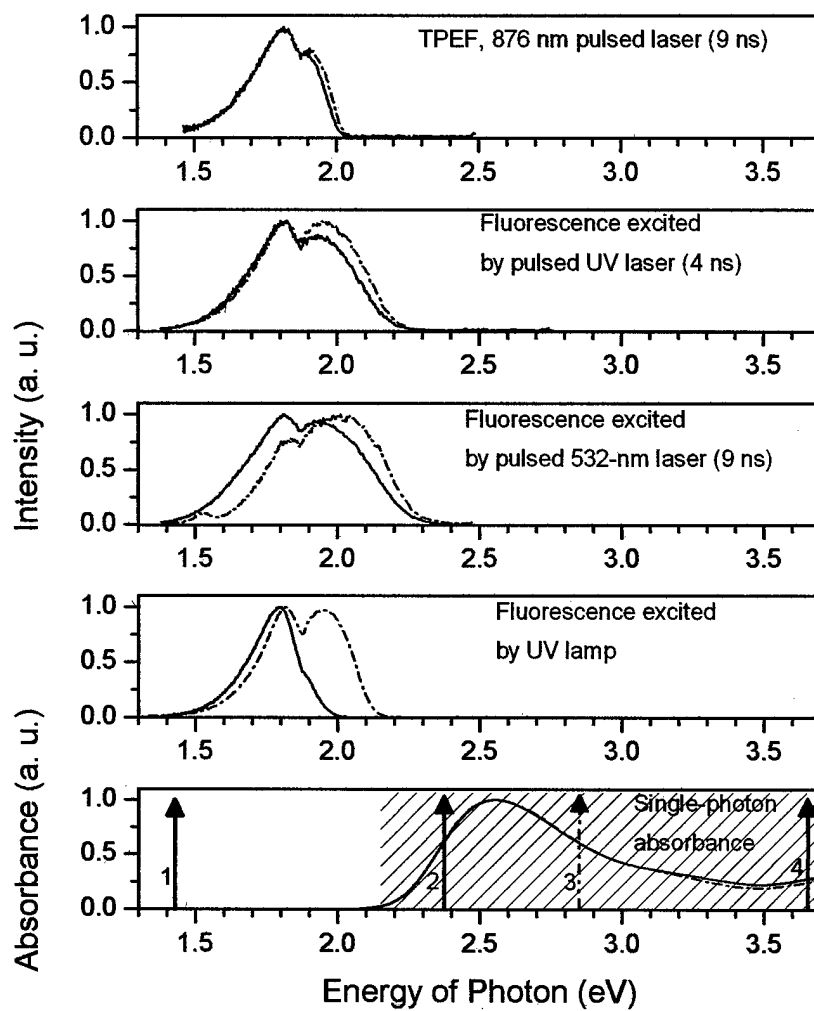


Fig. 17. Single-photon absorption, SPEF and TPEF of compounds 2 and 3 (dotted lines) both dissolved in chloroform. Notations and the conditions at which the spectra were taken are the same as for Fig. 16.

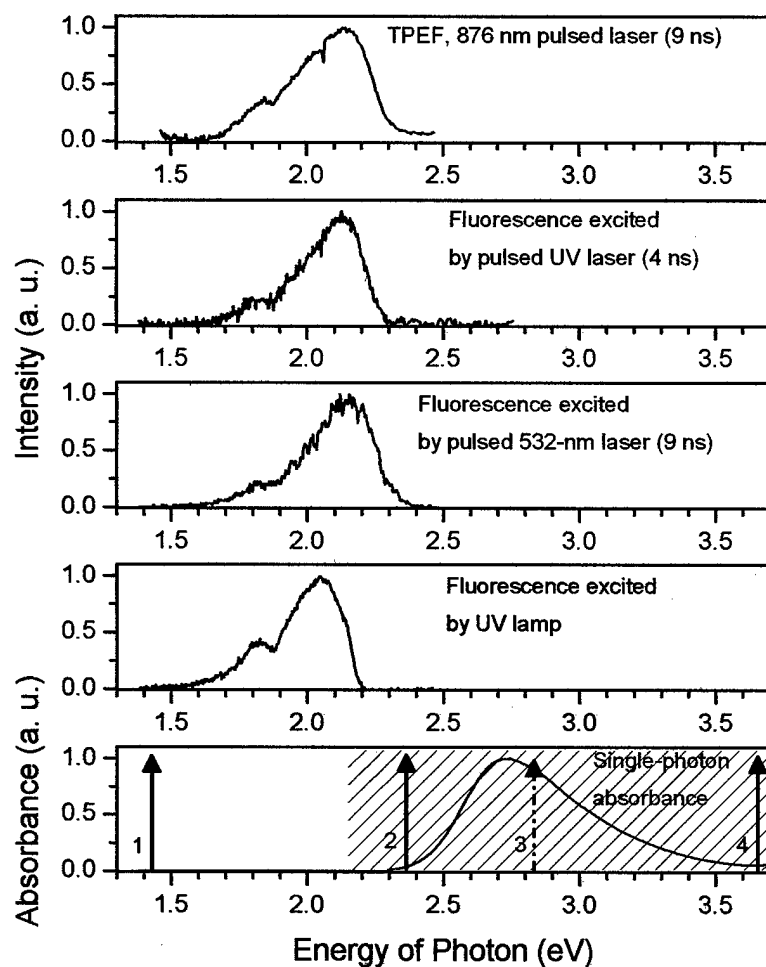


Fig. 18. Single-photon absorption, SPEF and TPEF of compound 4 dissolved in chloroform. Notations and the conditions at with the spectra were taken are the same as for Fig. 16.

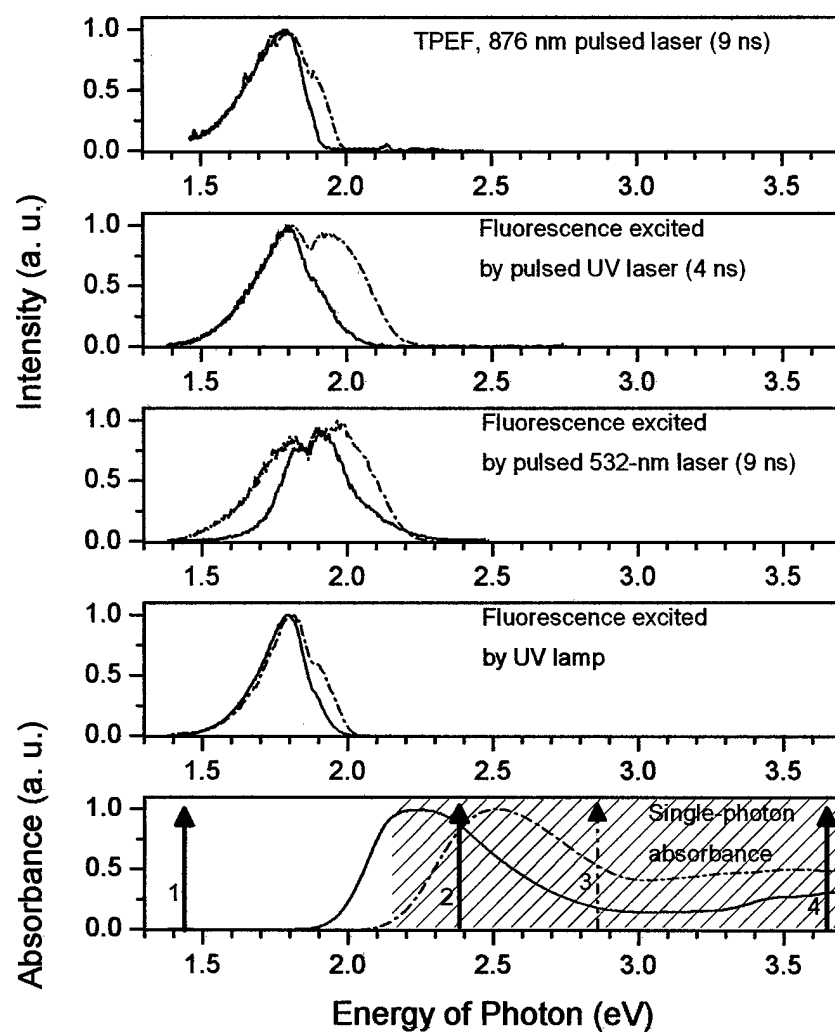


Fig. 19. Single-photon absorption, SPEF and TPEF of compounds 5 and 6 (dotted lines) both dissolved in chloroform. Notations and the conditions at which the spectra were taken are the same as for Fig. 16.

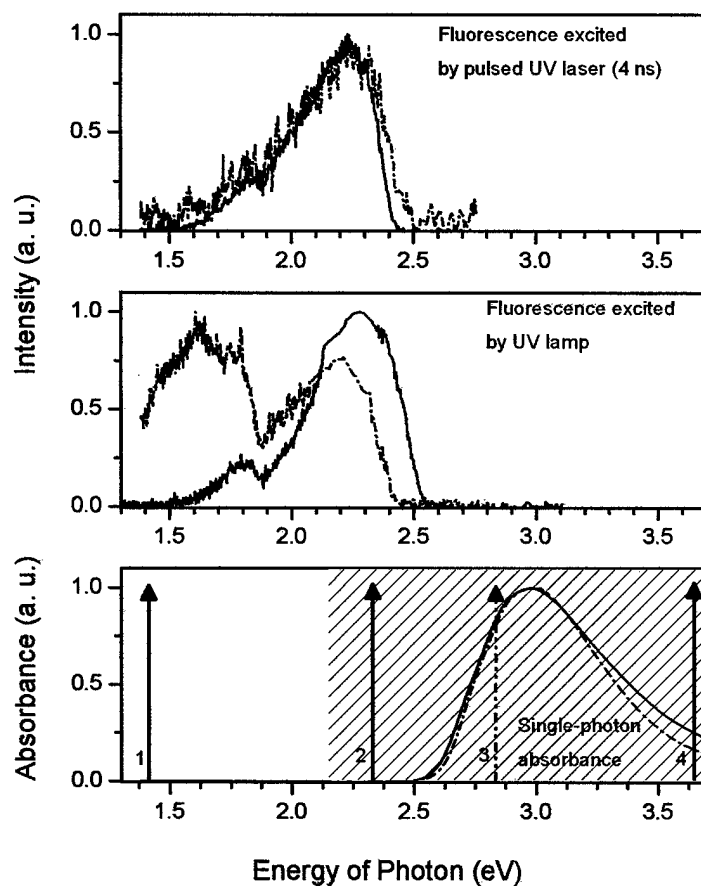


Fig. 20. Single-photon absorption and SPEF of compounds 7 and 8 (dotted lines) both dissolved in chloroform. Notations and the conditions at with the spectra were taken are the same as for Fig. 16.

Table 1. Energy position of vibrational spectra bands in COANP in solution and in solid phase.

COANP solution in CCl ₄	COANP solution in CS ₂	COANP solid film on ST-IR card	Solid COANP (data from Ref. 20)			Cracteristic vibrations
			Raman	IR-absorption		
				sing. cryst.	powder	
			479	479		
	502 vw	503-505m	505	495,505	500	
	527 w	530		520	523	
	546 w	548 m	550		545	
	577vw		573			CC in- plane bend
		581 w	584		576	
	618vvw	610-620			614	
678 m	679 s	677 s	674	679	677	
723 m	721 m		727	730	727	CH ₂ rock
	765 s	766 s	770	764	765	CC out-of-plane bend
	785vvw	797 vvw	796 vw			
	818 s		801 vw			
820m	825 s	830 s				
			841 m			
847w	847 w	847vw	843 m		845	CH out-of- plane-bend
			850 w			
860vvw	858 vvw	864vw	866 m			
			915 w			
	948 w	945 m		946	945	
951w		952vvw	951vw			
	965 vvw		974 w			
1001 m	1001 m	1000 m			999	
			1010w			
			1015w			
1071m	1070 w	1073m	1065w		1063	
1088 m			1090w			
1115s	1115 s	1115s	1115 m		1112	CH in-plane-bend ON in-plane-bend
1130 m	1129 w	1127vvw	1124 w			
1147vw	1145vvw	1143vw	1140 w			
			1151 w			
1159 w	1161 w	1165 m	1165 m			
			1190 m			
1228- 1243 w 1260 vw	1240 vw	1230 m		1231		CH ₂ twist C-C stretch CH ₂ wag
1293 vs	1292 s	1270- 1300 vs	1282 vs 1286 vs 1292 vs 1296 vs		1292	
1337 vs	1338 s	1324- 1340 s	1323 s 1329 s 1342 m		1325	
			1362 m			
1417 m						
1447m		1443 m				
			1459 m			CH ₂ deformation

1475m						NO stretch C-N stretch
1511 w	1498 w	1498 w	1498		1498	
1524 s	1510-1524 w	1531 m	1535 m			
			1581 w			
1597-1604 vs	1603	1601 s	1597 vw 1602 w		1603	C=C stretch
			1626 vw			
1804vww			1806 vw			C=N stretch
1897vww	1890 vw	1887 vww	1890	1886		
1931vww		1947vww				
2448vw	2445 vw	2439 vv w				
2492 vww	2486 vw					
			2580 vw			
2625	2621	2634 vww				
2698vww	2694			2692 vw	2691	
2855 m	2850 m		2862 vw		2865	CH stretch
			2917 m			
2926 s	2923 s		2921 w		2922	
			3059 w			
			3066 w	3068	3067	
3082 w						
		3184 vww				
		3248 vww				
3387 m 3416 m 3440 m	3405 m 3430 m (3340 in solid)	3337 m 3340 m	3344 m		3340	NH and OH stretch

Table 2. Cross-section of TPA of cyclohexanone/piperidone derivatives and reference materials.

Designation Number or Name of Compound	Derivative	Length of C-C bridge	Pending group	Linear Transmittance (1cm cell)	Coefficient of nonlinear absorption β [cm/GW]	Molecular cross-section of TPA $\sigma'_2 \times 10^{-50}$ [cm ⁴ s photon ⁻¹ molecule ⁻¹]
1	piperidone X = N R ₂ = CH ₃	n = 0	R ₁ = N(CH ₃) ₂	0.88	1.6±0.4	600±150
2	piperidone X = N R ₂ = CH ₃	n = 1	R ₁ = N(CH ₃) ₂	0.88	7.0±0.3	2650±100
3	cyclohexanone X = CH R ₂ = Ph	n = 1	R ₁ = N(CH ₃) ₂	0.90	6.5±0.2	2470±70
4	piperidone X = N R ₂ = CH ₃	n = 0	R ₁ = N(C ₂ H ₅) ₂	≈1.00	5.1±0.3	1950±110
5	piperidone X = N R ₂ = CH ₃	n = 1	R ₁ = N(C ₂ H ₅) ₂	0.91	8.5±0.2	3230±70
6	cyclohexanone X = CH R ₂ = Ph	n = 1	R ₁ = N(C ₂ H ₅) ₂	0.87	6.9±0.5	2600±200
7	cyclohexanone X = CH R ₂ = Ph	n = 1	R ₁ = OCH ₃	0.92	1.4±0.3	520±10
8	piperidone X = CH R ₂ = CH ₃	n = 1	R ₁ = OCH ₃	0.84	1.2±0.2	460±80
9	piperidone X = N R ₂ = CH ₃	n = 0	Benzene ring + R ₁ replaced by Fc	0.41	1.4±0.2	530±60
BDBAS ⁸ in acetone					3.2	17700
BBTDOT ⁹						2980
Rhodamine B (measured at the same conditions as materials 1 through 9)					3.3±0.7	1236±277

Table 3. Intensity of SPEF and TPEF of cyclohexanone/piperidone derivatives relative to reference dyes Rhodamine 6G and Rhodamine B respectively.

Designation Number	Derivative	Length of C-C bridge	Pending Group	UV lamp SPEF	Pulsed 532 nm SPEF	Pulsed UV 337 nm SPEF	Pulsed 876 nm TPEF
1	piperidone X = N R ₂ = CH ₃	n = 0	R ₁ = N(CH ₃) ₂	1.888E-05	2.72E-02	1.132E-02	1.42E-01
2	piperidone X = N R ₂ = CH ₃	n = 1	R ₁ = N(CH ₃) ₂	4.102E-02	6.25E-01	1.654E-01	3.74E-01
3	cyclohexanone X = CH R ₂ = Ph	n = 1	R ₁ = N(CH ₃) ₂	1.032E-02	7.17E-01	3.322E-01	3.37E-01
4	piperidone X = N R ₂ = CH ₃	n = 0	R ₁ = N(C ₂ H ₅) ₂	1.450E-03	8.17E-03	3.366E-03	4.35E-01
5	piperidone X = N R ₂ = CH ₃	n = 1	R ₁ = N(C ₂ H ₅) ₂	7.578E-05	3.72E-01	1.464E-02	4.03E-01
6	cyclohexanone X = CH R ₂ = Ph	n = 1	R ₁ = N(C ₂ H ₅) ₂	1.211E-04	5.16E-01	3.354E-01	3.65E-01
7	cyclohexanone X = CH R ₂ = Ph	n = 1	R ₁ = OCH ₃	5.310E-03		4.191E-04	
8	piperidone X = CH R ₂ = CH ₃	n = 1	R ₁ = OCH ₃	1.719E-05		1.993E-03	
9	piperidone X = N R ₂ = CH ₃	n = 0	Benzene ring + R ₁ replaced by Fc	2.460E-04			
Rhodamine 6G				1.000E+00	1.00E+00	1.000E+00	
Rhodamine B							1.00E+00

Part 3

Miniature Device Fabrication

1. Design

A miniature electro-optic (E-O) modulator that comprises a Fabry-Perot (F-P) etalon integrated with an optical fiber was theoretically analyzed. Basic design of the device is schematically shown in Fig. 1. The F-P etalon has to be fabricated on a cleaved end of a single-mode optical fiber. The etalon consists of two quarter-wave dielectric stacks and a spacer made of an E-O material. The etalon is surrounded by two conductive ITO electrodes. The fiber is connected to a laser source through a single-mode fiber splitter. Electric voltage from a signal applied to the electrodes changes the refractive index of the E-O material thus modulating the reflectivity of the etalon. This changes the intensity of the output light coming out from the second branch of the splitter. The device must have the advantages of a standard F-P E-O modulator such as low driving voltage and high extinction ratio plus a number of new features. It is simple and rigid. Everything is attached to fiber: there are no moving parts and nothing to be aligned and vibration isolated. The size of the electrodes is equal to the diameter of the fiber cladding (125 μm typically). This makes the capacitance low and increases the bandwidth of the modulator. The device has very loose requirements to the size of the optically uniform area of the E-O material. In fact, it must be slightly greater than the diameter of the fiber core (few microns). This makes the proposed design especially useful in case of single crystal E-O films, which cannot be grown bigger than fractions of millimeter in size.

2. Evaluation of the figures-of-merit

The theoretical evaluation of the performance of the modulator was conducted for a single crystal film of organic compound *N*-4-Nitrophenyl-*N*-(*L*)-prolinol known as NPP, which have been recently grown and used in a longitudinal E-O modulator known as a conventional Pockels cell.^{1,2} The normalized transmittance of a Pockels cell placed between crossed polarizers is given by the formula:

$$T = \sin^2(\Delta\phi), \quad (1)$$

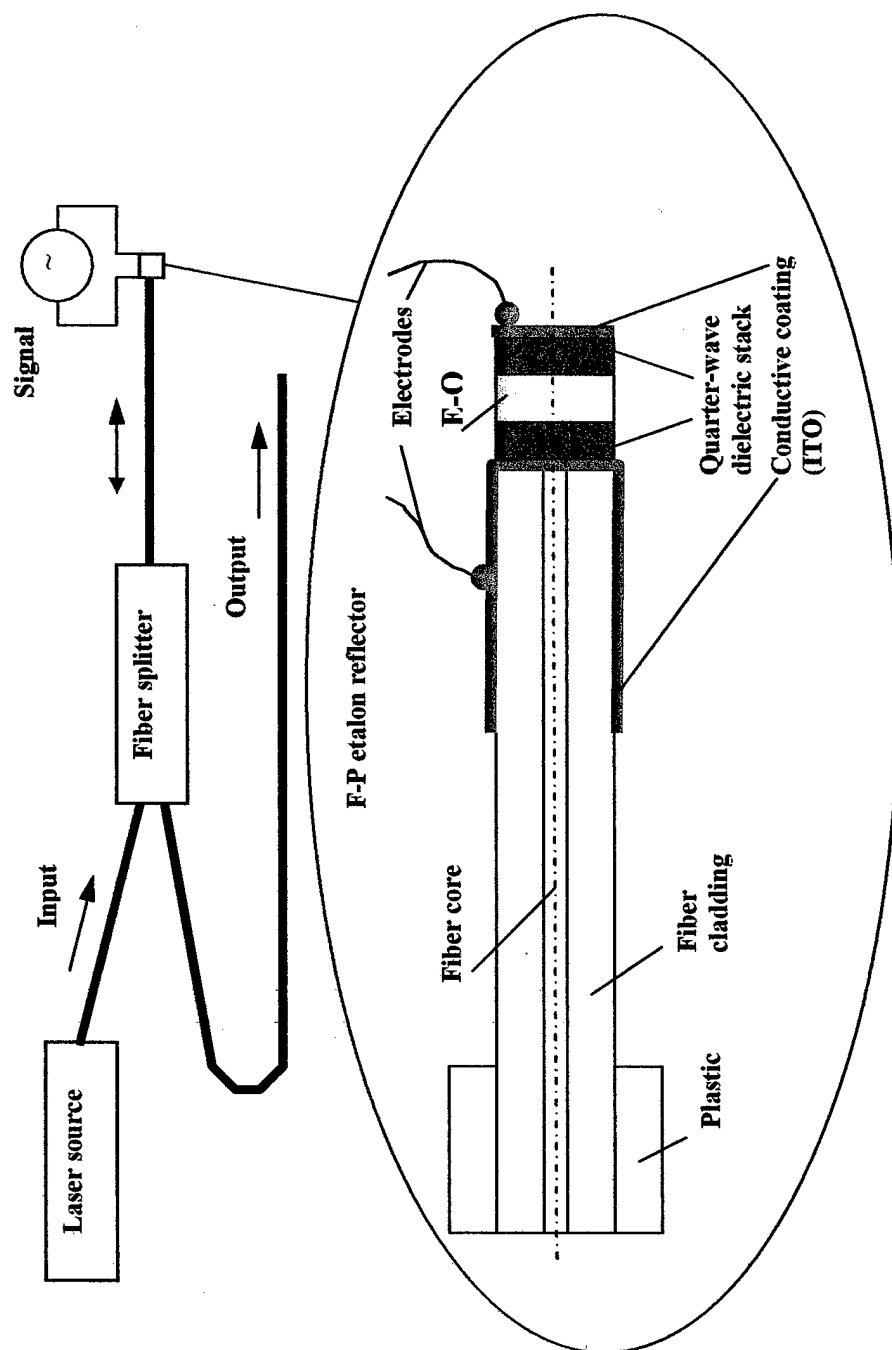


Fig. 1. Schematic of a miniature E-O modulator based on a Fabry-Perot (F-P) etalon integrated with an optical fiber.

where $\Delta\phi$ is the electrically induced phase shift between two components of the optical field with orthogonal polarizations passing through the cell. The normalized transmittance of the F-P modulator is given by the formula:

$$T = 1/[1 + F \sin^2(\Delta\phi)], \quad (2)$$

where F is finesse of the F-P cavity and $\Delta\phi$ is the electrically induced phase shift in a linearly polarized optical field (must be oriented along one of the optical axes of the NPP single crystal film filling the cavity). The transmittance of the modulator as compared to the transmittance of the Pockels cell is presented in Fig. 2.

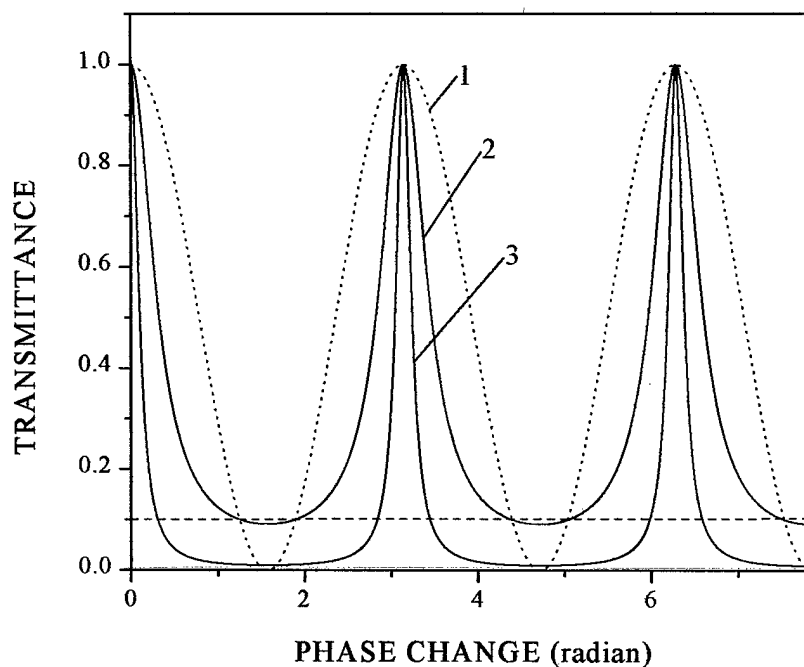


Fig.2. Transmittance of a F-P modulator (solid curves) as compared to a Pockels cell (dashed curve 1). Curve 2 corresponds to the finesse of the F-P cavity 10, curve 3 – to 100.

Constant phase shift $\pi/2$ is introduced into Pockels cell in order to have the transmittance peaks of both modulators overlapping. One can see that the proposed F-P modulator has much sharper response to an electrically induced phase change in the E-O

material. The greater is the finesse of the F-P cavity the sharper is the response. We previously measured the half-wave voltage V_π of the Pockels cell filled with NPP to be 3.24 kV. It gives us the factor c between the phase shift and the voltage V applied to the E-O film ($\Delta\phi = cV$) to be 9.7×10^{-4} rad/V. Using this value, we estimated the driving voltage V_{10dB} of the F-P modulator corresponding to an extinction ratio of 10 dB (one tenth of transmittance, which is marked in Fig. 2 by a horizontal dashed line) for various values of finesse in comparison with the driving voltage of the Pockels cell. The results of the calculations are presented in Table 1.

Table 1: Driving voltage V_{10dB} (V) of the F-P modulator for various values of finesse as compared to a Pockels cell. The material is a single crystal film of organic compound NPP

Pockels cell	Finesse of the F-P modulator							
	5	10	20	100	200	500	1000	2000
1290	-	1280	757	313	220	135	95	67

The proposed modulator with finesse of the order of few thousands can potentially have a driving voltage V_{10dB} close to tens of volts versus more than a kilovolt for a standard Pockels cell. These estimated indicate the feasibility of the proposed design and its potentially high figures-of-merit.

The estimations indicate that the finesse of the F-P cavity is a highly critical factor in achieving low driving voltage of the modulator. That is why in the modulator has to use quarter-wave dielectric stack reflectors on both sides of the E-O film. The dielectric stacks provide high reflectivity without introducing reflection losses as in case of metal films. The finesse of the F-P cavity in this case can be described by the formula³

$$F = \frac{4 \exp(-\alpha_r d)}{[1 - \exp(-\alpha_r d)]^2} \quad (3)$$

where α_r is the overall distributed loss coefficient in the cavity determined as

$$\alpha_r = \alpha_s + \frac{1}{2d} \ln \frac{1}{R_1 R_2}, \quad (4)$$

where α_s is the attenuation factor associated with the E-O spacer, d is the thickness of the spacer, R_1 , R_2 are the reflectance parameters of the dielectric mirrors. Neglecting the losses in the E-O material, we estimate that in order to achieve a finesses of the order of 2000 we must have dielectric reflectors with $R_1 = R_2 = 0.956$. The reflectors must have up to nine dielectric quarter-wave dielectric layers in each. This adds up to the distance between the electrodes of the E-O modulator thus decreasing the actual electric voltage applied to the E-O film. In fact, the actual voltage applied is determined as

$$V = V_e / \left[1 + 2 \frac{\epsilon_s d_r}{\epsilon_r d_s} \right], \quad (5)$$

where V_e is the external voltage applied to the electrodes, ϵ_r , ϵ_s are the dielectric constants of the reflector and spacer respectively, and d_r , d_s are the parameters of thickness of the reflector and spacer respectively. A nine-layer quarter-wave dielectric stack for 633-nm wavelength has a thickness of 1.42 μm . Assuming that we have a spacer made of a 6 - μm -thick E-O film of NPP, we can estimate that in order to get an actual voltage of 67 V applied to the film (see Table 1) we must apply to electrodes of the modulators a voltage close to 100V. The thinner the film, the higher must be voltage V_e . In reality, we might expect some losses in the E-O film, even if it is thin. An additional factor of losses will be a divergence of the light beam coming out of the fiber and reflected back in the fiber by the F-P cavity. Not all the rays will be equally participating in the interference interaction in the etalon. This will reduce the overall finesse, even if the reflectors are of good quality.

3. Alternative designs

Keeping in mind the problems mentioned above, an alternative design of the modulator was developed (Fig. 3). It is actually an implementation of a F-P etalon with fiber Bragg gratings. The F-P etalon made with fiber Bragg gratings can have a finesse of few thousands.⁴ The E-O film is squeezed between two fibers and the ITO electrodes are in direct contact with it thus making an external voltage directly applied to the film. Making a F-P etalon with Fiber gratings can be even simpler now than making a thin film

F-P etalon since fiber Bragg gratings are readily available from a variety of commercial sources.

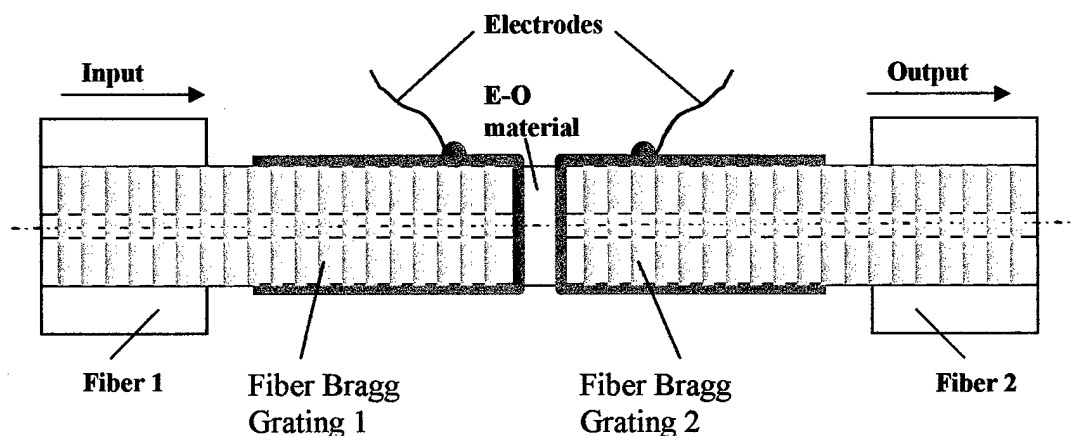


Fig. 3. A schematic of a F-P E-O modulator made of fiber Bragg reflectors.

In addition, intrinsic losses in the cavity can be easily compensated by inserting an optical fiber amplifier in the cavity between the Bragg reflectors. This can potentially make effective finesse very high thus reducing driving voltage of the modulator.

Fig. 4 shows the alternative design of a transversal E-O modulator with input and output optical fibers inserted in a single crystal film of an organic crystal (for example, NPP) grown by the plate guiding method as described in Refs. 1 and 2. The modulator is based on a cell, which has a quartz lid 1 and trough 2 with a trench 3 for an excessive material. The single crystal film 4 is grown from the melt between lid 1 and trough 2. The thickness of the film is equal to the depth d of the trough. Alternating voltage is applied to the modulator through leads 5 and 6, which are connected to transparent ITO electrodes 7 and 8. Optical fibers 9 and 10 with stripped and cleaved ends are immersed in to the organic material when it was melted and the crystal was grown. The fibers conduct polarized light in and out of the E-O film. When the light passes through the film, its polarization changes according to the applied alternating voltage thus resulting into E-O modulation effect. This design has two apparent advantages: (a) possibly low driving voltage due to long distance of interaction between light and the E-O material without need for multiple passes as in the F-P modulator; (b) efficient low-loss light input and output because of the direct optical contact between the fibers and the E-O film.

Fig. 5 shows the design of a longitudinal modulator using the same cell and the optical fibers with ITO coated ends. The cell has top lid 1 and trough 2 made of quartz. The excessive melted material is collected in trench 3 when lid 1 is placed on the top of trough 2. This time the lid and the trough do not have conductive ITP coating. Instead fibers 5 and 6 are coated with ITO and inserted in the trough with melted organic material used to produce a single crystal E-O film. Alternating voltage is applied to the modulator through leads 7 and 8 connected to the conductive ends of the fibers with conductive glue. When the polarized light passes through the film the alternating electric field is applied to the film along the propagation direction thus modulating the state of the polarization of the light (longitudinal E-O effect). With the fibers having Bragg grating on both ends the modulator can be converted into multi-pass F-P configuration with low driving voltage and high extinction ratio. The advantage of this design is that the growth direction and the orientation of the single crystal film are fully controlled by the cell thus making its properties more predictable.

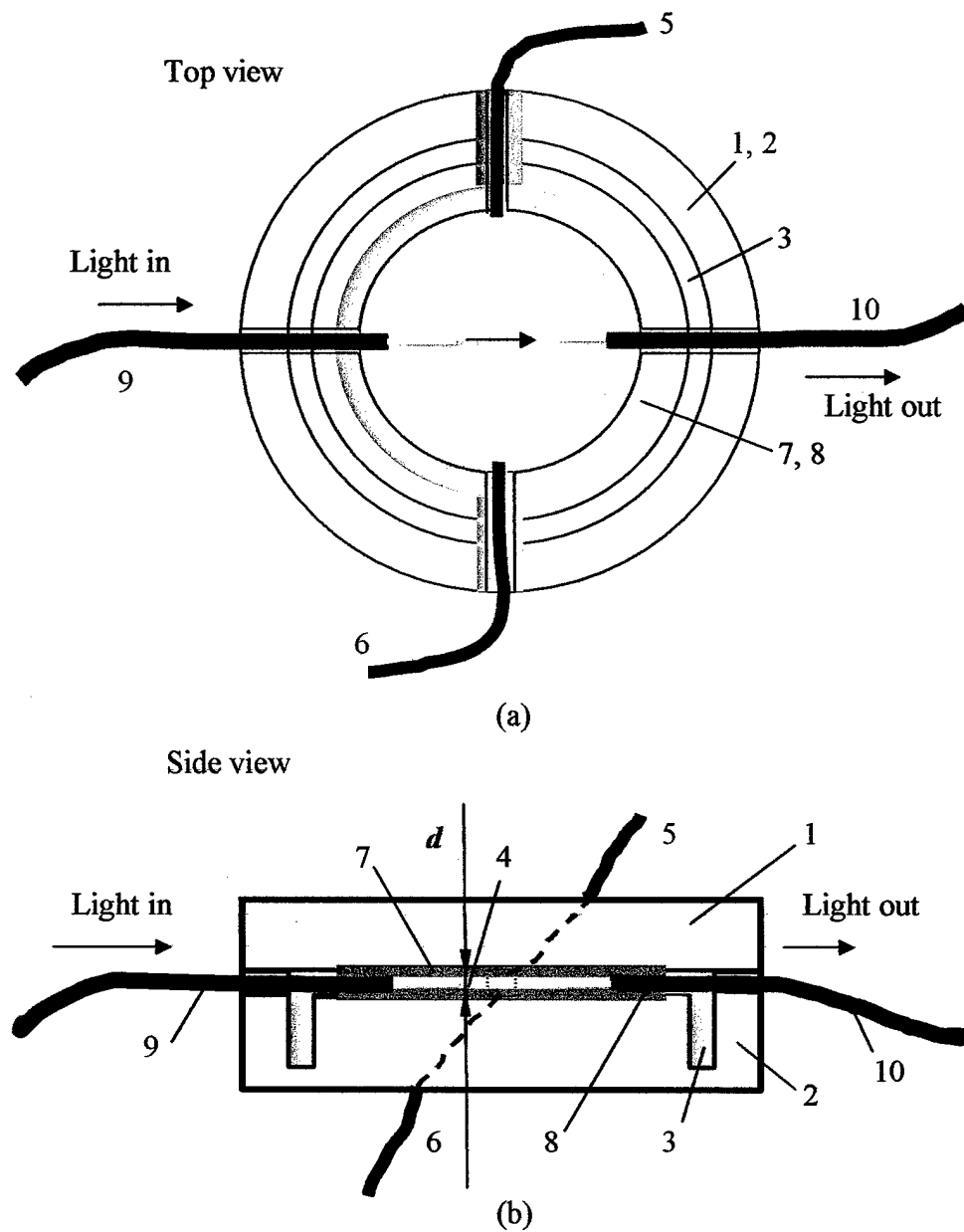


Fig. 4. Schematic of a transversal E-O modulator using optical fibers to inject light in and collect light out from a single crystal film of an organic crystal grown by the plate guiding method

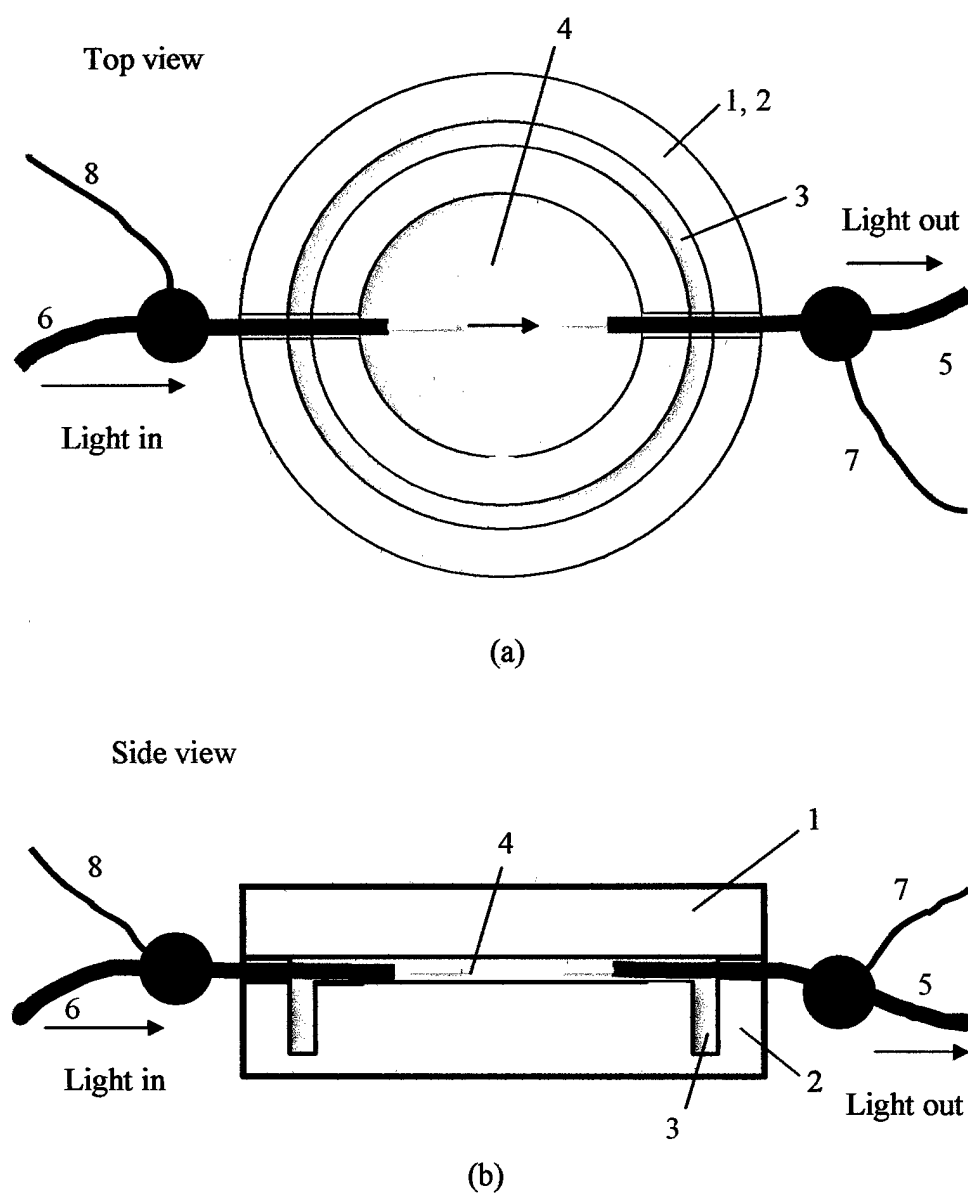


Fig. 5. Schematic of a longitudinal E-O modulator using optical fibers to inject light in and collect light out from a single crystal film of an organic crystal grown by the plate guiding method

4. Suggested fabrication procedure

The process of growth of a single crystal organic thin film within the vertical structure of the modulator is illustrated in Fig. 6.

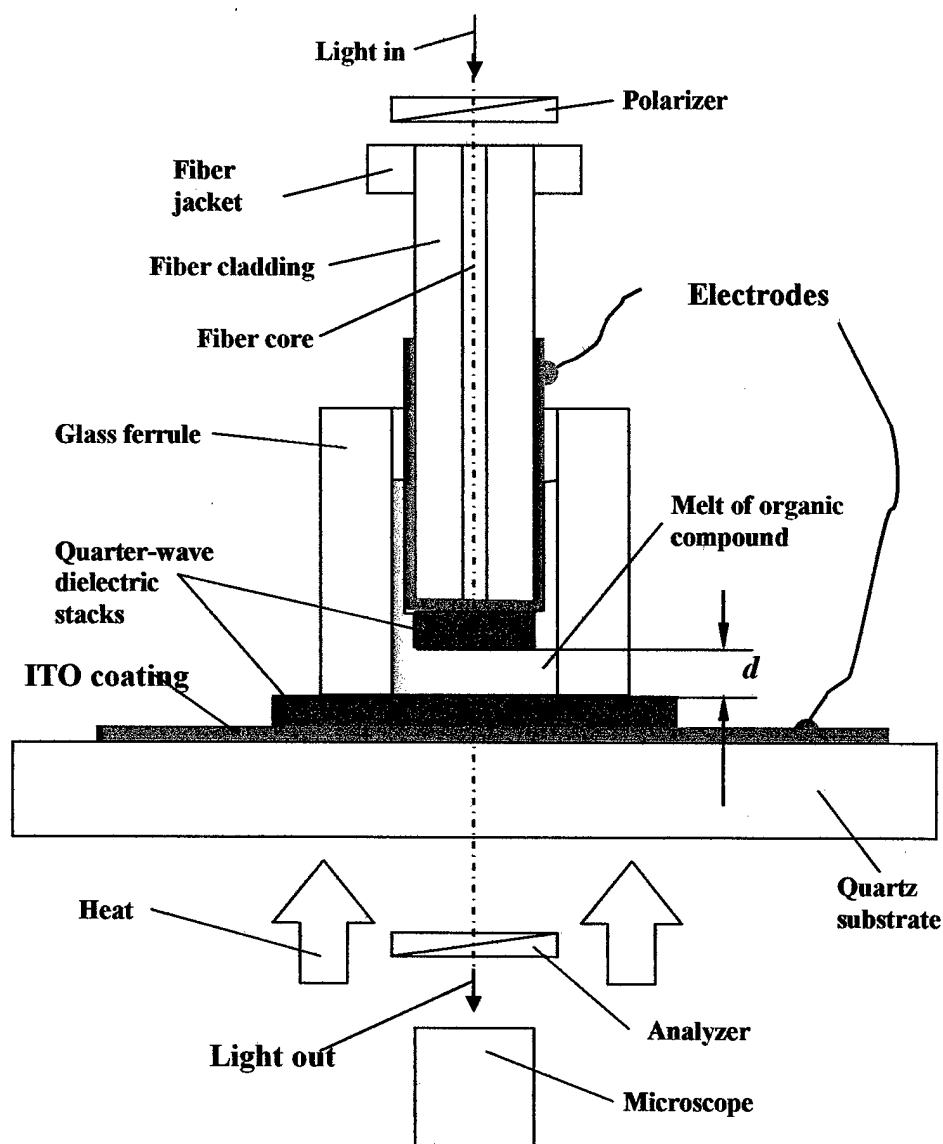


Fig. 6. The schematic of the suggested experimental cell for growing a single-crystal film of an organic E-O material as a part of a F-P E-O modulator.

The technique is still the plate guiding method described in Refs. 1 and 2. Cleaved end of a single-mode fiber is coated with an ITO conductive film and with interference multi-layer coating (quarter-wave dielectric stack). Then the fiber is pulled into a glass ferrule mounted on and glued to a quartz substrate coated with an ITO layer and with a quarter-wave stack. The gap between the fiber and the plate is filled with an organic E-O compound in powder form. Electrodes are attached to the ITO conductors. Quartz substrate is heated from below. The light is injected into the fiber through a polarizer. The light out of the fiber passes through the E-O material, plate, and an analyzer. Then the light goes into an optical microscope. The heat supplied to the assembly melts down the powder. When the heater is off, the organic compound undergoes re-crystallization. The crystalline state of the film can be observed with a microscope. If the film becomes a single crystal, an observer will see the dark uniform area corresponding to a single crystal placed between crossed polarizer and analyzer. If the film is polycrystalline, the area turns out to be bright and inhomogeneous. Repeated heating and cooling of the film in combination with microscope observation can eventually produce a uniform single crystal film of an organic E-O material of the size slightly bigger than the diameter of the fiber core (of the order of 10 μm). This will be enough for building a F-P E-O modulator. The thickness of the film can be easily controlled during the melting process by a fixing the tip of the fiber at a desirable distance from the plate. The process could be easily modified for a F-P modulator using fiber Bragg gratings (Fig. 3). In this case, the quartz plate must be replaced by the second fiber. Similar approach can be used for making polymer or glass E-O films within the F-P cavity. Instead of polycrystalline powder, we can fill the space between the fiber and the plate with a solution of an E-O polymer or with a sol-gel compound. Heating the polymer accompanied by application of high voltage to the electrodes does poling of the E-O polymer when it is melted and cooled down. For an E-O glass poling is accomplished when the voltage is applied during solidification of the gel.

5. Experimental results: conductive coating of optical fibers

We have developed and successfully carried out the process of deposition of conductive ITO coating on the cleaved ends of optical fibers. In our experiments we used standard Ge-doped single-mode fibers for a wavelength of 633 nm (Thorlabs FS-SN-3224). A 1-m-long piece of fiber with both ends having 2.5 cm of plastic jacketed stripped off and being cleaved was rolled over a special revolving drum placed into an RF magnetron sputtering system as is shown in Fig. 7. Fiber 1 is fixed in such a way that one of its ends 3 freely protrudes through a protecting cover of drum 2. The drum rotates clockwise. RF magnetron sputtering gun 4 loaded with an ITO target is placed over the drum. Rays 5 show the directions of atoms of indium oxide/ tin oxide coming on the stripped end of the fiber. The ground plate 6 is located under the drum, which is also grounded. Test substrate 7 is placed near the fiber. It is used to measure the thickness of the ITO coating. Rotation of the drum prevents overheating of the fiber. The fiber is

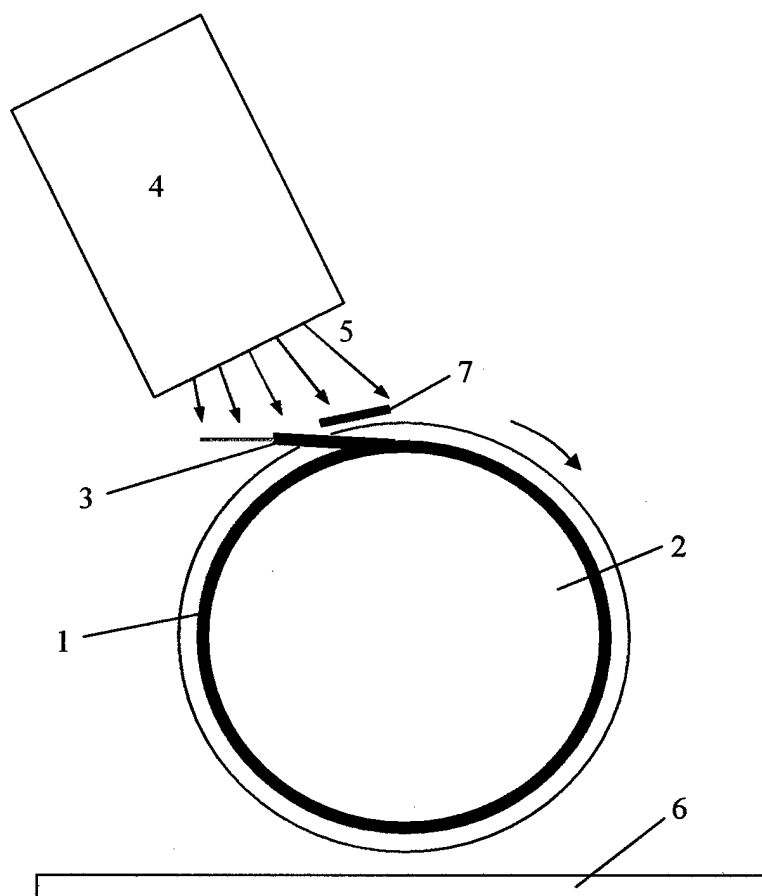


Fig. 7. The schematic of the experimental set-up used to deposit ITO conductive coating on the end of an optical fiber using the RF magnetron sputtering technique.

exposed to the gun only for a short period of time during the revolution of the drum. The rest of the time the fiber is being cooled down. The sputtering was conducted in atmosphere of argon. Operation was repeated for the second end of the fiber. It resulted into ITO coating deposited on both ends with a resistivity close to $100 \Omega/\square$.

The next step was to check if there is a sufficient electric contact between the ITO coated sidewalls of the fiber and its end face, which must actually interact with the E-O material squeezed between the fibers. The test was performed experimental set-up presented in Fig. 8. A movable pipette-like container 1 with a fiber 2 coming through it is filled with mercury 3. Metal wire electrode 4 provides an electric contact to the mercury and through it to the ITO coated sidewall of the fiber. Container 2 is movable in vertical

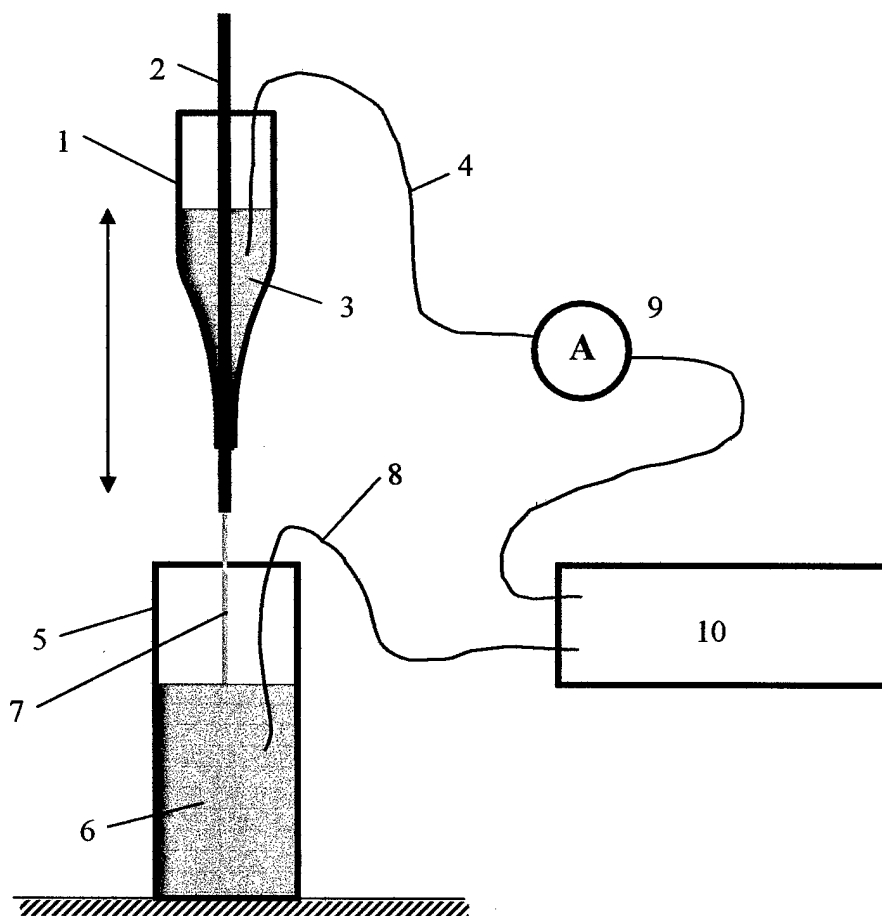


Fig. 8. The schematic of the experimental set-up used to test the electric contact between the sidewalls of the ITO coated fiber and its end face.

direction. Bottom cylindrical container 5 is also filled with mercury 6. Upper container 1 is moved down until the end face of the fiber makes a contact with the surface of mercury 6 in bottom container 5. Metal wire electrode 8 provides an electric contact to mercury 6 and through it to the ITO coated end face of the fiber. Wires 4 and 9 are connected to an external electric circuit made of an ammeter 9 and power supply 10. The electric current through the circuit measured by ammeter 9 gives an idea about the conductivity of the ITO coating between the sidewall of the fiber and the cleaved end face. Table 2 presents the results of the measurements for three pieces of optical fiber coated on both ends with ITO.

Table 2. Resistance of the ITO coating between the sidewall and the end face of optical fibers

Fiber	End	Resistance (k Ω)
1	1	10.0
	2	8.0
2	1	9.0
	2	8.5
3	1	7.5
	2	7.0

The resistance in all the cases is of the order of few kilohms. The third fiber was coated from both sides with respect to the sputtering gun and has less resistance. The resistance is low enough to provide an electric connection between the generator of the alternating voltage and the E-O material. We thus can conclude that the fibers can be used in the E-O modulator.

6. Electro-optic modulator based on a planar waveguide

E-O modulator based on a planar thin film waveguide is another alternative to a miniature E-O device. Thin films of E-O polymers were prepared using spin casting technique. Two polymers were used: commercial E-O polymer LD-3 from AdTech and a

E-O high-temperature polyimide. Polymeric material should be prepared in the form of a solution before spin casting on a substrate. After numerous experiments we found out that cycloheptanone is a good solvent for LD-3. The following procedures for LD-3 were used:

- (a) Dissolving powder of LD-3 in cycloheptanone at concentration 0.1 g of solids per 1.5 ml of liquids using stirring with a magnetic stirrer and heating at a hot plate for 4 hours at a temperature of 50°C. This results in a clear viscous solution of red color.
- (b) Filtering the solution through a 1- μm PTFE filter.
- (c) Filtering the solution through a 0.2- μm PTFE filter.
- (d) Spin casting the solution on a fused quartz substrate at a speed of 1000 rpm for 120 s. The process was repeated twice. This resulted in a high optical quality film of red/yellowish color.
- (e) Cold drying of the film in a vacuum oven for 3 hours.

Gamma-butyrolactone was identified as a good solvent for polyimide. The following procedures were used:

- (a) Dissolving powder of polyimide in gamma-butyrolactone at concentration 1 g of solids per 8 ml of liquids using stirring with a magnetic stirrer and heating at a hot plate for 24 hours at a temperature of 50°C. This results in a clear viscous solution of dark yellow/red color.
- (b) Filtering the solution through a 1- μm PTFE filter.
- (c) Spin casting a polyimide precursor at 4000 rpm and baking the substrate.
- (d) Spin casting the solution on a fused quartz substrate at a speed of 500 rpm and 100 rpm for 180 s. This resulted in a film of yellow/red color.
- (e) Baking the film.

The refractive indices were measured to be $n_{TE} = 1.7148$ and $n_{TM} = 1.7124$. The film has an anisotropy of the refractive index $\Delta n = n_{TE} - n_{TM} = 0.0024$, which is a typical

feature of a polyimide film attributed to the conditions of the packing of the molecules of the polymer on a substrate.

Corona poling is a convenient way of poling a film of E-O polymer without direct mechanical contact to its surface. A corona poling apparatus was designed with a needle and a control grid placed right above the film. A polymer film had to be kept in liquid phase during the poling process in order to ease up orientation of the E-O molecular fragments of the polymer along the electric field. In case of polymer LD-3 heating up to 150°C was used in order to melt the polymer. In case of polyimide poling was conducted with the film right after spin casting before the solvent dried out.

An experimental setup for characterization of electro-optic properties of poled polymer films was built. The setup is similar to that of ellipsometer with Soleil-babinet compensator initially proposed in Ref. 5. The electro-optic coefficients of poled polymer films were measured. Coefficient r_{33} was found to be between 3 and 5 pm/V and approximately 2 pm/V for LD-3 and polyimide respectively.

The oscillogram of real modulation signal obtained from the sample is presented in Fig. 9. Fig. 10 shows the amplitude of the signal proportional to the varying intensity of light reflected by the sample of poled polyimide film versus the amplitude of the alternating voltage. The dependence is apparently linear, which might serve as additional evidence of the true linear E-O (Pockels) effect in the corona poled polyimide.

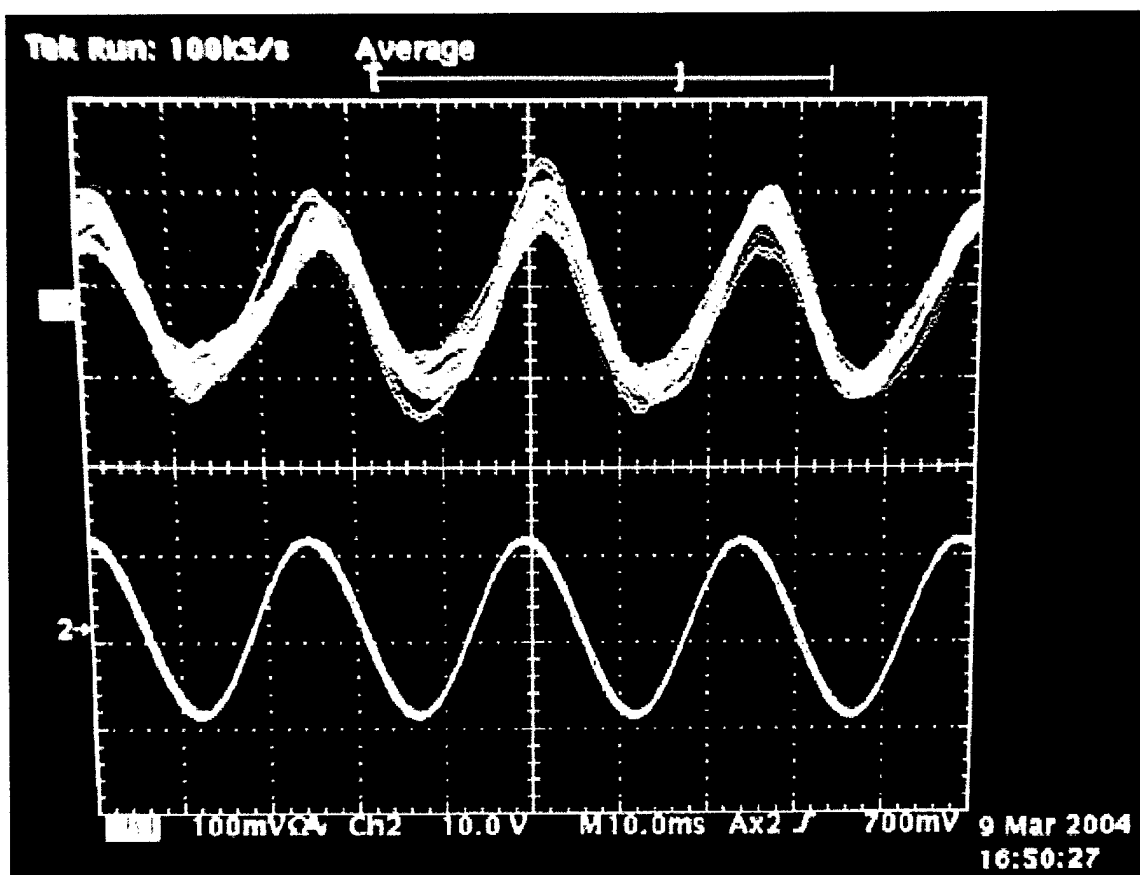


Fig. 9. The oscillogram of the signal proportional to the varying intensity of light reflected from the film of poled polyimide from GSU (top) and the alternating voltage applied to it (bottom).

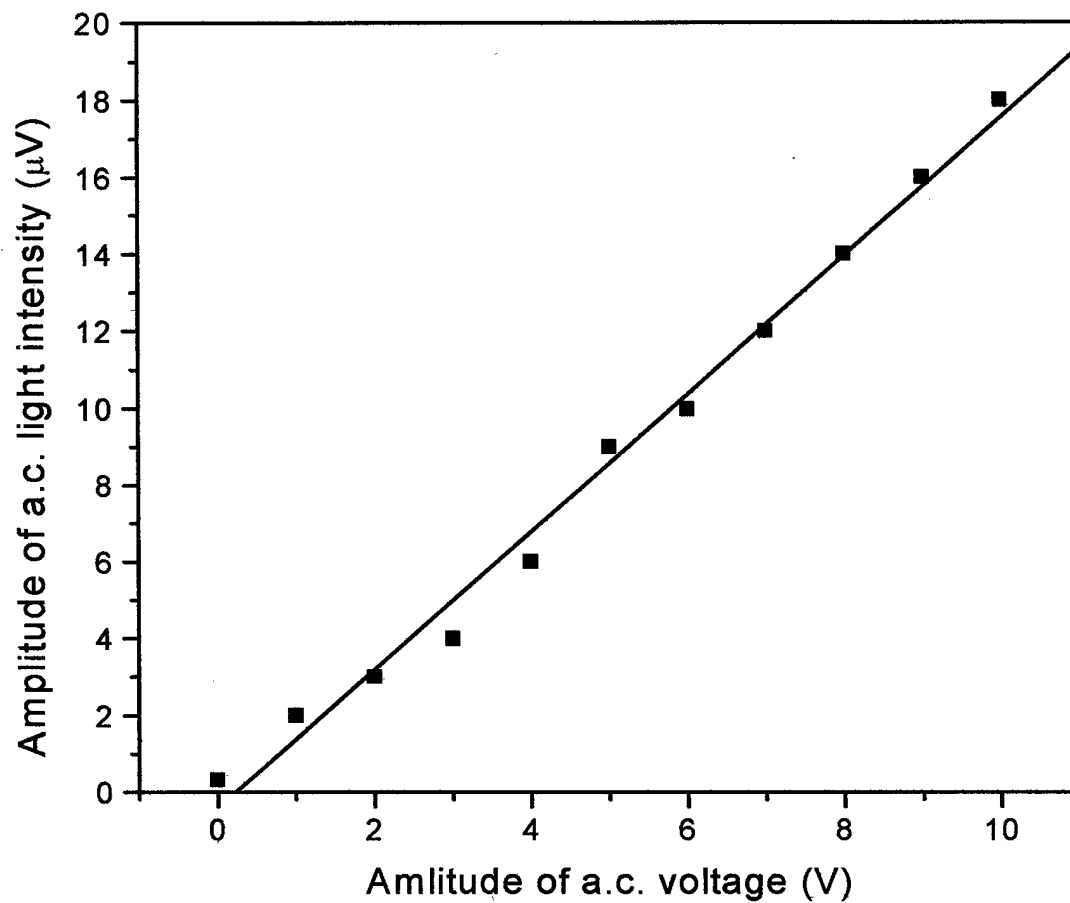


Fig. 10. Amplitude of the modulation signal from the E-O polyimide film versus amplitude of the alternating voltage in (a) linear and (b) log-log scale.

7. Conclusions and recommendations

A miniature electro-optic (E-O) modulator that comprises a Fabry-Perot (F-P) etalon integrated with an optical fiber was theoretically analyzed. The theoretical evaluation of the performance of the modulator was conducted for a single crystal film of organic compound *N*-4-Nitrophenyl-*N*-(*L*)-prolinol known as NPP, which have been recently grown and used in a longitudinal E-O modulator known as a conventional Pockels cell. The estimations indicated that the finesse of the F-P cavity is a highly critical factor in achieving low driving voltage of the modulator. An E-O modulator based on a planar thin film waveguide was also considered as another approach to a miniature E-O device. Thin films of E-O polymers were prepared using spin casting technique. An experimental setup for characterization of electro-optic properties of poled polymer films was built. The electro-optic coefficients of poled polymer films were measured. Coefficient r_{33} was found to be between 3 and 5 pm/V.

References for Part 3

1. Alexander Leyderman, Yunlong Cui, Javier Wu Li, Sergey Sarkisov, Michael Curley, Curtis Banks, Benjamin Penn, "Growth and characterization of single crystal organic thin films for electro-optic modulators," in *Operational Characteristics and Crystal Growth of Nonlinear Optical Materials*, Ravindra B. Lal, Donald O. Frazier, Editors, Proceedings of SPIE Vol. 3793 (1999) 45-54.
2. Zhifu Liu, Sergey S. Sarkisov, Michael J. Curley, Alexander Leyderman, Yulong Cui, Javier Wu Liu, and Benjamin Penn, "Diagnostics and growth of organic thin films for electro-optic modulators with low driving voltage," in *Optical Devices and Diagnostics in Material Science*, D.L. Andrews, T. Asakura, S. Jutamulia, W.P. Kirk, M.G. Lagally, R.B. Lal, J.D. Trolinger, Editors, Proceedings of SPIE Vol. 4098 (2000) 40-51.
3. B.E.A. Saleh and M. C. Teich, *Fundamentals of Photonics*, John Wiley and Sons, Inc., New York, 1991, 319.

4. A. Othonos and K. Kalli, Fiber Bragg Gratings, Artech House, Norwood, MA, 1999.
5. C.C. Teng and H.T. Man, Appl. Phys. Lett. 56, 1990, 1734.\
6. Sutherland, R. L., 1996. Handbook of nonlinear optics. Marcel Dekker, Inc., New York. 541.

Appendix

A1. Participants

Faculty and staff

UPRM

Principal Investigator:

Dr. Felix E. Fernandez (in replacement of the late Dr. Alex Leyderman)

Department of Physics, University of Puerto Rico, Mayaguez, PR 00680

787-265-3844, FAX: 787-832-1135, e-mail: f_fernandez@feynman.uprm.edu

NMHU

Principal Investigators of sub-contract:

Dr. Tatiana V. Timofeeva

Depart. of Chemistry, New Mexico Highlands University, Las Vegas, NM 87701, Tel.:

505-454-3362, FAX: 505-454-3301, e-mail: t_timofeeva@yahoo.com.

Staff:

Dr. Vladimir N. Nesterov, Department of Chemistry, New Mexico Highlands University

AAMU

Principal Investigator of sub-contract:

Dr. Sergey S. Sarkisov

Alabama A&M University Research Institute, Normal, AL 35762, Telephone: 256-858-

8106, Fax: 256-851-5622, e-mail: sergei@caos.aamu.edu.

Staff:

Dr. Michael J. Curley, Dept. of Physics, Alabama A&M University

Students

UPRM

Ms Tatiana Manotas, MS student

NMHU

Mr. Jose Gallegos, undergraduate student.

Ms Frances Sena, undergraduate student.

Ms Tiffany Kinnibrugh, MS student.

Ms Ekaterina Bodaeva, MS student.

Mr. Ilya Kosilkin, MS student.

AAMU

Ms Courtney Boykin, MS student

Mrs. Aisha Fields, Ph.D. student

Mr. Burl Peterson, Ph.D. student

A2. Presentations

1. NASA Ames & GEAR UP 2nd Annual Student Symposium, April 28, 2004, New Mexico Highlands University. . "Chromophore coated silver nanoparticles", Jose B. Gallegas, Ilya V. Kosilkin, Tatiana V. Timofeeva.
2. NASA Ames & GEAR UP 2nd Annual Student Symposium, April 28, 2004, New Mexico Highlands University. . "Computer simulation of molecules with two-photon absorption properties" Frances Sena, Ekaterina A. Badaeva, Tatiana V. Timofeeva.
3. Joint Regional Meeting of the Northwest and Rocky Mountain Sections of the American Chemical Society, June 6-9, 2004, Utah State University. "Chromophore coated silver nanoparticles", Ilya V. Kosilkin, Tatiana V. Timofeeva, Jose Gallegas.
4. Joint Regional Meeting of the Northwest and Rocky Mountain Sections of the American Chemical Society, June 6-9, 2004, Utah State University, "Computer simulation of new materials with two-photon adsorption properties", Ekaterina A. Badaeva, Tatiana V. Timofeeva, Frances Sena.
5. American Crystallographic Association 2004 Annual Meeting, July 17-22, Chicago, Illinois. "Crystal engineering of thermo stable acentric crystals", Tatiana V. Timofeeva, Vladimir N. Nesterov, Volodymir V. Nesterov, Mikhail Yu. Antipin.
6. American Crystallographic Association 2004 Annual Meeting, July 17-22, Chicago, Illinois. "Theoretical modeling of crystal structure of three polymorphs

- of (2E)-2-cyano-3-[4-(dimethylamino)phenyl]prop-2-enethioamide”, Tiffany Kinnibrugh, Tatina V. Timofeeva.
7. SPIE Conference “Photonics West’03”, San Jose, CA, Jan. 24-31, 2003. Electro-optic modulators based on high-temperature polyimides, Michael J. Curley.
 8. 17th Annual National Conference of Black Physics Students, Rensselaer Polytechnic Institute, April 3-6, 2003. Study of novel organic nonlinear optical materials, Burl H. Peterson.
 9. SPIE Meeting “Photonics West ‘04”, San Jose, CA, Jan. 2004. Novel organic compounds combining anti-cancer action with two-photon fluorescent cellular imaging, Burl H. Peterson.
 10. SPIE Meeting “Photonics West ‘04”, San Jose, CA, Jan. 2004. Novel two-photon optical limiting materials, Burl H. Peterson.

A3. Papers published

1. Thermally Stable Heterocyclic Imines as New Potential Nonlinear Optical Materials. Nesterov, V. V.; Antipin, M. Yu.; Nesterov, V. N.; Moore, C. E.; Cardelino, B. H.; Timofeeva, T. V.; *J. Phys. Chem. B.*; (Article); 2004; 108(25); 8531-8539.
2. Thermally Stable Imines as New Potential Nonlinear Optical Materials. Nesterov, V. V.; Antipin, M. Yu.; Nesterov, V. N.; Penn, B. G.; Frazier, D. O.; Timofeeva, T. V.; *Cryst. Growth Des.*; (Article); 2004; 4(3); 521-531. Sergey S. Sarkisov, Connie Walton, Michael J. Curley, Leonid Yarovoi, J._C. Wang, “Electro-optic modulators based on high-temperature polyimides”, in Proceedings of SPIE Vol. 4991 *Organic Photonic Materials and Devices V*, edited by James G. Grote, Toshikuni Kaino, (SPIE, Bellingham, WA, 2003) 589-600.
3. B.H. Peterson, S.S. Sarkisov, J.C. Wang, and M.J. Curley, Study of novel organic nonlinear optical materials, Poster, 17th Annual National Conference of Black Physics Students, Abstract Booklet, Rensselaer Polytechnic Institute, April 3-6, 2003. Burl H. Peterson, Sergey S. Sarkisov, V.N. Nesterov, E.I. Radovanova, A.

- Leyderman, T. Timofeeva, M. Antipin, Michael J. Curley, Paul A. Fleitz, Charles Lee, J.-C. Wang, "Novel organic compounds combining anti-cancer action with two-photon fluorescent cellular imaging," in *Multiphoton Microscopy in the Biomedical Sciences IV*, edited by Ammasi Periasamy, Peter T.C. So, Proceedings of SPIE Vol. 5323 (SPIE, Bellingham, WA, 2004) 365-376.
4. Burl H. Peterson, Sergey S. Sarkisov, V.N. Nesterov, E.I. Radovanova, A. Leyderman, T. Timofeeva, M. Antipin, Michael J. Curley, Paul A. Fleitz, Charles Lee, J.-C. Wang, "Novel two-photon optical limiting materials," in *Organic Photonic Materials and Devices VI*, edited by James G. Grote, Toshikuni Kaino, Proceedings of SPIE Vol. 5351 (SPIE, Bellingham, WA, 2004) 181-190.
 5. Vladimir N. Nesterov, Tatiana V. Timofeeva, Sergey S. Sarkisov, Alexander Leyderman, Charles Y.-C. Lee, and Mikhail Yu. Antipin, 3,5-Bis[4-(diethylamino)benzylidene]-1-methyl-4-piperidone and 3,5-bis[4-(diethylamino)cinnamylidene]-1-methyl-4-piperidone: prospective biophotonic materials, *Acta Cryst. C* 59 (2003) o605-o608.
 6. Sergey S. Sarkisov, Elena I. Radovanova, Burl H. Peterson, Alex Leyderman, Michael Curley and Paul Fleitz, Optical spectroscopic and nonlinear transmittance study of fullerene C₆₀ in mixture with 2-cyclooctylamino-5-nitropyridine (COANP), *Journal of Nonlinear Optical Physics and Materials (JNOPM)* 13, No. 1 (2004) 113-127.

A4. Papers submitted

1. Vanishing Polymorphism of (2E)-2-Cyano-3-[4-(diethylamino)phenyl]prop-2-enethioamide: X-Ray Structural Study and Polymorph Prediction. Tatiana V. Timofeeva, Tiffany Kinnibrugh, Oleg Ya. Borbulevych, Boris B. Averkiev, Vladimir N. Nesterov, Andreanne Sloan, and Mikhail Yu. Antipin; *Cryst. Growth Des.*, August 2004.
2. Sergey S. Sarkisov, Burl H. Peterson, Michael J. Curley, Vladimir N. Nesterov, Tatiana Timofeeva, Mikhail Antipin, Elena I. Radovanova, Alex Leyderman, Paul A. Fleitz, Two-photon absorption and fluorescence of new derivatives of

cyclohexanone and piperidone, submitted to the Journal of Nonlinear Optical Physics and Materials (JNOPM).

A5. Students graduated:

Mrs. Aisha Fields, (graduated with Ph.D. degree in Physics in July 2004)

Mr. Burl Peterson, M.S. (graduated with M.S. degree in Physics in November 2004).

Ms Tatiana Manotas, M.S. (thesis defense scheduled for December 2004).